THEORETICAL STUDY OF FUNCTIONALIZED TWO-DIMENSIONAL MATERIALS TOWARDS THEIR APPLICATION IN SUPERCAPACITORS

Thesis

submitted in partial fulfillment of the requirements for the degree of

DOCTOR OF PHILOSOPHY

by

SRUTHI T

DEPARTMENT OF PHYSICS
NATIONAL INSTITUTE OF TECHNOLOGY KARNATAKA (NITK)
SURATHKAL, MANGALORE - 575 025
July, 2021

DECLARATION

by the Ph.D. Research Scholar

I hereby declare that the Research Thesis entitled **"The Theoretical Study of Functionalized Two-Dimensional Materials Towards Their Application in Supercapacitors"**, which is being submitted to the ***National Institute of Technology Karnataka, Surathkal*** in partial fulfilment of the requirements for the award of the Degree of ***Doctor of Philosophy*** in ***Physics*** is a *bonafide report of the research work carried out by me* under the guidance of Dr. Kartick Tarafder, Assistant Professor, Department of Physics, NITK. The material contained in this Research Thesis has not been submitted to any University or Institution for the award of any degree.

08/07/2021

Sruthi T
Reg. No. : 158030 PH15F05
Department of Physics
NITK Surathkal – 575025

Place: NITK-Surathkal
Date: July, 2021

CERTIFICATE

This is to *certify* that the Research Thesis entitled "**The Theoretical Study of Functionalized Two Dimensional Materials Towards Their Application in Supercapacitors**" **submitted by Sruthi T**, (Reg. No. : 158030PH15F05) as the record of the research work carried out by her, is *accepted as* the *Research Thesis* in partial fulfilment of the requirements for the award of *degree of* **Doctor of Philosophy**.

KTarafder 13/7/2021

Dr. Kartick Tarafder

Research Guide
Assistant Professor
Department of Physics
NITK Surathkal – 575025

13/7/2021

Chairman - DRPC
(Signature with Date and Seal)

ASSOCIATE PROFESSOR & HEAD
Physics Department
NITK Surathkal, Mangalore-575025
KARNATAKA

ACKNOWLEDGEMENT

The success and outcome of the research required a lot of advice and help from many people. In the accomplishment of this work, many have better possessed upon me their blessings and their hearts-plundered support. I am very grateful to my guide, Dr. Kartick Tarafder, for his valuable advice that has supported my efforts at every stage of my work. At each stage of the work, his supervision and advice shaped this research work to completion. His constructive guidance and motivation were responsible for my Ph.D.'s success. I never thought I'd have a better advisor and mentor for my doctoral degree. His insightful comments prompted me to refine my thinking and take my work to the next level. I, therefore, wish to express my heartfelt gratitude to my supervisor, Dr. Kartick Tarafder. I have a sisterly affection with the beloved wife of Dr. Kartick, Mrs.Mamtha, who helped me to overcome many difficult moments and who will always be cherished. I am grateful to his wife and beloved son Anshuk for their love and care. I would like to thank the members of my Research Progress Assessment Committee members, Prof. Panduranga Vittal K, The Department of Electrical and Electronic Engineering and Prof. M. N. Satyanarayanan, Department of Physics for their constructive and timely suggestions and continued support, who have always provided me with more energy to get my work done on time. I am grateful to all the faculty members of the Department of Physics of NITK Surathkal, Prof. G. Umesh, Prof. Kasturi. V. Bangera, Prof. N. K. Udayashankar, Prof. H. D. Shashikala, Dr. M. N. Satyanarayan, Dr. H. S. Nagaraja, Dr. Partha P. Das, Dr. T. K. Shajahan, Dr. Ajith K.M, Dr. Deepak Vaid, and Dr. Kishore Sridharan for their support, motivation, and help throughout my lifetime of research. I am also indebted to the Department's non-academic staff, Mrs. Saritha Shetty, Mr. Dhanraj, Mrs. Ashalatha, Mrs. Veena, Mr. Pradeep, Mr. Harshith, Mr. Karthik and Mrs. Suma, Mrs. Hemalatha, Mrs. Anasooya, Mr. Sarath, Ms. Reshmi, Mr. Santhosh, Mr. Janardhana Bhat, Mr. Ganesh for their continued support of my daily activities within the Department. I also want to thank all the staff at the Institute and the Hostel office for their cooperation and support throughout my research life. I would like to acknowledge the computational resources at NITK. I remember with gratitude all of my teachers and mentors who have always inspired and brought to light my personal and academic journey.

I would like to thank all the teachers of Ramadas Shishumandir, GUPS Pullur, UNHS Pullur, Chattanchal HSS, Nehru Arts and Science College Kanhangad, in particular Mrs. Sheeba, Mrs. Bindu, Mrs. Beena, Mrs. Shiny, Mrs. Jessy, Mrs. Sayanora, Mrs. Gracy, Mrs. Jacquilne, Mr. Pramod, Mr. Jose, Mrs. Sreeja, Mrs. Mari, Mrs. Sujatha, Mrs. Anitha, Mr. Ratheesh, Mr. Avaneendranath, Mr. Mohanan, Mr. Raghu, Dr. K. M. Udayanandan, Prof. R.K. Sathish, Prof. P. V. Siddharthan, Dr. K. V. Murali, Dr. Pradeep Kumar, Mr. Rameshan, Dr. Naseema, Mrs. Sreelekha, Mrs. Anitha, Mrs. Neena, and Mr. Balakrishnan.

I am blessed with a lot of friends and well-wishers in my life. First and foremost, I express my deep gratitude to Mrs. Nayana Devaraj, who has always been there to motivate me since 2016, to take me through the difficult moments of NITK as a research student. I also wish to thank my friends Mr. Jijth and Mr. Lallu Anthoor for their support in the course of my research. I am grateful to my colleagues from NITK's Computer Physics Laboratory (MPCL), Mrs. Vijaya, Mr. Ramesh reddy, Ms. Sulakshana, and Ms. Subhashmitha for their support. I thank all the researchers and students in the Department of Physics for being so kind to me, Dr. Sibi Thomas, Mr. Ahmed Rizwan C L, Ms. Rajani, Mr. Safir, Mr. Anandram, Mr. Ahamed Khasim, Mr. Sterin, Ms. Sukanya, Mr. Shreyas, Mr. Kartheek Hegde, Mrs. Amrutha S V, Mrs. Subhashini, Mr. Mahendra, Ms. Bindu, Mr. Achyutha, Mr. Brijesh, Ms. Amudha, Dr. Manoj, Mr.Nimith, Mrs. Manju, Mrs. Sherin, Ms. Anupriya, Ms. Anupama, Mr. Makesh, Mrs. Soujanya, Mr. Bharath, Mr. Biswajith, Mrs. Veena, Mr. Santhosh, Mr. S.Bhattacharya, Mrs. Akhila, Dr. Sreejesh, Mrs. Pranitha, and student friends at NITK who treated me like a sister and made my time at NITK Surathkal unforgettable. I would also like to thank all my friends at and around NITK, Dr. Pavan Pujar, Mr. Komal Krishna, Mrs. AnMary, Mr. Deepu, Mr. Sudheesh, Mrs. Karthika, Mr. Sanjay, Ms. Lekshmi, Mr. Omkar, Ms. Reshmi, Ms. Sarga, Ms. Megha, Mrs. Abhirami, Ms. Aswathi, Ms. Jithin, Mrs. Pooja, Mrs. Chandana, Mr. Sujan, Ms. Surabhi and Ms. Sruthi are few among them.

I would like to thank all members of the NITK community for their help during these years. I would like to thank all my classmates, graduates, and senior friends for their friendship and support. Thanks to all of you for your help and affection that will always be treasured. I thank all members of my family for their support and encouragement.

The success of this work is all because of my parents and my siblings who are my greatest strength and weakness. I owe them my love and gratitude for their unconditional love, their trust in me, and their unconditional support at every step of my life and my Ph.D. The overwhelming encouragement and inspiration I received from my parents, brothers, and sisters for this pursuit were magnificent. I am also deeply indebted to my in-laws who showered their love, care, help, and kindness to me during my research life. I would like to express my heartfelt thanks to Mrs. Leskshmi Parasuram and Mr. Parasuram for the love and support they showed during my stay with them. I remember gratefully all the people and supporters for the help, support, and blessings for the research work that I may not have mentioned without knowing it.

Finally, I would like to express my profound gratitude to my parents and Dr. Sukesh, my life partner, for providing me with ongoing support and encouragement throughout my years of study and the research and writing process of this thesis. This accomplishment was not possible without them.

Thank you
Sruthi T

ABSTRACT

This thesis investigates possible roots to enhance the quantum capacitance(C_Q) of two-dimensional materials based electrodes for supercapacitor applications through density functional theory(DFT) calculations. In this work, various two-dimensional materials such as graphene, molybdenum disulfide(MoS_2), and hexagonal boron nitride(h-BN) have been considered, subsequently, chemical functionalization of these systems has been performed to manifest the high quantum capacitance. The quantum capacitance of functionalized systems was estimated from the precise electronic band structures of the system obtained by using DFT calculations. It has been observed that ad-atom functionalization of graphene can significantly enhance the quantum capacitance of the system. Therefore, in the first stage, the quantum capacitance of ad-atom doped graphene with a varying doping concentration has been systematically studied. The effect of temperature on quantum capacitance has also been investigated. The temperature-dependent study of C_Q for functionalized graphene shows that the C_Q remains very high in a broad range of temperatures close to room temperature. In the second stage, the graphene functionalization has been done by doping with different aliphatic and aromatic molecules and their radicals. Our theoretical investigation reveals that aromatic and aliphatic radicals introduce localized density of states near the Fermi level of the functionalized systems, due to a charge localization which in turn significantly enhances the quantum capacitance of the system. The effects of atomic dislocation on graphene during functionalization has also been incorporated in our investigation. In the third stage, we have carried out our investigation in other two-dimensional materials such as MoS_2 and h-BN. Attempts have been made to enhance the quantum capacitance of these systems by introducing defects as well as performing chemical fictionalizations. The detailed study in this thesis suggests an efficient way to produce functionalized materials using two-dimensional materials that could be very suitable electrode materials of highly efficient supercapacitors.

Keywords: The supercapacitor; Quantum capacitance; Two-dimensional materials; Graphene; Molybdenum disulfide(MoS_2); Hexagonal boron nitride(h-BN); Functionalization; Vacancy defects; Density Functional Theory.

Contents

List of Figures vii

List of Tables xiii

Nomenclature xv

1 Introduction **5**

1.1 Important Two-dimensional materials 6

1.1.1 Graphene 6

1.1.2 Functionalization of Graphene 7

1.1.3 Graphene Oxide 7

1.1.4 Reduced graphene oxide (rGO) 8

1.2 Possible solutions for energy storage problem 8

1.2.1 Application of Ultracapacitors 9

1.3 Supercapacitors based on graphene 10

1.3.1 Quantum capacitance (C_Q) of supercapacitor electrodes 11

1.3.2 Correlation and Quantum Capacitance 11

1.4 Functionalization of supercapacitor electrode materials 12

1.4.1 Functionalization of graphene with ad-atoms 12

1.4.2 Functionalization of graphene with molecular fragments 13

1.5 Molybdenum disulfide (MoS_2) 14

1.6 Hexagonal Boron Nitride 15

1.7 Scope and Objectives of the Present Research Work 16

1.7.1 Scope 16

1.7.2 Objectives of the proposed Work 18

1.8 Organization of the Thesis 19

2 Methodology **21**

2.1 Many-body Interacting Electron Problem 21

2.2 Density Functional Theory (DFT) 23

2.2.1 Hohenberg-Kohn Theorems 24

2.2.2 Kohn–Sham(KS) equations 28

2.2.3 Calculation procedure for Kohn-Sham equation : 30

2.2.4 Estimation of Exchange-Correlation(XC) energy 31

2.3 Quantum capacitance of a Supercapacitor cell 32

2.4 Simulation methods 35

3 Enhancement of Quantum Capacitance by Ad-atom Functionalization of Graphene Supercapacitor Electrodes. **39**

3.1 Introduction 39

3.2 Methodology 40

3.3 C_Q in pristine Graphene 41

3.4 Functionalization of graphene with ad-atoms 43

3.5 Impact of ad-atom concentrations on graphene C_Q: 54

3.5.1 Effect of Oxygenation on graphene C_Q 55

3.6 Effect of co-doping on graphene C_Q 56

3.6.1 Co-doping effect of Nitrogen and Oxygen on graphene C_Q . . . 57

3.7 Impact of Vacancy defects on graphene C_Q 59

3.8 Impact of vacancy defects on functionalized graphene C_Q 60

3.9 Conclusion 61

4 Enhancement of Quantum Capacitance in graphene electrodes using molecular fragments and radicals functionalization. **63**

4.1 Methodology 64

4.2 Aliphatic Molecule functionalization on pristine graphene 65

4.3 Aliphatic Radical functionalization on pristine graphene 67

4.4 Aromatic molecule functionalization on pristine graphene 69
4.5 Aromatic Radical functionalization on pristine graphene 72
4.6 Conclusion 76

5 The enhancement of quantum capacitance in chemically modified MoS_2 and h-BN electrodes 77
5.1 Introduction 77
5.2 Quantum capacitance of functionalized MoS_2 monolayer 78
  5.2.1 Substitution of Sulfur with group-V ad-atoms 80
  5.2.2 Substitution of Sulfur with group VII ad-atoms 82
  5.2.3 Substitution of Mo with Transition Metal(TM) ad-atoms 83
  5.2.4 Impact of vacancy defects 86
5.3 Effect of functionalization on quantum capacitance for hexagonal boron nitride (h-BN) 89
5.4 Conclusion 90

6 Summary and Future Work 93
6.1 Summary 93
6.2 Future Scope of work 95

References 97
6.3 LIST OF PUBLICATIONS BASED ON THESIS WORK 113

Conference Presentations 114

List of Figures

1.1 Schematic diagram shows the differences between Conventional Capacitor(a) and Supercapacitor(b). 9

2.1 (color online)A flow chart of the Kohn-Sham iteration scheme. 31

3.1 (colour online)Optimized geometric structure for pristine graphene. Black ball represents Carbon atom. 41

3.2 Electronic band structure for pristine graphene. Horizontal green dashed line is the Fermi energy set at E=0. Dirac point is encircled in the bandstructure. 42

3.3 (a)Electronic density of states and (b) Quantum capacitance value for pristine graphene. Vertical red and blue line is the Fermi energy set at E=0. 43

3.4 Energy-optimized geometry of functionalized graphene with different ad-atoms. Black magenta, blue and green ball represents C, Al, N and Cl atoms respectively a) Preferred adsorption position for Al at hollow site b)Nitrogen at bridge site and (c) Chlorine at the top site. (d) A side view of top site Cl adsorption. 44

3.5 Electronic band structure and DOS for graphene functionalized with K. Contribution from doped atoms are represented by the coloured curve in the DOS and coloured circle in the band structure. Horizontal green dashed line is the Fermi energy set at E=0. 46

3.6 Atom projected density of states for functionalized graphene with (a)K (b)Na and (c)Al atoms. The shaded curve represents dos from the doped atom. The vertical blue dashed line is the Fermi energy set at E=0. . . . 47

3.7 Atom projected density of states for functionalized graphene with (a)N (b)P and (c)Cl ad-atoms. The shaded curve represents dos from the doped atom. The vertical blue dashed line is the Fermi energy set at E=0. 48

3.8 Electronic band and DOS for (a) FG-N and (b) FG-Sn. Colored curve in the DOS and circle in the band structure represents contribution from doped atoms. Horizontal red dashed line is the Fermi energy set at E=0. 49

3.9 Contour plots for electron density associated with (a)Pristine Graphene, Functionalized graphene with (b)Al, (c)N and (d)Cl. Relative density is indicated by the colour bar. 49

3.10 Variation of Quantum Capacitance with temperature in the range of 10K to 400K for (a)FG-N (b) FG-P and (c)FG-Cl. 51

3.11 Atom projected density of states for functionalized graphene with (a)Ac (b)B and (c)Ca (d)La (e)Si and (f)Ge atoms. Colored curve represents dos from the doped atom. Vertical blue dashed line is the Fermi energy set at E=0. 52

3.12 The different color curve represents the energy variations of quantum capacitance for graphene functionalized with various ad-atoms. 53

3.13 N atom projected DOS for nitrogenated graphene with two different N concentrations. Red line is for the 6.25% doping where the C_Q is maximum. Blue line represent the same for higher 8% doping. 55

3.14 Quantum capacitance for oxygen doped graphene with various degrees of functionalization. 56

3.15 (a) Atom PDOS and (b)Quantum capacitance for N, O dual doped graphene. 58

3.16 Atom PDOS for N, O dual doped graphene. 58

3.17 Optimized geometric structure for monovacancy defected graphene. . . 59

3.18 (a) Electronic DOS and (b) Quantum capacitance values for pristine and vacancy defected graphene systems. 60

4.1 Energy-optimized geometry of functionalized graphene with (a)Acetone(ketone), (b)piperidine(amine), (c)DMSO and (d)Hexane-1-thiol. Black, grey, blue, red and yellow ball represents C, N, H, O and S atoms respectively. 66

4.2 Projected density of states for functionalized graphene with (a)Acetone(ketone), (b)piperidine(amine), (c)DMSO (sulfoxide) and (d)Hexane-1-thiol. The colored curve represents dos from the aliphatic molecules. The vertical blue dashed line is the Fermi energy set at E=0. 66

4.3 Energy-optimized geometry of (a)Ethene, (b)Propene, (c)Acetone and (d)Butanone radical functionalized graphene. Black, blue, and red ball represents C, H and O atoms respectively. 68

4.4 Projected density of states for functionalized graphene with (a)Ethene, (b)Propene, (c)Acetone and (d)Butanone radicals. The colored curve represents dos from the aliphatic radical. The vertical blue dashed line is the Fermi energy set at E=0. 69

4.5 Energy-optimized geometry of (a)Benzene, (b)Aniline, (c)Phenol, (d)Anthracene, (e)Toluene and (d)Naphthalene molecule functionalized graphene. Black, blue, red, and grey ball represents C, H, O and N atoms respectively. . . 71

4.6 Projected density of states for functionalized graphene with (a)Benzene, (b)Aniline, (c)Phenol, (d)Anthracene, (e)Toluene and (d)Naphthalene molecule. The colored curve represents dos from the aromatic molecules. The vertical blue dashed line is the Fermi energy set at E=0. 72

4.7 Energy-optimized geometry of (a)Benzene, (b)Aniline, (c)Phenol, (d)Anthracene, (e)Toluene and (d)Naphthalene radical functionalized graphene. Black, blue, red, and grey ball represents C, H, O and N atoms respectively. . . 73

4.8 Projected density of states for functionalized graphene with (a)Benzene, (b)Aniline, (c)Phenol, (d)Anthracene, (e)Toluene and (d)Naphthalene radical. The colored curve represents dos from the aromatic radicals. The vertical blue dashed line is the Fermi energy set at E=0. 74

4.9 Distribution of transferred charge due to (a) benzene (b)anthracene and (c) phenol radical functionalization on graphene. The transferred charges are highly localized in the case of phenol but delocalized in benzene and anthracene radical adsorptions 75

5.1 The optimized geometric structure of monolayer MoS_2 showing a layer of molybdenum atoms (blue) sandwiched between two layers of sulfur atoms (yellow). 79

5.2 Electronic DOS and Bandstructure for MoS_2 Monolayer. Horizontal pink dashed line is the Fermi energy set at E=0. 79

5.3 The optimized geometric structure of monolayer MoS_2 where Nitrogen replaces Sulfur(a)top view and (b)side view. 80

5.4 Atom projected density of states for functionalized MoS_2 with (a)N, (b)As, (c)Sb and (d)Se atoms. Colored curve represents dos from the doped atom. Vertical majenta dashed line is the Fermi energy set at E=0. 81

5.5 Change in electron density associated with Functionalized MoS_2 Monolayer with (a)N, (b)As, (c)Sb and (d)Se doping. Red and green isosurface represents the charge accumulation and electron deficiency in the system. The blue and yellow balls represents Mo and S atoms in MoS_2 Monolayer. 82

5.6 The optimized geometric structure of monolayer MoS_2 where Clorine replaces Sulfur(a)top view and (b)side view. 83

5.7 Atom projected density of states for functionalized MoS_2 with (a)F and (b)Cl atoms. Colored curve represents dos from the doped atom. Vertical majenta dashed line is the Fermi energy set at E=0. 83

5.8 Isosurface plots for electron density associated with Functionalized MoS_2 Monolayer with (a)F and (b)Cl. Red and green isosurface represnts the charge accumulation and electron deficiency in the system. The blue and yellow balls represents Mo and S atoms in MoS_2 Monolayer. 84

5.9 The different color curve represents the energy variations of quantum capacitance for MoS_2 Monolayer functionalized with various ad-atoms(Group 5 & 7). 84

5.10 The optimized geometric structure of monolayer MoS_2 where Vanadium replaces Molybdenum. 85

5.11 Atom projected density of states for functionalized MoS_2 with (a)V, (b)Nb, (c)Co and (d)Ni atoms. Colored curve represents dos from the doped atom. Vertical majenta dashed line is the Fermi energy set at E=0. 85

5.12 The different color curve represents the energy variations of quantum capacitance for MoS_2 Monolayer functionalized with various ad-atoms. 86

5.13 Change in electron density associated with Functionalized MoS_2 monolayer with (a)V, (b)Nb, (c)Co and (d)Ni doping. The blue and yellow balls represents Mo and S atoms in MoS_2 Monolayer. The electron accumulation and charge deficiency is represented by the red and green isosurface respectively 87

5.14 The optimized geometric structure of monolayer MoS_2 with monovacancy at Molybdenum site. 87

5.15 Atom projected density of states for MoS_2 Monolayer with (a)One sulfur vacancy, (b)two sulfur vacancy, (c)three sulfur vacancy, (d)one Mo vacancy. Vertical blue dashed line is the Fermi energy set at E=0. 88

5.16 The different color curve represents the energy variations of quantum capacitance for MoS_2 functionalized with various ad-atoms 88

5.17 (a)Geometric structure for Li doped h-BN and (b)Atom PDOS for Li doped h-BN. 90

List of Tables

3.1 Adsorption energy per ad-atoms adsorbs on pristine graphene surface. . 44

3.2 Calculated C_Q value at 300 K for various ad-atom functionalized graphene with doping concentration 5.5%. 45

3.3 Adsorption energy per ad-atoms adsorbs on pristine graphene surface. . 51

3.4 Details of C_Q value calculated at Fermi energy for various ad-atom functionalized graphene. 52

3.5 Details of charge transferred for variuos ad-atom functionalized graphene. 53

3.6 Concentration dependence in C_Q for nitrogen and chlorine functionalized graphene at 300K. 55

3.7 Details of C_Q calculated at Fermi energy for Oxygenated graphene with varying O/C ratio. 56

3.8 Calculated C_Q values for Co-doped graphene(G18) with two different ad-atoms with 5.5 % doping concentration for each type. 57

3.9 Details of C_Q values calculated at Fermi Energy for co-doped graphene with Nitrogen, Oxygen in different concentration. 57

3.10 Calculated C_Q values for vacancy defected graphene with different vacancy concentration(G50) at 300K. 60

4.1 Calculated E_{ad} value, charge transferred and quantum capacitance value at 300 K for various Aliphatic molecules functionalized graphene with single molecule doping. 67

4.2 Calculated Adsorption value, charge transferred and C_Q value at 300 K for various aliphatic radical functionalized graphene with single radical doping. 70

4.3 Calculated E_{ad} value, charge transferred and quantum capacitance value at 300 K for various aromatics functionalized graphene with single molecule doping. 71

4.4 Calculated E_{ad} value, charge transferred and quantum capacitance value at 300K for various aromatic radical functionalized graphene with single radical doping. 75

5.1 Adsorption energy per ad-atoms adsorbs on MoS_2 Monolayer. 80

5.2 Details of C_Q value calculated at Fermi energy for various ad-atom functionalized MoS_2. 86

5.3 Calculated C_Q value at 300 K for various adatom functionalized h-BN. . 89

Nomenclature

C_Q	Quantum capacitance
h-BN	Hexagonal boron nitride
MoS_2	Molybdenum disulfide
DFT	Density Functional Theory
C_T	Total capacitance
C_{EDL}	Electrical double layer capacitance
DOS	Density of states
μ	Chemical potential
FG	Functionalized graphene
EDLCs	Electric double-layer capacitors
E_F	Fermi energy
PC	Personal computer
HF	Hartree-Fock
ρ(r)	Electron density
H-K	Hohenberg and Kohn
KS	Kohn–Sham
etc.	et cetera
e.g.	Example
$V_{ext}(\vec{r})$	External potential
K.E	Kinetic energy
KS-DFT	Kohn-Sham DFT

T_s	True kinetic energy functional
V_H	Hartree potential
E_{xc}	Exchange correlation energy
V_{eff}	Effective potential
ϕ_i	Orbitals
XC	Exchange and correlation
E_{ext}	External energy
r	Electronic coordinates
E_x	Exchange energy between electrons with the identical spin
E_c	Correlation energy between electrons
LDA	Local density approximation
GGA	Generalised gradient approximation
ΔQ	Variation of charge density
ϕ	Local potential
n(E)	Density of states
E	Relative energy with respect to the Fermi level
D(E)	Electron density of state
f(E)	Fermi-Dirac distribution function
e	Electronic charge
VASP	Vienaa Ab-initio Simulation Package
vdW	Van der Waals
PDOS	Atom projected density of states
E_{ad}	Adsorption energy

E_{tot}	Total energy of the unit cell
E_{gr}	Total energy of pristine graphene
E_{frag}	Per molecule energy of the fragment
E_{at}	Per atom energy of the ad-atom
$(CH_2)_5NH$	Piperidine
$(CH_3)_2SO$	Dimethyl sulfoxide (DMSO)
Å	Angstrom
μF	Micro farad
E_D	Dirac point energy
n	Number of adsorbed molecules present in the unit cell
$E(\bar{g})$	Energy of the deformed graphene
E(g)	Energy of pristine graphene
K	Potassium
Na	Sodium
Al	Aluminium
P	Phosphorus
N	Nitrogen
Cl	Chlorine
Sn	Tin
O	Oxygen
C	Carbon
Ac	Actinium
La	Lanthanum

Si	Silicon
Ge	Germanium
S	Sulfur
B	Boron
Ca	Calcium
H	Hydrogen
Mo	Molybdenum
As	Arsenic
Sb	Antimony
Se	Selenium
Li	Lithium
V	Vanadium
Cu	Copper
2D	Two-dimensional
eV	Electron volt
i.e.	That is
K	Kelvin
MD	Molecular dynamics

Chapter 1

Introduction

An adequate amount of energy production from sustainable energy sources, bypassing the utilization of fossil fuels is one of the greatest challenges to stifle the weather change. Large scale production of green energy from sustainable power sources is therefore highly essential in this current scenario (Res and Majumdar 2016). In tropical developing nations like INDIA with increasingly high energy demand, one must need to discover an effective method to generate renewable energies from a sustainable power source such as wind and sunlight. Harvesting energy from the sunlight is the most practical way to generate an adequate amount of renewable energy to satisfy our daily needs. However, energy can't be harvested from the sunlight consistently in a uniform way throughout the year in numerous parts of the globe. Consequently, proficient storage of the energy produced and its savvy transportation is an important part of the energy generation process. As a result, designing proficient energy storage devices is one of the most important and dynamic areas of research in the green energy production process. Designing supercapacitors or ultracapacitors made up of functionalized materials would be a hopeful technology that could provide a possible alternative for efficient storage of energy (Peng et al. 2014, El-Kady et al. 2016, Bissett et al. 2015, Kim et al. 2010). A proficient supercapacitor prototype for this purpose requires electrode materials (Shim et al. 2011) with a very large ion density. Two-dimensional materials could play a significant role in designing effective supercapacitor electrodes (Dž et al. 2015). With an extremely high surface area, conductivity, and mechanical robustness in many 2D materials recently synthesized, are therefore could be suitable alternatives for supercapacitor electrode applications (Zhang et al. 2009, Ke and Wang 2016, Wood 2015).

1.1 Important Two-dimensional materials

Two-dimensional(2D) materials are crystalline materials also referred to as single-layer materials, comprising of a single or few layers of atoms. The 2D confinement gives rise to extraordinary material properties. This class of materials has been proven to be very suitable for their applications in electrodes, water purging photovoltaics, and semiconductors (Amiri et al. 2016). 2D layered materials that are attracted with a great research interest in the direction of energy storage includes graphene, transition-metal dichalcogenides (TMDs), and h-BN.

1.1.1 Graphene

Graphene is the first ‘modern’ 2D material of single-atom thickness was created in 2004, in which carbon atoms are arranged in a honeycomb lattice. Andre Geim and Konstantin Novoselov for the first time were successfully able to separate the single carbon layer from bulk graphite with sticky tape and transfer it onto a silicon wafer. Graphene shows remarkable electrical and mechanical properties. The two-dimensional sp^2 - hybridized carbon material, is the thinnest, most powerful, and rigid material in the world (Novoselov et al. 2005, Allen 2009). Graphene from the machine’s point of view, to be even marvelous than other carbon allotropes like 1-dimensional nanotubes and 0-dimensional fullerenes, etc. Graphene has pulled in the interest of many scientists, physicists, and materials scientists for the past two decades, because of its remarkable geometrical, mechanical, and electronic properties. Recently it became an energizing field of experimental research (Cooper et al. 2012).

Pristine graphene is in demand for applications that require a high electrical conductivity. It has been observed that numerous functional materials suitable for different technological applications can be made out of graphene upon chemical functionalizations of graphene.

1.1.2 Functionalization of Graphene

Many different techniques have been reported for graphene functionalization (Iyakutti et al. 2015). Chemical functionalization is one of such techniques proven to be a very suitable and easy process for controlling graphene's electronic structure (Rani et al. 2015, Nakada and Ishii 2011). For example, the presence of oxygen functionalities on the graphene motif enhances the dispersibility of the compound in water and other natural solvents. This is highly beneficial when blending it with ceramic or polymer networks and attempting to enhance their electrical and mechanical properties. Graphene oxide is one of such chemically modified graphene compounds reported to be very suitable for many different electrochemical applications.

1.1.3 Graphene Oxide

Graphene enriched by various oxygenated functional groups on its basal plane and at its edges give rise to a hybrid structure (blend of sp^2 and sp^3 hybridized carbon atoms) of graphene oxide (Kang et al. 2014, Mkhoyan et al. 2009). Oxidation of graphite can be done using powerful oxidizing agents, oxygenated functionalities are embedded inside the graphite structure. This oxidation leads to enlarged layer separation and makes the surface hydrophilic (Dreyer et al. 2010). Therefore with proper sonication, one can obtain the single or fewer layer graphene attached with oxygenated functionalities, called graphene oxide (GO). The properties of graphene oxide can be further altered by functionalization (Dobrota et al. 2016).

The chemically modified graphenes(CMG) are undeniably more versatile for applications (Erickson et al. 2010). Depending on the specific application, there are numerous methods by which graphene oxide can be functionalized (Olaniyan et al. 2016). In the perspective of supercapacitor applications, GO have less π-π stacking steadiness and poor conductivity and hence it is not suitable for the supercapacitor anode material (Dž et al. 2015). The functionalization of GO is thus necessary. Experimentally it's been seen that functionalized GO shows higher capacitance than unmodified GO (Gu and Fein 2015, Karthika 2012). However, in general, the graphene oxide is typically depicted as an electrical insulator as far as electrical conductivity is a concern. This is mainly because of the interruption of its sp^2 bonding networks (Ito et al. 2008). So the reduction of graphene oxide is required to recoup the honeycomb hexagonal lattice and hence to gain the electrical conductivity.

1.1.4 Reduced graphene oxide (rGO)

Reduced graphene oxide (rGO) is accomplished from graphene oxide(GO) through different reduction processes such as electrochemical, chemical, and thermal reduction. Although different reduction process has different benefits, the ultimate goal is the same, which is to remove the oxygen groups and fix the defects in GO to restore the long-range conjugated network which will help to improve the conductivity.

Recently, experimental reports show that the electrochemically reduced graphene oxide demonstrated the electronic conductivity values which are more than that of silver. There are methods by which we can functionalize reduced graphene oxide(rGO) to be utilized in applications like supercapacitor electrode materials (Dž et al. 2015).

1.2 Possible solutions for energy storage problem

The energy demand is increasing day by day whereas the availability of fossil fuels is rapidly declining. Therefore, on one hand, efficient production of clean energy from a sustainable source is very essential and on the other hand, technology needs to be developed that can efficiently convert and store energy. Innovative work of new energy storage materials and gadgets are therefore attracts global concern and expanding research intrigue. Batteries, fuel cells, and supercapacitors are the three most important technological devices that help to convert and store energy. Researchers are constantly attempting to improve the efficiency of these devices. There exist batteries where we can store a larger than average measure of energy. In the present scenario, there are several issues with energy storage devices. Batteries used for these purposes are exceptionally large, extremely dense, and the liberation of energy is very slow. On the other hand, capacitors have the ability to rapid charging and discharge, however, can hold very little energy compared tore batteries. High capacity batteries set aside charges for a longer period.

A customary capacitor is framed from two layers of conductive materials, the positive and negative charged terminals, set-apart by an insulator.

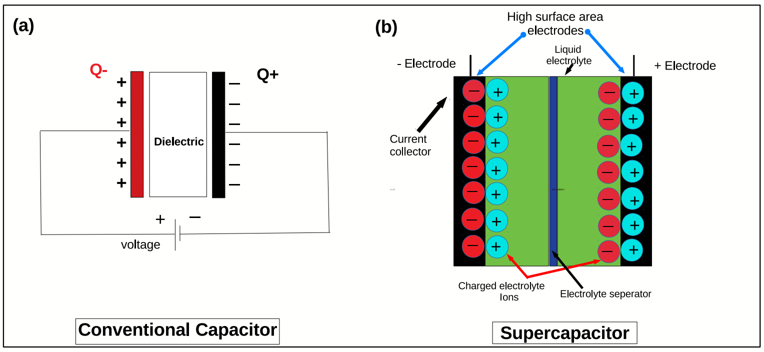
(a)
Q-
Q+
Dielectric
voltage
Conventional Capacitor
(b)
High surface area electrodes
Liquid electrolyte
- Electrode
+ Electrode
Current collector
Charged electrolyte Ions
Electrolyte seperator
Supercapacitor

Figure 1.1: Schematic diagram shows the differences between Conventional Capacitor(a) and Supercapacitor(b).

Supercapacitors are somewhat different from traditional capacitors, that they are not having a strong insulator between the electrodes. The two conductive electrodes in a cell are covered with a permeable material and the cells are immersed in an electrolyte solution as shown in Fig.[1.1]. The permeable material ideally will have a large surface area. The most commonly considered electrodes are carbon-based materials which have a large specific surface area with good electrical conductivity and stability (Huang et al. 2012, Hirunsit et al. 2016). Supercapacitors (are also called ultracapacitors) are, therefore, in this way appropriate as a substitution for electrochemical batteries in numerous commercial and business applications. In general supercapacitor, setup promises a high power density, long lifetime, good stability (Xu et al. 2019). It can store much more electrical energy than standardized capacitors. Also, supercapacitors can work at low temperatures; which is very useful in many circumstances where electrochemical batteries may stop working (Xu et al. 2019, Brousse et al. 2017). Nowadays the Transport sector predominantly depending upon supercapacitors. Furthermore, within a few years, we will start to decide on cell phones and other versatile electronic gadgets being fueled by supercapacitors. As a result, intense research on materials suitable for supercapacitor applications has recently gained the topmost priority.

1.2.1 Application of Ultracapacitors

- Industrial lasers, medical instrumentation.
- Electric vehicle.

- Wireless communication system for continuous service.
- In PCs, Railway, Cranes, Tractors, Buses, and so on.

Supercapacitors can temporarily store a large amount of electrical energy and release it when needed. However, their low energy density and high production cost are a hindrance to their progress (Wang et al. 2012). It is very essential to overcome these drawbacks to expand the use of supercapacitors. Intense research is going on to overcome the obstacle of low energy density by changing the electrode material of supercapacitors.

1.3 Supercapacitors based on graphene

Graphene-based supercapacitors have become important in recent years because of the low dimensionality and the insignificant production cost (Shim et al. 2011). Innovation in this area of supercapacitor research is expected to reach the market within a decade. Graphene is a remarkable two-dimensional carbon material that can be considered as a brilliant electrode for energy storage systems because of its high surface area, chemical steadiness, amazing electrical and thermal conductivity (Zhang et al. 2009). Compare to activated charcoal which is well known for electrode applications, graphene has a significantly larger surface area. Additionally, Graphene is lighter, being a fabric made from one single atomic layer of Carbon is environmentally friendly. Before the graphene era, researchers were able to make supercapacitors that can store 150 Farads for every gram. Graphene-based supercapacitor promises to increase this value to a multiple order.

Graphene has been tested in both supercapacitor and battery development (El-Kady et al. 2016). Graphene-based supercapacitors can supplant little batteries. Micro-supercapacitors might be effectively produced and incorporated into little gadgets like next-generation pacemakers. Graphene-based ultracapacitors would also be able to get charged at a higher rate compared to present-day lithium-ion batteries. They can last for a boundlessly more prominent length of time. The demand for innovative energy storage methods like supercapacitors will be increased in the upcoming years due to their effectiveness and less cost of manufacturing.

Two different factors determine the efficiency of supercapacitors namely the Quantum capacitance (C_Q) and double layer capacitance(C_{EDL}). Quantum capacitance (C_Q) plays a major role in a supercapacitor's overall capacitance.

1.3.1 Quantum capacitance (C_Q) of supercapacitor electrodes

Quantum Capacitance is characterized as the additional charge aggregated when a unit potential difference is applied between the electrodes. It is a material property that completely depends on the electronic configuration of the electrode materials. The origin of quantum impact is from the electron density confined near the Fermi energy (Kliros 2015). Quantum Capacitance can be varied by charging the electrode which will drive the electrons to accomplish higher energy levels. In this regard, two-dimensional material such as graphene can work exceptionally well in the devices as the quantum capacitance (C_Q) in these materials can be systematically improved.

1.3.2 Correlation and Quantum Capacitance

The variation in the electron chemical potential(μ) concerning the variation in carrier density leads to the origin of quantum capacitance(C_Q). The electron chemical potential(μ) relies legitimately upon the exchange-correlation energy functional. The correlation will change the density of states which intern influences the quantum capacitance of materials (Neilson et al. 2016). Therefore the estimation of Quantum Capacitance can be done through the density of states calculations incorporating a variety of fascinating many-body effects. Quantum Capacitance of the graphene base electrode materials is also identified from the electronic structure(DOS). There exist a non-zero minimum at the Dirac point. Charged impurities influence the value of C_Q with a linear increase on either side of the Dirac point. So the utilization of graphene inside the cutting-edge electronic gadgets, including supercapacitors, requires intentional control of the density of the charge carrier in the vicinity of the Dirac point. The usage of graphene within the next-generation electronics, including supercapacitors, requires careful control of the charge carrier density, Fermi energy, and Dirac point. This can be achieved through functionalization.

1.4 Functionalization of supercapacitor electrode materials

Electronic structures of materials can be often altered by introducing dopants, adding functional groups, and creating geometric as well as structural defects into the system (Paek et al. 2013, Rani and Jindal 2013). The effect of such chemical modification on the capacitor execution of graphene/electrolyte systems remains unexplored to a great extent, which needs further examination.

1.4.1 Functionalization of graphene with ad-atoms

The doping-induced change in the electronic structure of graphene and consequently the change on the electrode capacitance have been investigated recently by (Pak et al. 2014, Yu et al. 2013). Also, the impact of chemical modification of graphene-like electrodes on supercapacitor performance has been reported. Recently Zhan et al. (2015) examined the importance of quantum effects on the capacitance of electrode materials based on graphene. Their study content is on how quantum capacitance impacts their electrochemical performance. In most of the cases, it was observed that ad-atom functionalization on graphene leads to an enhancement of C_Q values. Marsden et al. (2015) have shown that nitrogen doping of graphene significantly improves quantum capacitance. Mousavi-Khoshdel et al. (2015) inspected the quantum capacitance of the Si-, S and P doped and co-doped with N on graphene-based supercapacitors. Their observation shows that co-doping significantly improves the quantum capacitance into the system.

Zhan et al. (2015) introduced a new DFT modeling technique to study the electrolyte/graphene interfaces and estimate the electric double layers (EDL) capacitance. The total capacitance of monolayer graphene mainly depends on the value of quantum capacitance. Vatamanu et al. (2015) reported a low-level total capacitance and energy density in an electric double layer (EDL) capacitor electrode materials due to an insufficient quantum capacitance. They have also shown that the electronic structure alterations that introduce the electronic density of states close to the Fermi energy, improve quantum capacitance of graphene electrodes, subsequently re-establishing the conducting property of those electrode materials. A significant difference in quantum capacitance observed when pristine graphene was doped nitrogen around the vacancy defects (Vatamanu et al. 2015). The interactions between graphene layers could lower quantum capacitances. This research paper recommends the probability to improve the graphene-based electrode quantum capacitance utilizing the combined impact of vacancy defects and functionalization. Hirunsit et al. (2016) examined the impact of graphene functionalization using adatoms like Al, B, N, and P. They have incorporated monovacancy and studied the impact on electronic structures and consequently on its quantum capacitance by applying DFT computations (Zhu et al. 2016, Taluja et al. 2016). They observed a considerable enhancement in electrode quantum capacitances due to functionalization when there exist vacancy defects (Chen et al. 2017). Song et al. (2018) explored the effect of functionalization on reduced graphene oxide to enhance quantum capacitance utilizing Density Functional Theory calculations. They also have tested graphene oxide as supercapacitor electrode materials.

1.4.2 Functionalization of graphene with molecular fragments

Lazar et al. (2013) analyzed the consequence of organic molecule functionalization on graphene electrodes both, experimentally and theoretically (Su et al. 2009). They have selected seven organic molecules such as acetonitrile, dichloromethane, hexane acetone, toluene, ethanol, and ester. They also have evaluated the strength of interactions between graphene and the organic molecules using DFT (De Oliveira and Miwa 2015).

Rubio-Pereda and Takeuchi (2013) introduced the DFT simulations for hydrogen-terminated graphene functionalized with organic molecules like acetylene, ethylene, etc. The outcomes are compared with the earlier study of similar doping processes on hydrogen-terminated silicon [111] surfaces and silicene.

Lonkar et al. (2015) explored the basic geometrical modification of graphene through chemical functionalization. It uncovers the different opportunities for tuning its structure; various chemical and physical functionalization techniques are investigated to hike the stabilization and modification of graphene.

During this survey, they revealed the ongoing advancement towards the chemical modification of graphene, including both covalent and non-covalent techniques, to be utilized in different applications (Milowska et al. 2013).

Majumdar (2016) investigated the functionalized-Graphene/Polyaniline nanocomposites as capable energy storage material. Polyaniline (PANI), with remarkable high electrical conductivity, doping/codoping properties, and high environmental stability, has likewise been explored in detail (Majumdar 2016).

Plachinda et al. (2017) has utilized first-principle computations to survey change in the electronic structure of atomic and molecular group functionalized graphene. They have used covalent functionalization with atomic and molecular groups like amines, PFPA, and epoxides. They demonstrated that this functionalization brings about a gap inside the bandstructure of graphene yet additionally gives rise to a decrease in electrical conductivity. They have also reported the impact of charge exchange on electron transport properties by calculating the charge exchange between the conjugated electrons in graphene and the functionalizing molecule (Stauber et al. 2017, Mirlin 2005).

Studies have been carried out by considering graphene, chemically modified graphene, and graphene-based composites as electrodes of supercapacitors Stoller et al. (2008), Tan et al. (2015). But the poor scalability, low yield, and expense lead to the search for other suitable supercapacitor electrode materials.

1.5 Molybdenum disulfide (MoS_2)

Graphene-like materials such as layered MoS_2 grabs significant attention in their application in this direction due to its ionic conductivity with minimal doping, large surface area, and high specific capacitance (Ke and Wang 2016, Jiang 2015). MoS_2 is a sandwich structure having two layers of S atoms and one layer of Mo atoms. These layers are interconnected by the force of Van der Waals. The separation between layers is about 0.65 nm. The carrier transport in MoS_2 mainly originates from the electron correlation between the Mo layers in the sandwich structure (Ahmad and Mukherjee 2014). This will enhance the energy density and power density of supercapacitors. Monolayer MoS_2 is having a large surface area, which is the essential requirement for a supercapacitor (Peng et al. 2014, Soon and Loh 2007). Superior electrical and electrochemical properties, various electronic states (semiconductor and metallic state), and mechanical flexibleness lead us to use layered MoS_2 as electrode materials for energy storage systems.

Kumar et al. (2015) explored the possibility of enhancing quantum capacitance by making a hybrid structure of graphene and MoS_2. Graphene is chemically unreactive and a gapless semimetal. Graphene and MoS_2 are two notable two-dimensional materials with a hybridized form that may provide interesting functional materials suitable for energy applications. Jiang (2015) *et al.* provides a short review on graphene versus MoS_2. Li and Zhu (2015) have studied preparation, properties, and applications of 2D MoS_2. Even though these 2D nanomaterials separately have a large importance in different applications, the mix of these materials could open another paradigm could play a key role in electrochemical energy storage and electronic gadget applications (Bissett et al. 2015). This encourages further investigation of graphene/MoS_2 heterostructures.

In 2007, Soon and Lohz investigated the double-layer electrochemical capacitance of nanowall MoS_2 film using electrochemical impedance spectroscopy. Through this work, they have shown that edge-aligned MoS_2 thin films can act as a supercapacitor at various current frequencies, which can be compared to a carbon nanotube array electrode. They also have found that ion diffusion at slow scanning speeds results in faradaic capacitance, which greatly improves the capacitance (Soon and Loh 2007). In 2013 Ma et.al reported a method to synthesize a polypyrrole/MoS_2 (PPy/MoS_2) nanocomposite as an innovative electrode material for efficient supercapacitors (Ma et al. 2013).

1.6 Hexagonal Boron Nitride

Hexagonal boron nitride (h-BN) is another material that can be separated into its two-dimensional form and could be suitable for energy storage applications. The structure of h-BN consists of three (BN) rings with alternate boron and nitrogen hexagonal structure. It is constructed from equivalent numbers of boron (B) and nitrogen (N) atoms. Two-dimensional h-BN is also called white graphene. Similar to graphene, h-BN is a honeycomb structure having sp^2 covalent bonds. Hexagonal boron nitride is a good dielectric material like graphite which is having high dielectric breakdown strength, good chemical, and thermal stability. h-BN is a 5 to 6eV broad bandgap semiconductor. h-BN is a material having various applications. Functionalized h-BN can be used as supercapacitor electrode materials (min Ding et al. 2016, Weng et al. 2016).

Albe *et al.* (1996) introduced the ab initio DFT-LDA and empirical simulation methods to figure the properties of various BN structures. Kaloni *et al.* (2011) considered the ground state properties of graphene and h-BN utilizing the pseudopotential plane-wave method utilizing DFT. They performed an LDA simulation with a (6×6×4) K-point mesh. Both LDA and GGA give the most exact outcomes in all the determined physical properties.

Ooi et al. have investigated the electronic and basic properties of h-BN using density functional theory calculations (Ooi et al. 2006). They utilized various exchange-correlation energy to ascertain the properties of this system. Min-Ding et al. reported that ad-atom doping techniques enhance the n-type conductivity in h-BN monolayers (min Ding et al. 2016). Cassabois et al. showed an exceptionally high thermal and chemical steadiness of the wide bandgap semiconductor h-BN that is utilized in gadgets working under outrageous conditions (Cassabois et al. 2016). The properties of h-BN monolayers have been contemplated utilizing first-principles calculationsmin Ding et al. (2016). An increase in the concentration of electrons and conductivity was observed in their study. These outcomes are important for improving the performance of h-BN based two-dimensional optoelectronic nanodevices. Weng et al. explored the functionalization of h-BN to introduce new properties and applicationsWeng et al. (2016). Dean *et al.* (2010) and Yankowitz et al. (2014) *et al.* reported that hexagonal boron nitride can be used as a substrate for high-quality graphene electronic devices. The recent studies encourage more careful investigations of the G/MoS_2 as well as G/h-BN heterostructure as the potential electrode material for supercapacitor applications (Bhauriyal et al. 2019).

1.7 Scope and Objectives of the Present Research Work

1.7.1 Scope

It is evident from the above discussion that per capita energy demand is increasing day by day in modern society and that creates a drastic rise in the demand for innovative energy storing systems. Hence the finding of relevant raw materials is inevitable for such applications. Numerous scientific studies have been shown that graphene and other two-dimensional materials are the most competent materials because of their unique and versatile characters related to the storage of energy. Therefore investigation of 2D materials as the electrodes for supercapacitors is more focused on modern scientific researches. On the other hand research in this field also have great scopes in many fundamental areas of applications such as wearable electronics, medical implanting, etc. Medical implants such as pacemakers, knee implants equipped with supercapacitors can receive energy from body heat and movements which can make them truly self-sufficient.

Supercapacitors have been started to use in much modern equipment such as robots, trains, and other vehicles, and in near future, it will be the essential parts of the renewable energy system, smart grids as well as mini-grids. Overall, from the current market trends, it is obvious that supercapacitors will have a much bright future and exponential growth is expected henceforward.

The existing literature in this area of research reveals that two-dimensional materials will be the best option for supercapacitors electrode (Bissett et al. 2015, Takahashi et al. 2014, Olaniyan et al. 2016). Computational simulations using DFT is an effective tool for the study of the electronic characteristics of the electrode materials (Iyakutti et al. 2015, Zhan et al. 2017). In DFT, the accuracy of the predicted properties strongly depends on the accuracy of the pseudopotential used in the simulation. In my research, I have developed a feasible route to estimate an accurate value of quantum capacitance in different materials. The main focus of my research was to find out suitable two-dimensional materials for supercapacitor electrode application. In this regard, I have studied the change in the electronic structure of differently functionalized two-dimensional materials and subsequently, the estimated change in quantum capacitance(C_Q). I have also attempted to investigate the effect of temperature and vacancy defects on the C_Q values (Fang et al. 2007, Kliros 2010) I have mainly considered three different two-dimensional materials in my work such as graphene, MoS_2, and h-BN. All there of these materials shows a negligible quantum capacitance in their pristine form. Therefore I have chemically modified them with different ad-atoms and functional groups and ligands and perform a detailed investigation of electronic structure and quantum capacitance behavior. In summary, the objectives of my proposed work are the following.

1.7.2 Objectives of the proposed Work

The main objective of this present work was to find suitable electrode materials with a very high quantum capacitance suitable for supercapacitor applications. In this regard, I had set the following goal in my Ph.D. research.

- To develop a suitable method to estimate an accurate quantum capacitance value of 2D materials.
- To study adatom adsorption, functionalization of graphene aiming at manipulating electronic and magnetic properties of the system to meet various requirements in carbon-based electronic device applications such as supercapacitors.
- Since the functionalization with molecular radicals introduces strong correlation into the system which intern may improve the quantum capacitance of graphene. Therefore one of my objectives in this thesis was to calculate the quantum capacitance of the molecular fragment/radical functionalized graphene-based supercapacitor electrodes.
- Dislocation in the graphene sheet incorporates strong charge localization which can improve the quantum capacitance in the system. Therefore my objective was to calculate the quantum capacitance in defected graphene with a variable degree of defects.
- Finally I would also like to see study other two-dimensional materials such as MoS_2, h-BN, etc for their application in supercapacitor electrode materials.

1.8 Organization of the Thesis

The rest of the thesis is organized as follows:

CHAPTER 2 presents a concise introduction of the computational approach relevant to the analysis of the electronic structure. In particular, Density Functional Theory and its application for quantum capacitance calculation have been thoroughly discussed.

In **CHAPTER 3**, I have discussed the ad-atom functionalization of graphene. The impact of n- and p-type doping, concentration dependence of doped atoms, the combinational effect of co-doping on graphene are systematically analyzed. The alteration in electronic bandstructure and density of states have been scrutinized using DFT calculations. The consequent change in quantum capacitance has been studied. To determine the origin of a large enhancement in C_Q and reasons for localization of ad-atom dominated density of states near Fermi energy(E_F), the charge re-distribution and charge transfer upon functionalization are analyzed. The temperature-dependent behavior of C_Q has been studied to understand the localization of states near the Fermi energy. This chapter also addresses the impact of vacancy defects/structural disorder in the electronic structure of pristine graphene. The last part of this chapter discusses the effect of vacancy defect concentration and the role of vacancy defect position in the graphene sublattice with variable degrees of defects on the C_Q value.

CHAPTER 4 explains our investigation of the molecule and radical functionalization of graphene for supercapacitor electrode applications. DFT calculations have been performed to analyze the electronic band structure of the functionalized graphene. This chapter is dedicated to the enhancement of quantum capacitance in graphene electrodes by chemical modifications utilizing non-covalent functionalization of graphene with different fragments of aliphatic and aromatic donor and acceptor molecules and their radicals. Overlap of atomic orbitals due to the covalent functionalization and charge transfer/redistribution has been estimated to have a microscopic understanding of related change.

CHAPTER 5 discusses quantum capacitance in the other two-dimensional materials like MoS_2 and h-BN. The semiconducting nature of MoS_2 gives rise to a lower level of C_Q which hinders it from supercapacitor applications. This chapter explains the substitutional doping of molybdenum and sulfur in MoS_2 monolayer and the impact of vacancy defects, which leads to the electronic bandstructure modification. I have analyzed the ad-atom functionalized h-BN structure for supercapacitor electrode applications.

Finally, **CHAPTER 6** is devoted to the conclusion drawn from all the investigations carried out on two-dimensional materials and summarizes the findings of the present research work by highlighting the important results of the thesis. This chapter also comprises the scope for further research work in the area.

Chapter 2

Methodology

This chapter will mainly focus on the theoretical foundation for calculating quantum capacitance in the system. Since the calculation of the quantum capacitance in materials is truly a many-body problem and information of the electronic structure is an essential part to understand these properties of the material. Therefore I shall first briefly discuss the salient feature of the many-body theory. Subsequently, I shall discuss how to use this theory to obtain the electronic structure information and finally, I shall discuss the procedure for quantum capacitance calculation in detail.

2.1 Many-body Interacting Electron Problem

The many-body problem is an overall name for a large class of physical problems relating to the properties of infinitesimal frameworks created from a larger than the average number(in the range of 3 to infinity) of collaborating particles (Yeh 2008). This kind of quantum framework has a large number of collaborations between particles that offer ascent to quantum connections, or on the other hand entrapment. As an outcome, the wave function of the framework might be a confounded object holding a lot of data, which for the most part makes diagnostic counts a complicated one. Consequently, many-body hypothetical material science most frequently depends on a set of approximations specific to the current issue.

The Schrödinger differential equation,

$$\hat{H}\psi(r_1, r_2, ..., r_n) = E\psi(r_1, r_2, ..., r_n),$$

is unquestionably a work of genius that supported the very origin of material science. Unfortunately, the condition is useful by and by only for the easiest frameworks because of the hidden difficulties of the many-body quantum impact (Neilson et al. 2016). It is being heard that first- principles techniques require just one information, the atomic number, and nothing else for the count. This is regularly evident in principle, yet the fact of the matter is not as basic as the announcement sounds. The explanation is that the wave equation of a many body interacting electron problem is a function that relies upon the 3n coordinates of n electrons. Regardless of whether we knew an approach to do such an estimation, a personal computer(PC) that can deal with such a gigantic undertaking isn't accessible. This may be true in the future regardless of how fast PCs are.

There are a number of approximations available to determine the electronic ground state of many-electron frameworks. Some of the different methodologies are:

- Exact diagonalization
- Many-body perturbation theory
- Hartree-Fock method
- Quantum Monte Carlo
- Density Functional Theory.

The Hartree–Fock (HF) strategy had the option to facilitate the estimation of ground state energy keeping up the parameter-free nature, by presenting the wave function as Slater determinant and the mean-field approximation (Sherrill 2000).

However, because of the computational heaviness, applications of this method is being confined to little systems with atoms of a few tens or less, which are far away from the system of materials. Eventually, the improvement happened when Hohenberg and Kohn in 1964 have presented two hypotheses concerning electron density and energy functionals. Kohn and Sham (1965) thought of a rare plan called the density functional theory (DFT). Thus one can have the simplest definition of DFT because it could be a strategy for acquiring an estimated answer for the Schrödinger condition of a many-body framework.

2.2 Density Functional Theory (DFT)

DFT is a computational quantum mechanical procedure utilized in physics, chemistry, and material science to study essentially the ground state electronic structure of many-body frameworks, explicitly atoms, molecules, and the condensed phases (Zeng et al. 2012). In this hypothesis, we first express the full Hamiltonian as different components which are functions of electron density. The properties of a many-electron framework will be dictated by solving this Hamiltonian. Since electron density is a function of electron's positions, the overall energy becomes a function of another function, which is called the functionals. The utilization of functionals of the electron density leads to the name DFT. Density functional theory is one of the first well-known and adaptable methods accessible in computational physical science, and chemistry.

DFT has been exceptionally mainstream for computations in physical science since the 1970s. Nevertheless, density functional theory wasn't viewed as precise enough in the field of quantum science before the 1990s, when the guesstimate used in the hypothesis have been incredibly fine-tuned to better model the exchange and correlation(XC) interactions. Computing expenses are quite low when contrasted with conventional techniques, similar to exchange only the Hartree-Fock hypothesis. DFT includes its theoretical origins inside the Thomas-Fermi model. The Kohn and Sham methodology utilized the density of electron as the principal variable to take care of the n-electron issue. This new approach fundamentally changed the matter of 3n-dimensional to n separate three dimensions by using the density of electrons. In this way, there is no individual electron, however, as it was a 3-dimensional density of electrons, ρ(x, y, z). So now the quantum mechanical framework is an electron density subordinate issue. This may lessen the computational efforts. Moreover, the skipped correlation energy inside the HF technique is explained by guess, is also included here, and hence, all essential energy terms are available inside the DFT. The electron densityρ(r) determines all details in an electron quantum framework in its ground state. Let us initially characterize electron density, the key participant inside the DFT. Furthermore, we move on to the two assumptions that form the basis of DFT.

If we construct the squared wave functions at one spot, it will fabricate the density of electrons at that specific point per unit volume (ρ(r)) in an n-electron framework. The system groundstate electron density not just gives data about wave function and the complete number of electrons, yet is moreover straightforwardly connected with energies, and accordingly all other properties.

2.2.1 Hohenberg-Kohn Theorems

DFT is made conceivable by the presence of two keenly straightforward hypotheses suggested and demonstrated by Hohenberg and Kohn in 1964 (Superzeure1964). Researchers knew that the density of electrons might play a conclusive job in electronic structure estimations. It had been exposed to formal check at last when Hohenberg and Kohn(H-K) in 1964 demonstrated it with two hypotheses. The hypotheses in this manner clarified the relations between electron density, external energy, and wave function.

Theorem I

The primary Hohenberg-Kohn hypothesis demonstrates that the properties of the ground state of a many-electron framework are particularly dictated by the density of electrons which relies upon just three space co-ordinates. It lays the foundation for decreasing the issue of many-body of N electrons with spatial coordinates of 3N to three space co-ordinates, through the use of electron density functionals.

For any arrangement of interacting particles within an external potential $V_{ext}(r)$, the density is particularly determined(i.e., the external potential might be a unique function of the density).

$$\hat{H} = -\frac{1}{2}\sum_{i}^{N}\nabla_i^2 + \hat{V}_{ext} + \sum_{i<j}^{N}\frac{1}{\mid r_i - r_j \mid} \tag{2.1}$$

where the first and the last terms are electronic kinetic energy(K.E) and electron-electron interaction potential respectively. The external potential, $\hat{V}_{ext}$ represents the amount of the interaction between electron and nuclei. The interaction energy of the external potential can be explained as:

$$V_{ext}[\rho] = \int \hat{V}_{ext}\rho(r)dr \tag{2.2}$$

The number of electrons presents inside the framework will be obtained by the integral of the electron densities.

$$\int \rho(r) = N \tag{2.3}$$

It is obvious that nucleus-electron densities are very limited near the nucleus, and the valence electrons are somewhat diffused around. Therefore there will be an immediate relation between the density of the electrons and the outside potential. The term external in the V_{ext} shows that, from the electron's perspective, the interaction from the nucleus is external and therefore system dependent. The internal potential independent of the system (the electronic K.E. and the electron-electron interaction energy) is free from such external potential (Aikebaier et al. 2015). We can now write the electronic total energy functional as:

$$E[\rho] = T[\rho] + V_{ext}[\rho] + V_{ee}[\rho] \tag{2.4}$$

In this way for an N electron framework, the first theorem is often summed up as:

1. The density of electrons only can characterize the outer potential and vice versa for any given framework is in the ground state.

2. Since the kinetic energy of the electrons is framework independent and doesn't depend on the external potential, a density-dependent kinetic energy term ought to be there as a universal functional while the external potential differs from one framework to another relying upon the sort of nuclei.

3. Distinctive Hamiltonians contrast in their outer possibilities, that is their external potentials.

4. Along these lines the electron density decides external potential, accordingly the Hamiltonian, wave function, and all the ground-state properties of the framework.

Various external potentials will constantly offer ascent to different electron densities. Furthermore, if we limit our curiosity only to the properties of the ground-state of a framework, at that point the electron density at any external potential decides the overall energy and other properties of the framework.

Theorem II

A universal functional for the energy E[n] will be characterized regarding the density. The specific ground state is that the overall minimal estimate of this functional. This theorem builds up variational for the energy in terms of electron density. The second H-K hypothesis presented energy functional for the framework and shows that the correct density of electrons in the ground-state minimizes this energy functional.

This hypothesis recognized how to locate the minimum energy of a framework. It has been demonstrated that the ground state of a framework can be examined utilizing the principle of variation. If we minimize the energy of the framework at a certain V_{ext}, with varying electron density, at that point we will arrive at the ground state of the energy level. This is often referred to as the variational principle within the DFT structure, and in this manner, the electron density which minimizes the energy of the system is the ground-state electron density, ρ_0.

$$E[\rho(r)] = E_h[\rho(r)] + E_{ext}[\rho(r)] \geq E_{gs} \tag{2.5}$$

where E_h represents the one-electron Hamiltonian. The idea offers us an incredible strategy for finding the ground-state energy and different properties. We furnished with both electron density and variational principle for the search and may begin calculating for the energy from any known guess in density. DFT was set on a firm hypothetical balance using both Hohenberg-Kohn hypotheses (H-K).

Kohn-Sham Approach

In Kohn-Sham DFT (KS-DFT), the complex issue of electrons interacting during a static external potential is diminished to a manageable problem of electrons not interacting moving into an effective potential (Aikebaier et al. 2015). The effective potential comprises the outer potential and the exchange and correlation interaction impacts. Modeling the last two potential terms is the most troublesome task, one needs to approximate these energies. The local density approximation (LDA) the simplest approximation, which is based upon the precise exchange energy for a uniform electron gas. Non-interacting frameworks are generally simply because the wavefunction will be shown as a Slater determinant of orbitals. In addition, the K.E. functional of such a framework is seen precisely. We have to apply some approximation in the exchange-correlation portion of the total energy functional which stays obscure. Based on the two hypotheses of Hohenberg and Kohn, Kohn and Sham in 1965 formed an imaginary framework, which is of one-electron in nature. This approach is outlined in the following sections.

$$\hat{H} = -\frac{1}{2}\sum_{i}^{N} \nabla_i^2 + \hat{V}_{ext} + \sum_{i<j}^{N} \frac{1}{| r_i - r_j |} \tag{2.6}$$

In the Hamiltonian, the last term gives the electron-electron connection where the summation covers up all situations where $i \neq j$ to avoid the self-connection. Significant trouble lies during this final term, the interrelated interaction among all n electrons. As the final term incorporates different interactions that are hard to be solved, Kohn and Sham (1965) took an alternate route around this issue. In the case of an interacting system, the full energy functional is often expressed as

$$E[\rho] = T_s[\rho] + V_{ext}[\rho] + V_H[\rho] + E_{xc}[\rho] \tag{2.7}$$

where T_s is that the true K.E functional, V_{ext} is that the external potential, V_H is the Hartree potential and E_{xc} is that the exchange-correlation energy. The last term E_{xc} is difficult to calculate accurately because it involves multielectron interactions. The solution of the above equation is additionally difficult to get due to this term. Since the variational principle allows us to urge the charge density from any coordinate system, the only requirement is that charge density should minimize the above total energy functional. Kohn and Sham first calculated the charge density from a non-interacting system

$$\Sigma_i[-\frac{1}{2}\nabla_i^2 + V_{eff}]\psi_i = \varepsilon_i \psi_i \tag{2.8}$$

assuming that each electron is getting an effective potential V_{eff}. Then he used this density and apply the variational principle to calculate the ground state energy of the specific framework.

2.2.2 Kohn–Sham(KS) equations

In this segment, we are going to discover the energetic functionals and their derivatives with reference to the density of the electrons to find the ultimate KS equations. First of all, we have to show each in terms of the density of electrons, then we should find the derivative relative to it.

Kinetic energy :

In this arrangement of non-interacting decoupled co-ordinates, the electronic density can be written as a straightforward sum over a group of squared non-interacting orbitals ϕ_i called KS orbitals:

$$\rho(r) = \sum_i^N |\phi_i|^2 \tag{2.9}$$

The development of the electronic density can be done accurately from a gathering of orbitals and it can be made from an asymmetric wavefunction. The K.E and the density of electrons are specifically known from the orbitals ϕ_i.

$T_{ks}[\rho] = \frac{1}{2}\sum_i^N \langle \phi_i \mid \nabla^2 \mid \phi_i \rangle$

This non-interfacing K.E. represents a considerable amount of the entire kinetic energy, and the neglected interacting K.E. is incorporated inside the XC expression, E_{xc}.

External energy :

As we examined already, the external potential, $V_{ext}(r)$, originates from the interaction between an electron and other nuclei. In this case, the external energy, $E_{ext}[\rho(r)]$ is a functional that involves a function of $\rho(r)$, that could progressively be a r functionality(electronic co-ordinates). This means that a functional accepts a function as an input and yields a number. External energy is therefore represented in terms of electron density as the single variable.

Hartree energy :

The interaction between the electrons is given by the Coulomb potential. Each electron moves freely of each other, just experiencing the typical electric field because of all the contrary electrons in addition to the field because of the atoms. That is, the starting point of the potential is the electron density dispersion and ionic lattice yet ignores exchange and correlation impacts. With highly non-interacting charge distribution, the Hartree potential is due to the interaction between an electron at position r and the average density of the electrons at r' out of an approximation of the mean-field:

$$V_H(r) = \int \frac{\rho(r')}{|\vec{r} - \vec{r'}|} dr' \tag{2.10}$$

This condition calls for the calculation of an integral part of r' for assessing Hartree's potential at r. As far as this potential is concerned, Hartree's energy is often shown as an expectation value,

$$E_H[\rho(r)] = \int V_H(r)\rho(r)dr = \frac{1}{2}\int\int \frac{\rho(r)\rho(r')}{|\vec{r} - \vec{r'}|} drdr' \tag{2.11}$$

Here we have expressed the non-interacting Hartree energy as a functional of electron density.

Exchange-Correlation(XC) energy (E_{xc}) :

Exchange-Correlation(XC) energy is exclusively the aggregate of the error committed while employing a non-interacting K.E. and the classical treatment of the interaction between electrons. The exchange-correlation energy comprises two energies: E_x is the energy of exchange that is between electrons having identical spin, and E_c is the energy of correlation that is between electrons with an alternative spin.

Exchange energy, E_x is identified by the Pauli exclusion principle, which is connected to the nature of antisymmetric electron waves. On the opposite side, two electrons with various spins can possess identical orbital. An electron in one position r will cause the approach of another electron at that position difficult. Those electrons are repelled by these electrons, too. This is due to the identical negative charges they hold. It can be termed as the electronic correlation effect. This electron correlation makes a reduced electron density around the electron thus creating a little attractive energy. This can be named a correlation hole.

This is the obscure n-electron impact that has not been considered in the Hartree-Fock strategy. Therefore we have to apply some approximations to resolve this issue.

Thus we have got the variation with respect to density:

$$\frac{\delta E[\rho(r)]}{\delta\rho(r)} = \frac{\delta T_{ks}[\rho(r)]}{\delta\rho(r)} + V_{ext} + \int \frac{\rho(r')}{|\vec{r}-\vec{r'}|}dr' + \frac{\delta E_{xc}^{new}[\rho(r)]}{\rho(r)} \tag{2.12}$$

where

$$E_{xc}^{new} = E_{xc} + T_s - T_{ks}$$

It demonstrates that the DFT, at last, encloses all terms of energy, leads in the most minimal curve, and approaches near the exact value.
The computation method is as follows and shown in Fig.[2.1].

2.2.3 Calculation procedure for Kohn-Sham equation :

1. Guess an initial charge density $\rho(r)$.
2. Determine the effective potential V_{eff}.
3. Put this effective potential V_{eff} in Kohn-Sham equation and acquire a brand new charge density.
4. With this charge density, evaluate the energy of the single-particle framework.
5. Ascertain the ground state energy of the framework.
6. Ascertain the entire energy functional E [$\rho(\vec{r})$].
7. Compare the energies acquired in stage 5 and stage 3. If they're equivalent, this energy is the ground state energy, otherwise, head to the next step.

8. Evaluate V_{eff} with the new charge density and repeat steps from 3 to 7.

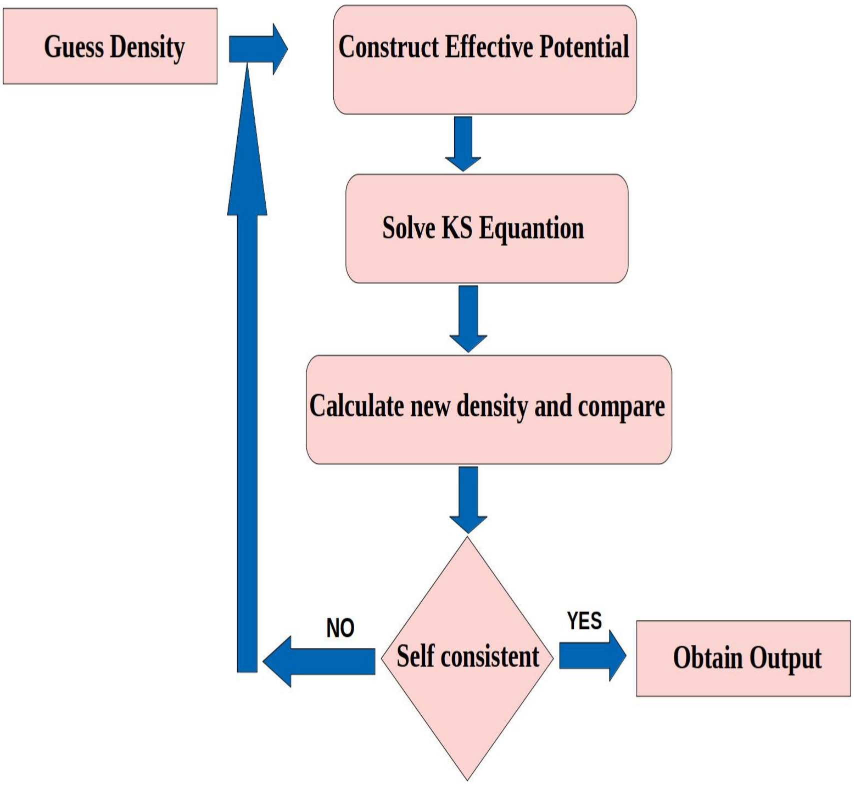
Guess Density
Construct Effective Potential
Solve KS Equantion
Calculate new density and compare
NO
Self consistent
YES
Obtain Output

Figure 2.1: (color online)A flow chart of the Kohn-Sham iteration scheme.

2.2.4 Estimation of Exchange-Correlation(XC) energy

The core of the Density Functional Calculation is the elucidation of the Kohn-Sham equation. As described earlier, here the system is taken into account to be made of non-interacting electrons. And therefore, the neglected part of the K.E. term is going to be included within the exchange-correlation functional.

The electronic ground state issue might be solved if the electron density is given and the properties can be determined using the Kohn-Sham equations. The selection of excellent XC functional figures out what proportion error is involved within the DFT calculations. Therefore the perfection of DFT simulation depends mainly on the accurate XC energy which we have selected.

There are various XC functionals accessible with different exactnesses and computational expenses. DFT precision improves when a more specific depiction of the XC energy is given. The three typical functionals which are used usually are Local Density Approximation(LDA), Generalised Gradient Approximation(GGA), and hybrid functionals. In local density approximation[LDA], the whole system is split into numerous bits of uniform electron density. At this point, the exchange-correlation energy for every electron with the electron density which is expected to be consistent within this piece is determined. Finally, the energies associated with the electrons in the different pieces are calculated and added up to get the total energy. The LDA calculation works perfectly only within the limit of homogeneous electron gas or frameworks within which charge density varies relatively slowly like in metals. There are drawbacks to Local Density Approximations like they overestimate cohesive energy and modulus of elasticity of the solids. It calculates band gaps that are smaller (eg: Silicon) or maybe no gap(eg: Germanium). It can not depict transition metal and its oxides. Real systems do not appear to be homogeneous. Consequently, its electron density will not be uniform. It will be different. Therefore the rate of this variation must even be incorporated. The approximation method which considers the variation is that the Generalised Gradient Approximation (GGA) (Perdew et al. 1997). Numerous alternative styles of GGA are proposed and therefore the mainstream possibilities are PBE, PW91, and Perdew and Wang(1992) (Perdew et al. 1996). Pseudopotential documents incorporate these GGA or LDA functionals. PW91 has been widely used in applications to a huge set of materials as a result of its sensible precision. The PBE incorporates features like local electron density, gradient, and second-order gradient. GGA functions admirably with most frameworks giving the system properties inside a 1% to 3% inaccuracy. Generalized Gradient Approximation ascertains bandgap more precisely than Local Density Approximation. There are improved functionals like meta-GGA, hybrid functional like B3LYP, etc., which have better precision.

2.3 Quantum capacitance of a Supercapacitor cell

The accurate electronic structure of the materials enables us to predict the quantum capacitance of the system. The total capacitance of a Supercapacitor cell comprises of two nonparallel capacitances, the quantum capacitance C_Q and the double layer capacitance C_{EDL}, which are related to the following equation.

$$1/C_{Total} = 1/C_Q + 1/C_{EDL} \tag{2.13}$$

The entire charge in the electrode material is in proportion to the weighted sum of the electronic DOS up to Fermi energy (E_F). In this manner, when the DOS is understood, the C_Q of an electrode at a particular temperature can be easily determined (Mousavi-Khoshdel et al. 2015). C_Q has a predominant job in the overall capacitance of the monolayer graphene. The quantum capacitance value diminishes as the number of graphene layers increments. Quantum capacitance (C_Q) is dependent upon the electronic structure of materials, and the double layer capacitance (C_{EDL}) is dependent upon the electrode-electrolyte interfacial structure.

Analytical solution for quantum capacitance,

$$C_Q = e^2 g_s g_v \frac{2e|\phi_G|}{\pi(\hbar V_F)^2} \tag{2.14}$$

where,

$$\frac{2e|\phi_G|}{\pi(\hbar V_F)^2} = D(E) \tag{2.15}$$

$$e|\phi_G| = E_F \tag{2.16}$$

Where the g_s & g_v represents the spin and the valley degeneracy respectively. Chemical modification leads to a broken sublattice symmetry, which will alter the valley degeneracy in two-dimensional structure. Therefore g_v is very difficult to calculate in functionalized systems. So the analytical solution is very difficult to attain. This problem can be accomplished through DFT calculations.

Quantum capacitance is given by,

$$C_Q = \frac{\Delta Q}{\Delta \phi} \tag{2.17}$$

Where ΔQ is the variation of charge thickness, $\Delta\phi$ is the local potential applied.

Excess charge density on the electrode is given by,

$$Q = e\int_{-\infty}^{+\infty} n(E)[f_e(E) - f_e(E - e\phi)]dE \tag{2.18}$$

in which n(E) is the electronic DOS,

$$f_e(E) = \frac{1}{e^{(\frac{E}{k_B T})} + 1} \tag{2.19}$$

is the distribution function of Fermi-Dirac, E is the relative energy as far as the Fermi level is concerned. Note that the quantum capacitance is directly dependent upon the density of states of electron D(E) and the Fermi−Dirac distribution function f(E).

Derivative of (2.19) with respect to ϕ and using the hyperbolic functions (2.20) and (2.21),

$$sech(x) = 2e^x/(e^{2x} + 1) \tag{2.20}$$

$$sech^2(x) = 4e^{2x}/(e^{2x} + 1)^2 \tag{2.21}$$

we will get (2.22), where β = 1/(KT)

$$\frac{\partial f(E - e\phi)}{\partial \phi} = e\beta/4 sech^2 \beta(E - e\phi)/2 \tag{2.22}$$

Derivative of 2.18 with respect to ϕ using 2.22, we will get

$$C_Q = e^2\beta/4\int_{-\infty}^{+\infty} D(E) sech^2(\beta(E - e\phi)/2)dE \tag{2.23}$$

Finally,

Quantum Capacitance(C_Q)

$$C_Q = \frac{dQ}{d\phi} = \frac{e^2}{4kT}\int_{-\infty}^{+\infty} D(E) sech^2\left(\frac{E - e\phi}{2kT}\right)dE \tag{2.24}$$

Here extra charge is given by Q and electronic charge $(1.6 \times 10^{-19}C)$ is given by e. In this manner, we have assessed the C_Q for all the framework from the density of states (Zhan et al. 2015) which can be calculated from DFT (Bhushan and Srivastava 2018).

Thermal Broadening function

$$F_T(E - e\phi) = 1/(4KT)sech^2((E - e\phi)/2KT) \tag{2.25}$$

Modification of electronic bandstructure is possible through substitutional dopants, functional groups, and structural disorders. The impact of such chemical modifications on the capacitor performance remains undiscovered, which needs further examination.

2.4 Simulation methods

We have performed plane wave-based density functional theory calculations utilizing the Vienna Ab-initio Simulation Package(VASP) (Kresse and Furthmüller 1996a,b). The projected augmented wave method was utilized to optimize the geometric structure of the functionalized 2D materials (Blöchl 1994a). The exchange-correlation energy functionals were approximated utilizing generalized gradient approximation with PBE parametrization (Perdew et al. 1996, 1997, Vanderbilt 2006). We have considered 10^{-6}H tolerance in total energy in electronic self-consistency. Inter-atomic forces were obtained using the Hellmann-Feynman theorem and subsequently reduced by moving atoms using a conjugate gradient algorithm to obtain the optimum geometry. The process continued until all inter-atomic forces were reduced to 0.01 eV/Å. A sufficiently large plane-wave kinetic energy cut-off (>400eV) was utilized in each one of our calculations for accurate outcomes. An adequately enormous vacuum has been considered along the out of the plane direction of the 2D structure unit cells (height>10Å) to evade the association with periodic images.

In order to examine the consequences of various adatom functionalization on the quantum capacitance, calculations were done utilizing supercells of respective 2D materials. The impact of dislocations was studied on a larger supercell of the planer structure and by removing few atoms randomly from it. In order to accommodate molecular fragments and their radicals on the 2D surface, we generated large supercells and placed one fragment inside it so that the fragments are separated by at least 5 Å from each other in the periodic cells. We have removed one hydrogen atom from the molecule to form radicals. The correction due to the vdW interactions is also considered in these types of calculations.

We have used a Γ point pack of k-point mesh to sample the Brillouin zone for geometry optimization. A denser k-point grid was utilized for the precise extraction of electron density of states D(E) and atom projected density of states(PDOS).

The stability of the functionalized structure was investigated by estimating average adsorption energy E_{ad} for ad-atoms using

$$E_{ad} = \frac{1}{n}[E_{tot} - E_{gr} - nE_{at}] \tag{2.26}$$

where E_{tot} is the total energy of the functionalized graphene unit cell, E_{gr} is the total energy of pristine graphene in the same unit cell, E_{at} is the per atom energy of the ad-atom and n represents the number of ad-atoms present in the unit cell (Xu et al. 2020).

The quantum capacitance of the materials can be seen as the rate of change of excessive charges(ions) with respect to the change in applied potential (Xia et al. 2009). Therefore, it is directly related to the electronic energy configuration of the electrode materials and can be defined as the derivative of the net charge on the substrate/electrode with respect to electrostatic potential. The total charge is proportional to the weighted sum of the electronic density of states up to the Fermi level E_F (Dröscher et al. 2010). Therefore, when the density of states (DOS) is known, the quantum capacitance C_Q of a channel at finite temperature can be calculated as equation(1) (Mousavi-Khoshdel et al. 2015).

The expression for quantum capacitance was obtained as,

$$C_Q = \frac{e^2}{4kT} \int_{-\infty}^{+\infty} D(E) Sech^2 \left(\frac{E - e\phi}{2kT} \right) dE \tag{2.27}$$

Therefore, when the density of states (DOS) is known, the quantum capacitance C_Q of a channel at a finite temperature T can be calculated from equation (2.27).

The DOS profiles extracted using the VASP package have been processed through MATLAB programming to obtain quantum capacitance. and we have analyzed the charge transferred in functionalized 2D systems by using Bader charge analysis.

Chapter 3

Enhancement of Quantum Capacitance by Ad-atom Functionalization of Graphene Supercapacitor Electrodes.

3.1 Introduction

Functionalization alters the electronic structure of graphene. Dirac cones get reshaped due to strong interactions which change the electronic density near the Fermi energy, and consequently, the quantum capacitance (C_Q) get modified (Elias et al. 2011, Ito et al. 2008, Cities 2016). The density of state near the Fermi level for a given material can be tuned by means of an efficient chemical modification of the system using external ad-atoms or creating defects (Iyakutti et al. 2015, Mukherjee and Kaloni 2012). This is also an effective way to control the type and concentration of charge carriers in the system. The electronic energy levels of the parent material may also be modified/shift in these process (Sun et al. 2015). The change in an electronic structure depends on dopant type, concentration, and doped position in the sublattice (Li et al. 2018, Bottari et al. 2017).

3.2 Methodology

It is evident from the expression of C_Q in equation (2.27) that the quantum capacitance is directly proportional to the density of state present near the Fermi energy. Since $(E - e\phi)$ represents the energy with respect to Fermi level and $sech^2(x)$ rapidly goes to zero for $|x| > 0$, the states which are energetically far from the E_F are not contribute much on C_Q. Hence, it is important to understand the proper change in electronic structure upon ad-atom functionalization (Dimakis et al. 2017, Marsden et al. 2015, Sun and Peng 2014). To start with, I, therefore, have studied the change in the electronic structure of the functionalized graphene with various ad-atoms. Subsequently, I have calculated the total quantum capacitance and identified the most favorable ad-atoms for maximum enhancement of C_Q. In the second stage, I have performed a similar study by varying the doping concentration of the favorable ad-atoms as well as the combinational effect of co-doping on graphene. Finally, I extend my investigation by considering defected graphene structure (Mukherjee and Kaloni 2012, Xu et al. 2019).

In order to explore the impact of various adatom functionalization on the quantum capacitance, calculations were done using $3\times3\times1$ supercells of graphene unit cell, having 18 carbon atoms of the graphene sheet (G18) with one functional group. The vacancy defected configurations were realized on a $5\times5\times1$ supercell of graphene unit cell (50 C atoms of graphene, G50) with a variable concentration of vacancy in the range from 2 to 8 percent. A sufficiently large vacuum has been considered along the out of the plane direction of the graphene sheet (height$>$10Å) to avoid the interaction with periodic images. I have used a $6\times6\times1$ Γ point pack of k-point mesh to sample the Brillouin zone for geometry optimization with 10^{-6}H tolerance in total energy for convergence. A denser $24\times24\times1$ k-point grid was used for the precise extraction of electron density of states D(E) and atom projected density of states(PDOS). I, therefore, have estimated the C_Q using the equation (2.27) for all the system form the density of states obtained from DFT calculations.

3.3 C_Q in pristine Graphene

The geometric structure of graphene is a hexagonal honeycomb lattice having sp^2 hybridized carbon atoms as shown in Fig.[3.1]. The hexagonal ring is comprised of two perfectly equivalent triangular sublattices. The formation of sp^2 hybridization in graphene is between the 2s and 2p outer-shell orbital electrons. There is a formation of three sp^2 hybridized orbitals is from three of the four outer-shell electrons, that is a blend of orbitals s, px, and py. Carbon atoms in the graphene are associated with its three closest neighbor atoms through a σ-bond. The length of these bonds is about 0.142 nanometers. The leftover p$_z$ outer-shell orbital is oriented perpendicularly to the plane, form two half-filled bands, π, and π^*. These bands are liable for the vast majority of graphene's outstanding electronic properties. Long-range π-conjugation in graphene modifies the elementary character, yields exceptional thermal, mechanical, and electrical properties, which have for quite some time been the enthusiasm for numerous theoretical physicists.

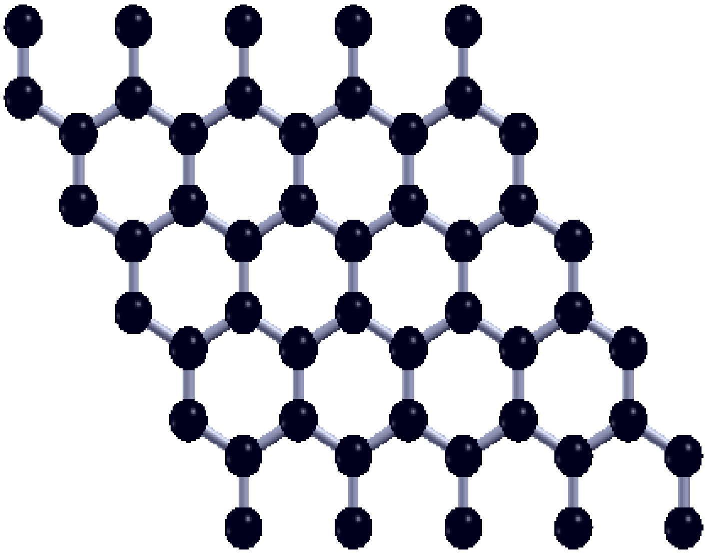

Figure 3.1: (colour online)Optimized geometric structure for pristine graphene. Black ball represents Carbon atom.

Pristine graphene is semimetallic, whose properties incorporate electron-electron interactions in its honeycomb lattice (Aikebaier et al. 2015, Kotov et al. 2012). It does not have a bandgap unlike the band structure of semiconductors and insulators as shown in Fig.[3.2]. The electron-filled valence band and the vacant conduction band in graphene are continuous in nature. Graphene is having a linear dispersion in its electronic bandstructure. These two bands are depicted by two cones called Dirac cones whose intersecting point is the unique feature of graphene called the Dirac point. There exist a zero density of states and no bandgap at the Dirac point as shown in Fig.[3.2].

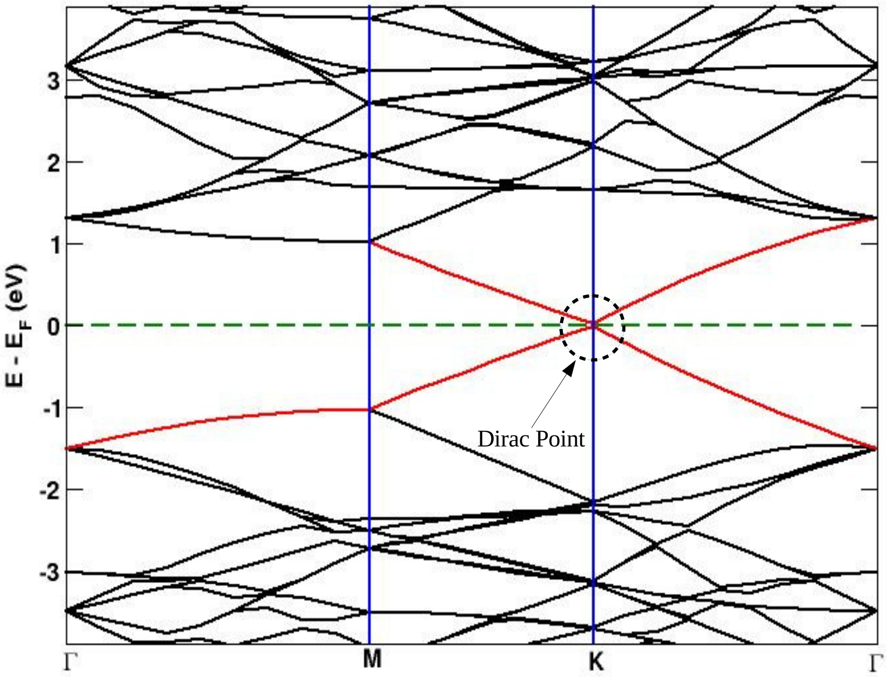

Figure 3.2: Electronic band structure for pristine graphene. Horizontal green dashed line is the Fermi energy set at E=0. Dirac point is encircled in the bandstructure.

These unique characteristics indicate that the graphene charge carriers are acting like massless electrons whose mobility is extremely high at the Fermi level. Charge transporters can travel sub-micrometer distances without scattering (Xia 2010). The graphene electronic properties can be modified by the method of functionalization, which will alter the electronic behavior and this may give rise to some of the interesting properties (Plachinda et al. 2017).

Since the availablity of the DOS near the Fermi-level is less, the quantum capacitance in pristine graphene is very low as shown in Fig.3.3.

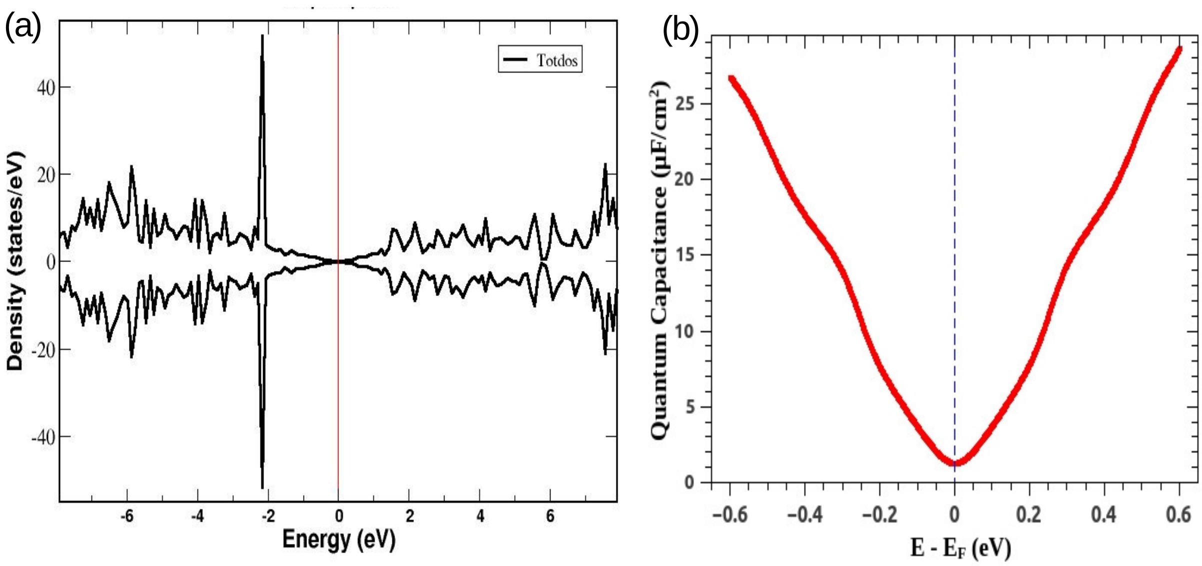

Figure 3.3: (a)Electronic density of states and (b) Quantum capacitance value for pristine graphene. Vertical red and blue line is the Fermi energy set at E=0.

3.4 Functionalization of graphene with ad-atoms

The type and concentration of charge carriers in graphene can be controlled effectively by functionalization (Pumera 2014). The carrier density at the band edges varies with dopant types and concentration (Fujimoto 2015). In this study, I have considered atoms from different groups in the periodic table with increasing order of electronegativity such as K< Na< Al< P< N< Cl, to functionalize the graphene (Nakada and Ishii 2011, Bouša et al. 2016). There are three different absorption sites for an ad-atom to sit on the graphene lattice, namely the top(on vertically top of the graphene C atoms) hollow (at the center of the hexagon in the sheet), and bridge site (in between two graphene C atoms). The most stable adsorption position of ad-atoms on graphene was found by comparing the ground state energies (Kang et al. 2014, Marsden et al. 2015). The hollow position was found to be the most favorable position for ad-atoms like K, Na, Al, bridge position for P, N and top position for Cl and all other ad-atoms (Kang et al. 2014, Hussain et al. 2016). The optimized structure of functionalized graphene with different adsorption positions is shown in Fig.[3.4].

The adsorption energies for different ad-atoms are listed in the Table.[3.1] confirms the stable adsorption of ad-atoms on the graphene sheet. The calculation shows that the adsorption of N on pristine graphene surface is most favorable compare to other ad-atoms. However, relatively large adsorption energies for P, Cl, and Al clearly indicate that these can be easily adsorbed on the pristine graphene surface. The ad-atoms are adsorbed on graphene at distances varying from 1.5 Å to 3.3 Å from the surface. Interestingly, the planar structure of graphene is not disturbed by these adsorptions.

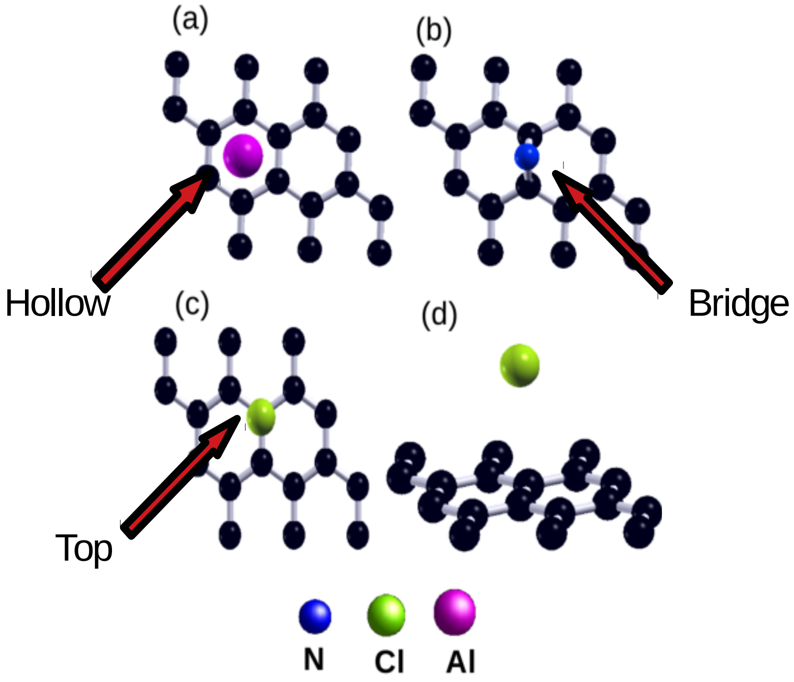

Figure 3.4: Energy-optimized geometry of functionalized graphene with different ad-atoms. Black magenta, blue and green ball represents C, Al, N and Cl atoms respectively a) Preferred adsorption position for Al at hollow site b)Nitrogen at bridge site and (c) Chlorine at the top site. (d) A side view of top site Cl adsorption.

Table 3.1: Adsorption energy per ad-atoms adsorbs on pristine graphene surface.

ad-atom	**adsorption energy(in eV)**	**ad-atom**	**adsorption energy(in eV)**
Na	-0.525	Cl	-1.142
K	-0.790	P	-1.234
Al	-1.117	N	-2.372

The electronic structure and subsequently the quantum capacitance of functionalized graphene were calculated in the optimized adsorbed geometry. The calculation shows a slight shift of band energies in graphene due to functionalization.

The calculation shows that quantum capacitance in functionalized graphene varies with the type, concentration, and distributions of ad-atoms. The calculated C_Q values in functionalized graphene with ad-atoms from different groups with a 5.5% doping concentration are shown in Table.[3.2].

Table 3.2: Calculated C_Q value at 300 K for various ad-atom functionalized graphene with doping concentration 5.5%.

Configuration	**Electronegativity of ad-atom**	**C$_Q$ (μF/cm^2)**
Pristine Graphene	-	1.294
FG - K	0.82	26.790
FG - Na	0.93	75.905
FG - Al	1.61	57.497
FG - Sn	1.96	249.477
FG - P	2.19	346.116
FG - N	3.04	256.422
FG - Cl	3.16	553.684

The table shows a clear enhancement in quantum capacitance due to functionalization in comparison with the pristine graphene which is $\sim 1.3\mu F/cm^2$. Notice that the enhancement of C_Q is proportional to the increase of electronegativity of ad-atoms.

The doped atoms in this study can be broadly categorized into two different groups. Group 1-3 metals such as K, Na, and Al ad-atoms are behaving as electron donors for graphene. They are donating electrons from their outer shell to the graphene and shift the Fermi level of graphene into the conduction band. As a result, the system shows an n-type behavior. On the other hand group, 15 and 17 elements such as N and Cl are electron-accepting ad-atoms (p-type doping).

The density of states contributed from alkali metal ad-atoms, are far from Fermi energy and shows a weak dispersion. K doped graphene band structure is shown in Fig.[3.5] with colored squares.

In the case of n-type functionalization, the Dirac cone structure of the graphene bands is preserved as shown in Fig.[3.6]. The Fermi level is located at the conduction cone, indicating a large amount of ad-atom induced free electron density between the Dirac point energy (E$_D$) and E$_F$, which can be controlled by tuning the n-type ad-

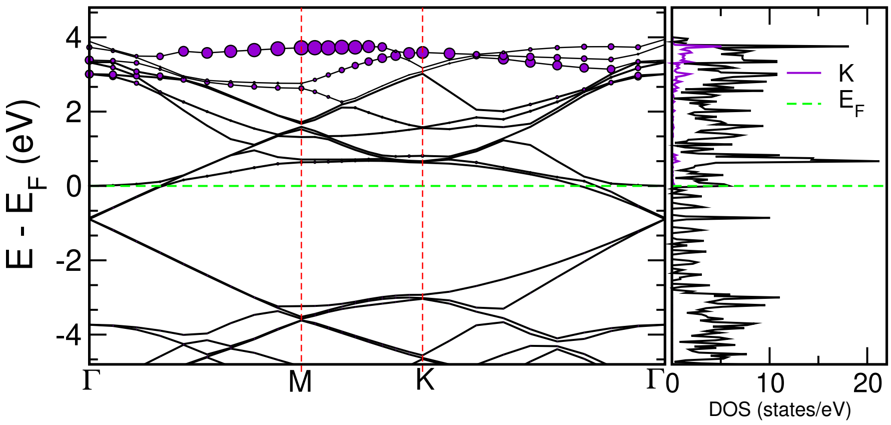

Figure 3.5: Electronic band structure and DOS for graphene functionalized with K. Contribution from doped atoms are represented by the coloured curve in the DOS and coloured circle in the band structure. Horizontal green dashed line is the Fermi energy set at E=0.

atom concentration. Since the conduction in pristine graphene is mainly due to the de-localized π cloud from p$_z$ orbitals of carbon, only p-states are expected to be found around the Fermi-level. A very similar change in the electronic structure was observed for Na and Al-doped graphene shown in Fig.[3.6(b)&(c)]. The overall change in density of state near the Fermi energy very small. As a result, the change in quantum capacitance compared to pristine graphene is expected to be very small. The maximum value of C$_Q$ among all alkali metal-doped graphene is found to be $\sim 76\mu F/cm^2$ for Na doping.

The electronic behavior of p-doped graphenes is entirely different from the alkali metal-doped graphene. In all of the p-doped graphene systems, the Dirac cone structure got distorted and the Fermi level is located at the valence Dirac cone. The atom projected density of states for N, P, and Cl doped graphene are shown in Fig.[3.7]. Free hole density appears between E$_D$ and E$_F$. The energy states near the Fermi energy are mainly contributed from the dopant atoms. I have observed a maximum change is for Cl doped system. It shows strong peaks near E_F which are $3p_z$ states from the doped chlorine ad-atom as shown in Fig.[3.7(c)].

Accumulation of large density of state near the Fermi energy was found in all p-doped graphene. Since the quantum capacitance is directly proportional to the measure of electron density near the Fermi level, there is a significant enhancement observed in

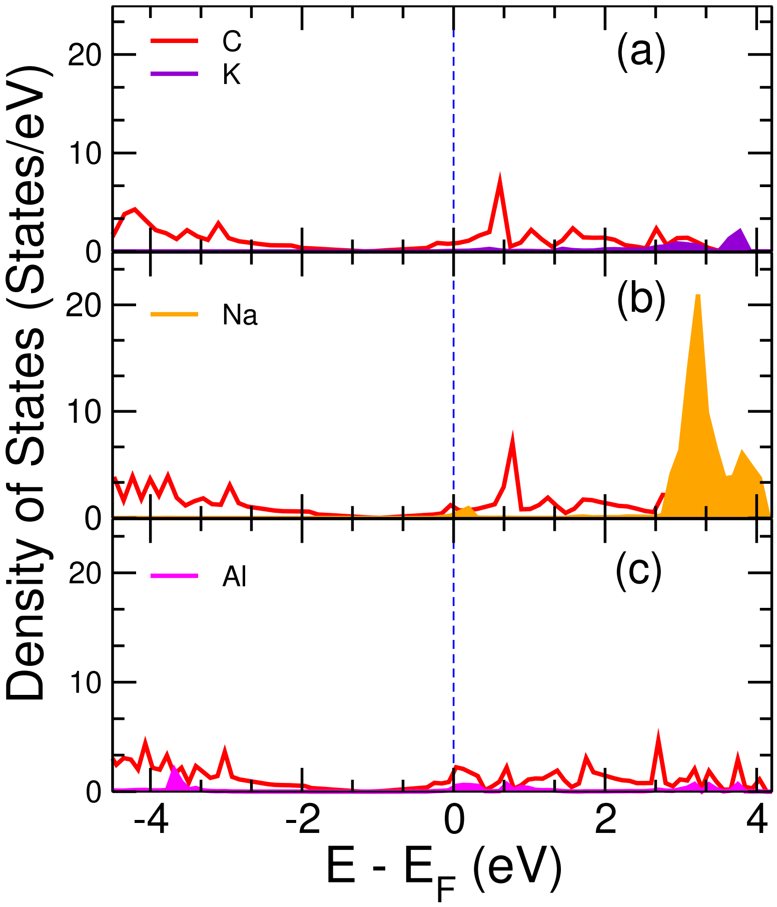

Figure 3.6: Atom projected density of states for functionalized graphene with (a)K (b)Na and (c)Al atoms. The shaded curve represents dos from the doped atom. The vertical blue dashed line is the Fermi energy set at E=0.

the case of the p-type doping system shown in Table.[3.2]. I found the maximum value of $C_Q = 553\mu F/cm^2$ for Cl-functionalized graphene with a 5.5% doping concentration.

For Sn and N functionalized graphene, a large amount of density of state accumulated near Fermi level as shown in Fig.3.8[(a) & (b)], as result high quantum capacitance value of 249.47 μF/cm^2 and 256.42 μF/cm^2 for Sn and N respectively were observed in these systems.

Next, the origin of large enhancement in quantum capacitance in p-type doping on graphene has been investigated. Charge redistribution in presence of ad-atom could be one of the main reasons. I have performed a Bader charge analysis on functionalized graphene and observed that there is a significant charge transfer between graphene and the ad-atoms.

In the case of Cl and N doping, the charge transfer is remarkably high. I found 0.6e

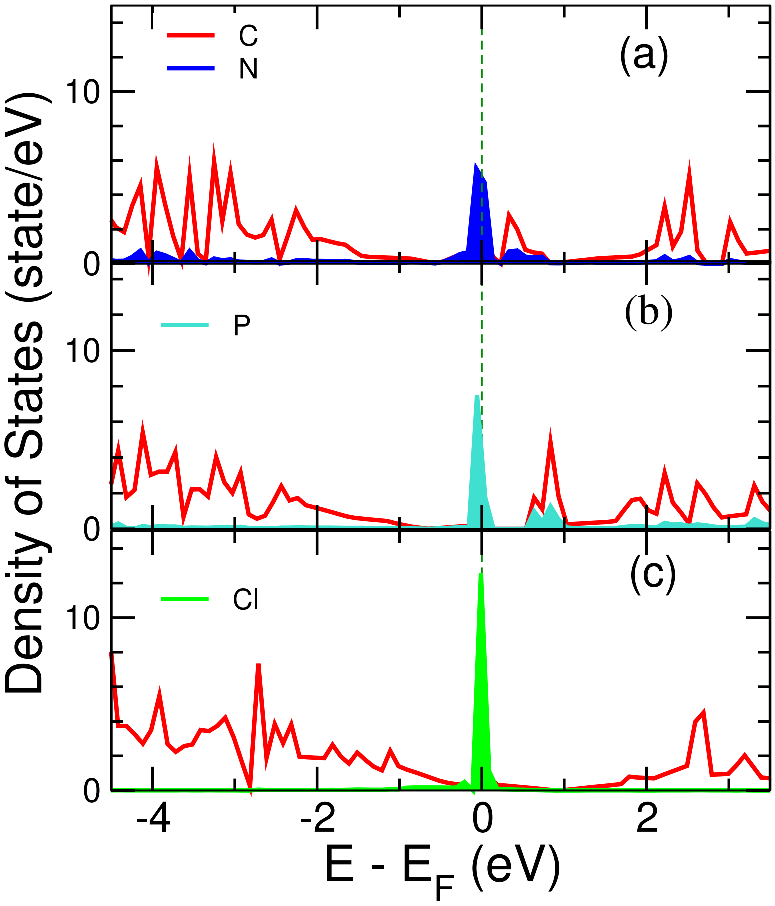

Figure 3.7: Atom projected density of states for functionalized graphene with (a)N (b)P and (c)Cl ad-atoms. The shaded curve represents dos from the doped atom. The vertical blue dashed line is the Fermi energy set at E=0.

and 0.5e charge transfer to Cl and N atoms respectively from the graphene sheet. A small change in the sublattice structures has also been observed. The introduction of the electron-accepting ad-atoms disrupts the homogeneity of the charge distribution due to the strong correlation effects. Fig.[3.9] shows the charge redistribution upon functionalization of graphene with Al, N, and Cl ad-atoms. Uniform homogenous charge distribution can be seen in the case of pristine graphene monolayer (See Fig.[3.9](a)).

We have observed that the charge inhomogeneity systematically increases with the increasing atomic number of the ad-atom. The localization of charges near the dopant site increases systematically as we have moved from the Na to Cl. This can be ascribed to the fact that the strong on-site Coulombic interaction dominates in the case of heavier p-block elements. I found maximum charge re-distribution on graphene caused by Cl. Further charge transfer leads to a change in the average DOS near the Fermi level, which

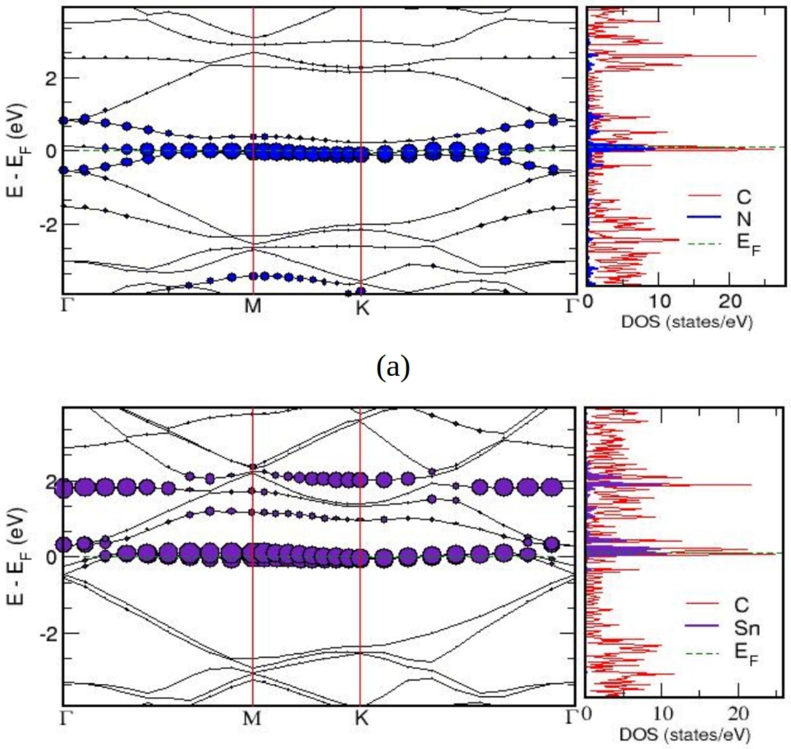

(a)

(b)

Figure 3.8: Electronic band and DOS for (a) FG-N and (b) FG-Sn. Colored curve in the DOS and circle in the band structure represents contribution from doped atoms. Horizontal red dashed line is the Fermi energy set at E=0.

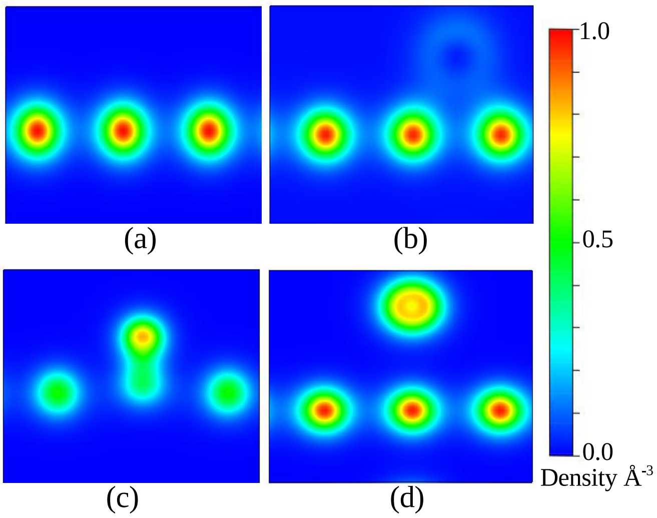

(a) (b)

(c) (d)

Figure 3.9: Contour plots for electron density associated with (a)Pristine Graphene, Functionalized graphene with (b)Al, (c)N and (d)Cl. Relative density is indicated by the colour bar.

in turn affects the quantum capacitance. Interestingly the density of states from $3p_z$ orbitals of Cl, N, and P are localized very near to Fermi level as shown in Fig.[3.7], which provides the maximum contribution to the quantum capacitance. To understand the localization of states near the Fermi energy from the doped atom I have carried out my investigation taking temperature into account. Considering a uniform variation of temperature from 10K to 400K I have studied the temperature-dependent behavior of the C_Q (Kliros 2010). In the case of pristine graphene monolayer, the value of C_Q remains nearly unchanged and it is close to $\sim 1.3\mu$F/cm^2. However, C_Q changes dramatically with temperature when Cl, P, and N atoms are added to the graphene. The calculation shows a sharp increase and then a gradual decrease of C_Q, upon increasing the temperature. With a 5.5% doping concentration the maximum value of $C_Q = 648\mu F/cm^2$ appears at 200K in Cl doped graphene and 263 $\mu F/cm^2$ arises at 234K in N-doped graphene. A significantly large value of $C_Q = 1992\mu F/cm^2$ was observed for the p-doped system at 30K with the same doping concentration. The variation of C_Q with temperature for N, P, and Cl doped graphene is shown in Fig.[3.10]. One possibility of such variation of C_Q with temperature could be due to the Kondo behavior of the doped graphene where ad-atoms may behave as the magnetic impurities. To confirm this, I have performed spin-polarized DFT calculations for these systems and observed that $0.371\mu B$, $0.75\mu B$, and 0.45 μB magnetic moment lies on the doped Cl, N, P atoms respectively, which confirms the magnetic behavior of the doped ad-atoms and localization of DOS near the Fermi energy.

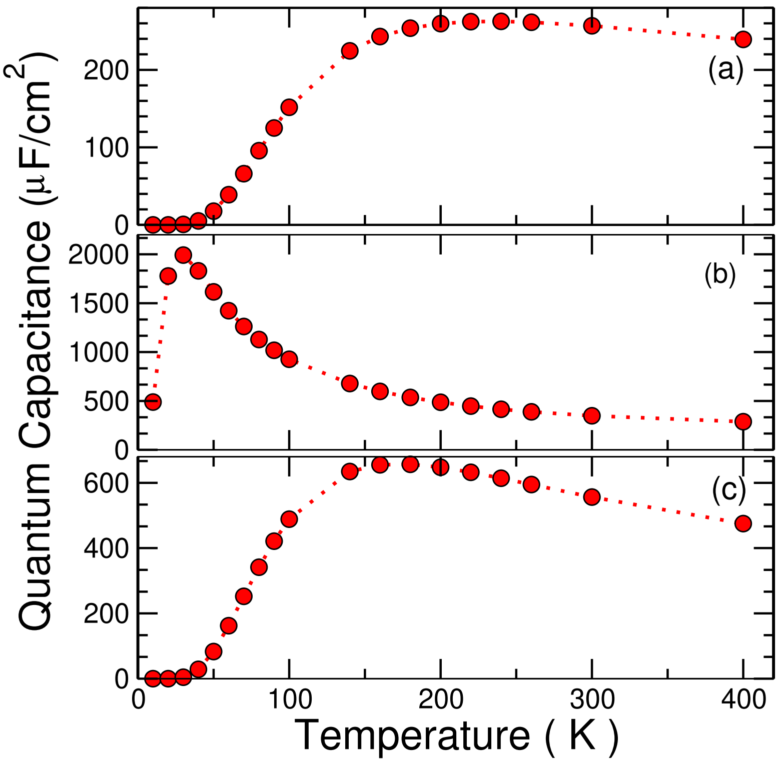

Figure 3.10: Variation of Quantum Capacitance with temperature in the range of 10K to 400K for (a)FG-N (b) FG-P and (c)FG-Cl.

I have extended my study of functionalization of graphene for the improvement of C_Q, considering many other ad-atoms such as Ac, B, Ca, La, Si, and Ge. The stability of functionalized graphene is checked by calculating the adsorption energy, which is listed in Table.[3.3].

Table 3.3: Adsorption energy per ad-atoms adsorbs on pristine graphene surface.

ad-atoms	**adsorption energy(in eV)**	**ad-atoms**	**adsorption energy(in eV)**
Ac	-1.416	La	-1.537
B	-1.268	Si	-1.244
Ca	-0.346	Ge	-1.015

In these functionalized graphenes the DOS near to the Fermi level is mainly contributed from ad-atoms as shown in Fig.[3.11].

The calculated C_Q for various ad-atom doped graphene are ploted in Fig.[3.12]. The calculated value of C_Q in Si and Ge doped graphene are 174.82 μF/cm^2 and 253.46 μF/cm^2 respectively listed in Table.[3.4].

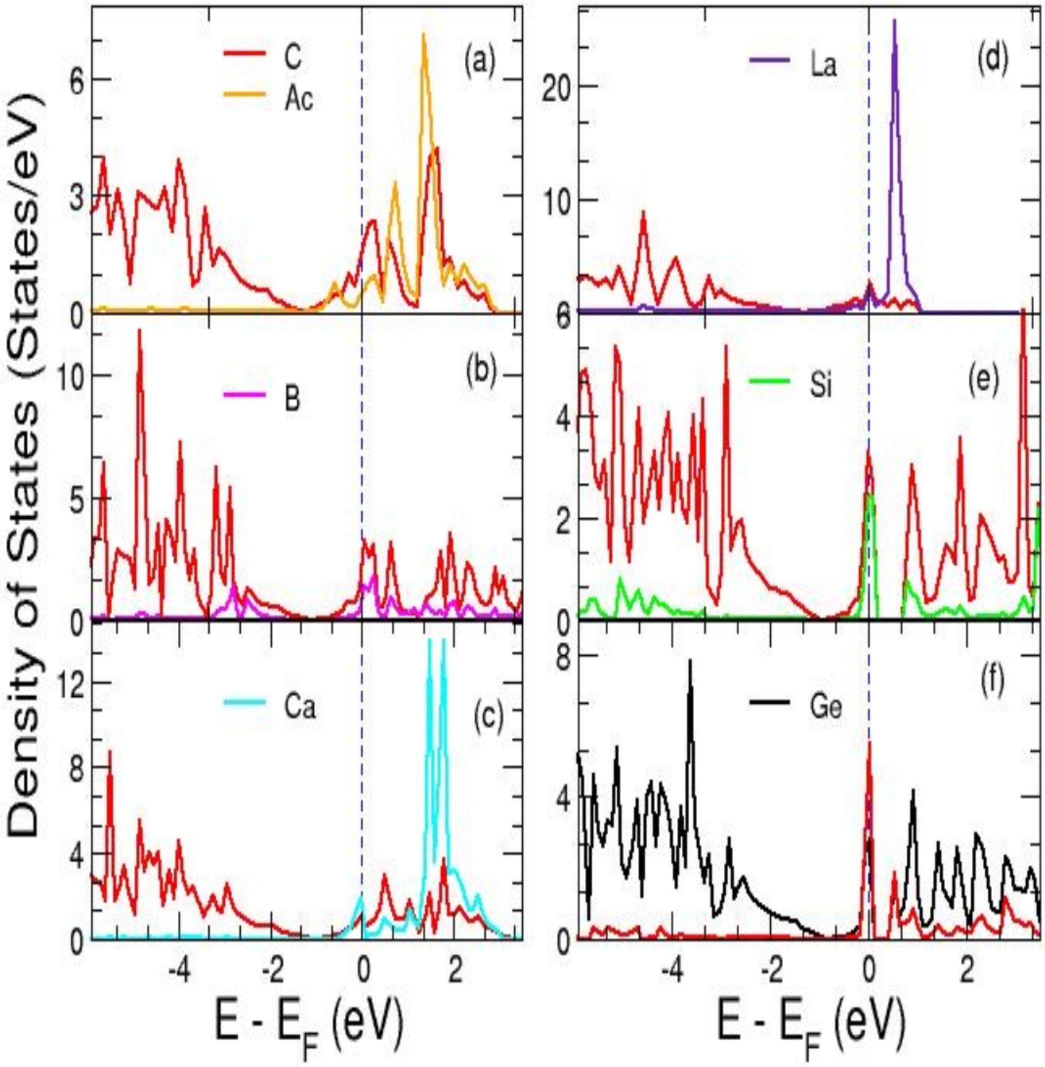

Figure 3.11: Atom projected density of states for functionalized graphene with (a)Ac (b)B and (c)Ca (d)La (e)Si and (f)Ge atoms. Colored curve represents dos from the doped atom. Vertical blue dashed line is the Fermi energy set at E=0.

Table 3.4: Details of C_Q value calculated at Fermi energy for various ad-atom functionalized graphene.

Configuration	**C_Q (μF/cm^2)**	**Configuration**	**C_Q (μF/cm^2)**
FG - Ac	60.319	FG - La	145.131
FG - B	60.847	FG - Si	174.825
FG - Ca	137.200	FG - Ge	253.457

An increase in C_Q is due to these localized DOS at the Fermi level, which is maximum for Si and Ge compared to other ad-atoms as depicted in Fig.[3.11]. One possi-

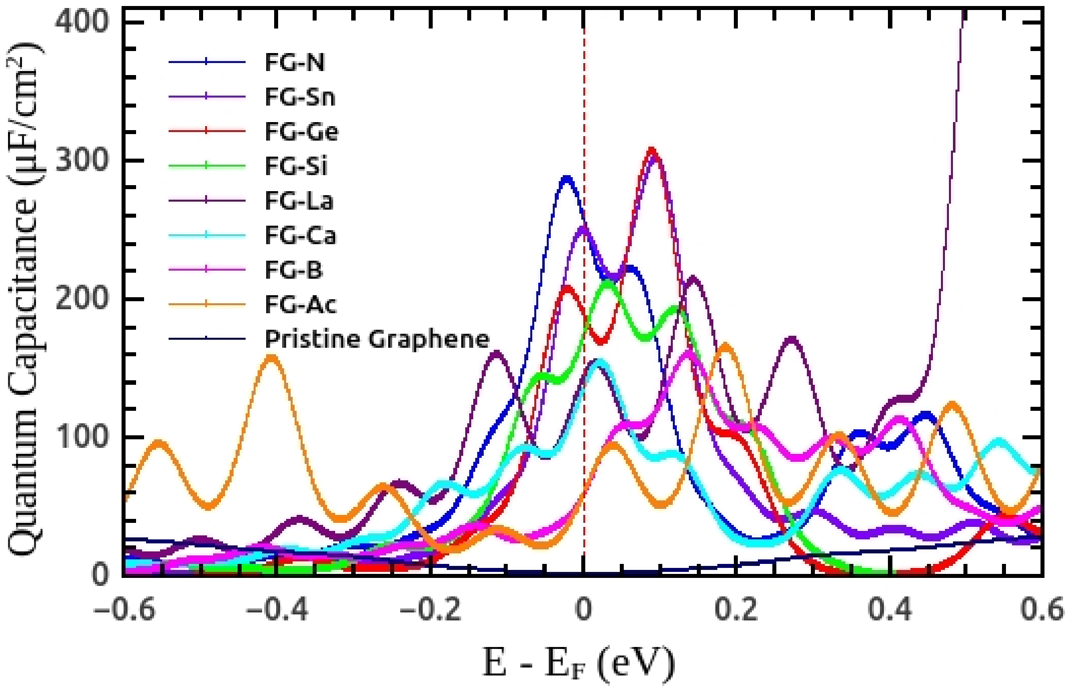

Figure 3.12: The different color curve represents the energy variations of quantum capacitance for graphene functionalized with various ad-atoms.

bility of obtaining a high C_Q value is that a significant charge reorganization happens due to the functionalization of graphene. Therefore I have investigated the charge redistribution in the functionalized graphene using Bader charge analysis and observed a large amount of charge transfer between graphene and the ad-atoms. I found 0.4e charge transfer to N and 0.5e charge transfer from silicon to graphene, where N and Si are the most and the least electronegative ad-atom in this study as shown in Table.[3.5].

Table 3.5: Details of charge transferred for variuos ad-atom functionalized graphene.

System	**Charge transferred (e)**
FG-B	0.364
FG-Si	0.524
FG-Ge	0.379
FG-Sn	0.316
FG-N	-0.413

3.5 Impact of ad-atom concentrations on graphene C_Q:

Next, I have carried out my investigation to study the impact of doping concentration on graphenes' quantum capacitance. I have chosen Cl, N, and P as ad-atoms to dope graphene with variable concentrations, as doping with these atoms with a similar concentration shows comparatively large C_Q value at room temperature.

It has been observed that a steady increment of C_Q for N and Cl doped system up to a certain concentration and then it decreases. However, in the case of the p-doped system, the C_Q decreases significantly with the increase of doping concentration. The maximum value of C_Q appears to be $280\mu F/cm^2$ and 1142 $\mu F/cm^2$ for N and Cl doped systems with doping concentration 6.25% and 12% respectively at room temperature. The concentration dependence of C_Q for different systems are summarized in the Table.[3.6]. The calculation also shows that the C_Q is sensitive to the adsorption site of the graphene lattice and it reduces drastically when ad-atoms are very close to each other. Moreover, the calculated value of C_Q is very small, when more than one ad-atom adsorbs on a single ring unit of the graphene or in equivalent sites of the adjacent ring. Since the N prefers to adsorb on the bridge position and Cl prefers to adsorb on the top position of the graphene lattice, therefore maximum concentration with such restriction is possible only for 6.25% and 12% doping concentration for N and Cl adsorption respectively. When the doping concentration is more than the critical value, impurity centers are interacting with each other which affects the localized states near the Fermi energy, which in turn reduces the C_Q value.

This can be understood by comparing the projected DOS of the impurity N atom in N-doped graphene with critical doping concentration(red curve) and higher than the critical doping concentration (blue curve) as shown in Fig.[3.13], where the impurity bandwidth is extended for the concentration which is higher than the critical value. Dense decoration of Cl on a graphene surface leads to the desorption of Cl from the surface in the form of Cl_2 due to a stronger Cl$-$Cl interaction.

One possibility of reduced C_Q value is due to the interaction between ad-atoms in functionalized graphene. The interaction between ad-atoms becomes much more powerful when the ad-atom concentration crosses the optimal value. These interactions

Table 3.6: Concentration dependence in C$_Q$ for nitrogen and chlorine functionalized graphene at 300K.

Concentration of ad-atom	**FG-N:C$_Q$ (μF/cm^2)**	**FG-Cl:C$_Q$ (μF/cm^2)**
2%	254.344	315.727
4%	269.484	1066.193
6.25%	279.770	976.114
8%	249.099	980.303
10%	195.319	279.753
12%	269.786	1141.655

affect the localized states near the Fermi level. As a result reduction in the C_Q value is observed as shown in Table.[3.6]. However, in the case of the N doped system, there is a steady increment of C_Q up to a 6.25% concentration as listed in Table.[3.6]. In case of higher doping concentration more than 6.25% C$_Q$ drastically reduced. Similar behavior has been observed in the case of Sn ad-atom.

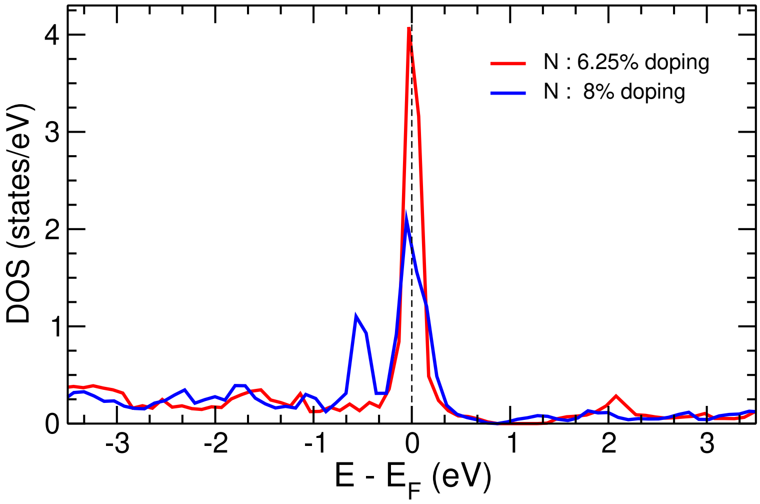

Figure 3.13: N atom projected DOS for nitrogenated graphene with two different N concentrations. Red line is for the 6.25% doping where the C_Q is maximum. Blue line represent the same for higher 8% doping.

3.5.1 Effect of Oxygenation on graphene C_Q

The investigation also shows that the enhancement of quantum capacitance is possible with oxygen doping as shown in Fig.[3.14]. A quantum capacitance of 247.379μF/cm^2 has been observed for oxygenated graphene with an O-C ratio 7:18 as listed in Table.[3.7].

Table 3.7: Details of C_Q calculated at Fermi energy for Oxygenated graphene with varying O/C ratio.

O-C Ratio	$\mathbf{C_Q}$ **(μF/cm^2)**
1:50 (0.02)	19.997
3:18 (0.17)	20.722
7:18 (0.39)	247.379

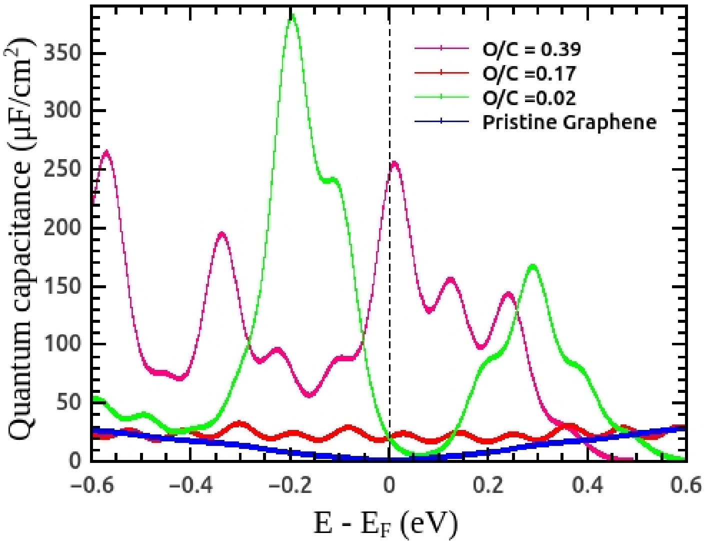

Figure 3.14: Quantum capacitance for oxygen doped graphene with various degrees of functionalization.

3.6 Effect of co-doping on graphene C_Q

In the case of co-doping of Cl, N, and P ad-atoms the interaction between ad-atoms are much stronger and instabilizes the absorption of ad-atoms on the graphene surfaces. The C_Q also reduces significantly as shown in the Table.[3.8].

Table 3.8: Calculated C_Q values for Co-doped graphene(G18) with two different ad-atoms with 5.5 % doping concentration for each type.

Co-doped ad-atoms	**C_Q(μF/cm^2)**
N,Cl	110.05
N,Sn	118.22
P,Sn	118.45
Sn,Cl	102.57

3.6.1 Co-doping effect of Nitrogen and Oxygen on graphene C_Q

The enhanced quantum capacitance can be obtained from reduced graphene oxide when functionalized with ad-atoms as predicted by Song Ce *et al.* Song et al. (2018). Therefore I have explored the combined effect using N and O ad-atoms. A clear enhancement of quantum capacitance value in nitrogenated graphene, in the presence of oxygen, is observed. I have then simultaneously varied the O and N concentration and found that the increment in C_Q is maximum when C:O: N ratio is 50:8:4 as listed in Table.[3.9] and the variation of C_Q in different N and O doping concentrations are shown in Fig.[3.15]

Table 3.9: Details of C_Q values calculated at Fermi Energy for co-doped graphene with Nitrogen, Oxygen in different concentration.

C:O:N Ratio	**C_Q (μF/cm^2)**	**C:O:N Ratio**	**C_Q (μF/cm^2)**
50:8:2	103.327	50:8:3	189.767
50:8:1	132.915	50:8:4	423.73

We have observed that the value of C_Q in nitrogenated graphene increases twofold (423.73 μF/cm^2) in presence of O in the above-mentioned concentration. The enhancement in C_Q can be realized as, there is a significant charge transfer from the graphene sheet to the O atom, which intern reduces the hybridization between the graphene carbon atom and the doped N atoms. As a result, the bandwidths of the impurity bands due to N atoms became narrower and extended only in a very small energy range near Fermi energy. Fig.[3.16] clearly shows the localization effect of nitrogen DOS near the

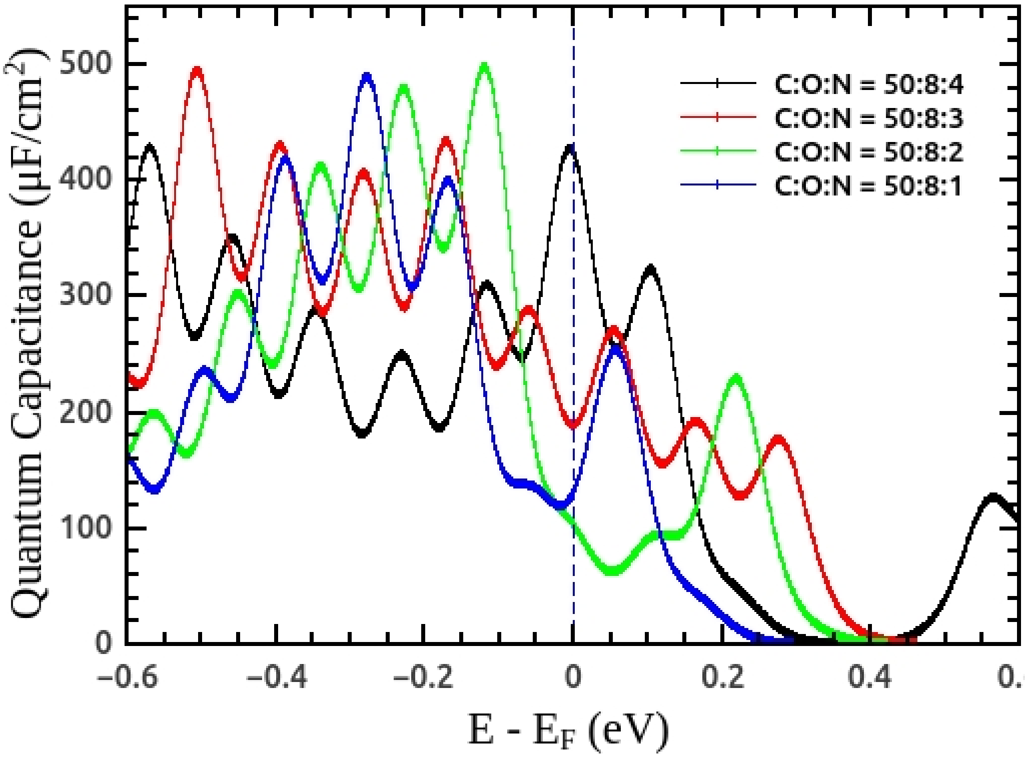

Figure 3.15: (a) Atom PDOS and (b)Quantum capacitance for N, O dual doped graphene.

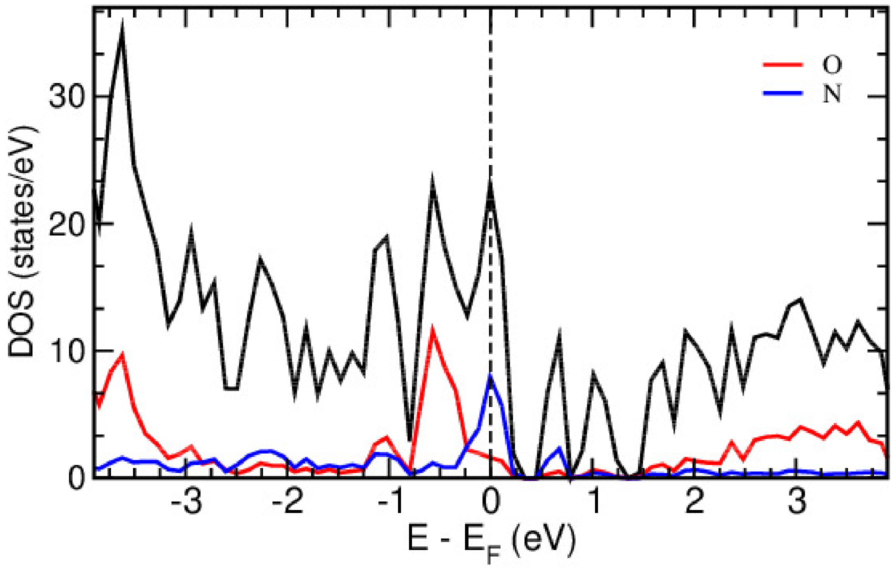

Figure 3.16: Atom PDOS for N, O dual doped graphene.

Fermi energy, which effectively helps to increase the charge carrier density and hence the quantum capacitance.

3.7 Impact of Vacancy defects on graphene C_Q

Imperfections are ubiquitous in any material and the point by point computational investigation of any material incorporating defects gives a more realistic picture prior to experimental analysis (Terrones et al. 2010). On the other hand, dislocation or defect on pristine graphene also causes charge localization, which intern may improve the quantum capacitance. Therefore in the next step, I have investigated the quantum capacitance of graphene in presence of vacancy defects. The effect of vacancy defects/structural disorder in the electronic structure of pristine graphene, subsequently the impact of vacancy defect concentration and the role of vacancy defect position in the graphene sublattice were systematically analyzed. The vacancies were created by simply removing the C atom from the graphene lattice as shown in Fig.[3.17]. The calculation shows that C_Q increases with defect concentration up to 4 % and then it decreases. The C_Q values with different vacancy concentrations are listed in Table.[3.10].

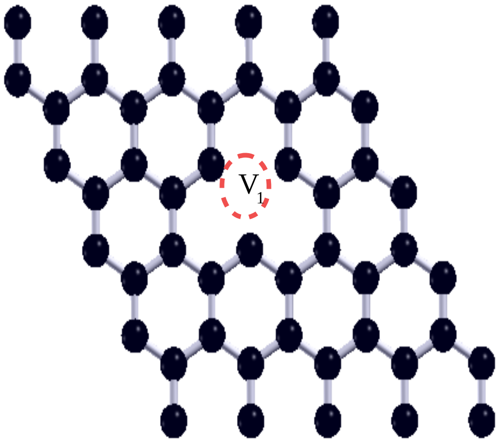

Figure 3.17: Optimized geometric structure for monovacancy defected graphene.

The main reason behind the enhancement of the quantum capacitance is due to the formation of localized states near Fermi energy, induced by defects as shown in Fig.[3.18(a)], which is very similar to the effect of ad-atom doping on graphene. It was also observed that the localized states are spin-polarized induces $\sim$ 0.3 μB magnetic moment for each vacancy created. The value of C_Q in different vacancy concentration are listed in the Table.[3.10]. We have noticed that vacancy defected graphene with more than 8% defect is difficult to study as the structure itself is unstable. Interestingly

Table 3.10: Calculated C_Q values for vacancy defected graphene with different vacancy concentration(G50) at 300K.

Vacancy concentration(%)	**C_Q(μF/cm^2)**
0	1.294
2	99.064
4	260.328
6	244.588
8	127.880

the position of the created vacancy site also has an impact on C_Q, very similar to the ad-atom's positions in doped graphene. The calculation shows that a significant reduction of C_Q in 4% defect configuration when the distance between two defect sites is less than 5$\AA$ as shown in Fig.[3.18(b)] where V_1, V_2, V_3, V_4 stand for graphene with 1,2,3,4 vacancies respectively.

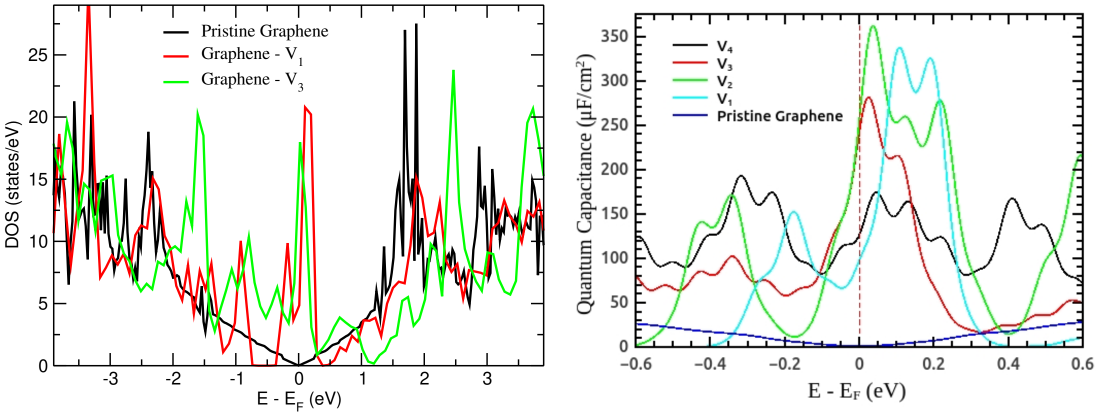

Figure 3.18: (a) Electronic DOS and (b) Quantum capacitance values for pristine and vacancy defected graphene systems.

3.8 Impact of vacancy defects on functionalized graphene C_Q

In the final step, I have incorporated vacancy defects in graphene functionalized with N, P, Cl ad-atoms. In presence of vacancy defect, I have observed a slight variation in C_Q only for Cl doped system. In 2% and 4% chlorine concentration, when one vacancy was created in a 50 C atom unit cell of graphene, the C_Q increases to 486 μF/cm^2 and 1091 μF/cm^2 respectively. Further increment in Cl doping concentration, the C_Q

reduces drastically. This is due to the strong interaction between the localized charge in the doped atom and the defected site. No considerable changes are found in C_Q for N and P doped graphene with vacancy defects.

3.9 Conclusion

In conclusion, the functionalization of graphene with ad-atoms from different groups in the periodic table was analyzed systematically. Our density functional theory calculations indicate that the quantum capacitance in functionalized graphene mainly depends on the sublattice positions and the concentration of ad-atoms. The quantum capacitance of 249.477 $\mu F/cm^2$ was observed for Sn functionalized graphene. The nitrogenated graphene gives generally a high C_Q of 279.385 $\mu F/cm^2$ which was further expanded to 423.73 $\mu F/cm^2$ in presence of an oxygen atom in the system. We observed that the enhancement is significant when the graphene was functionalized with N, Cl, and P ad-atoms with certain concentrations. These ad-atoms are behaving as magnetic impurities in the system, generates localized density of states near the Fermi energy. Atom projected density of states for these systems show that new DOS are appearing near the Fermi-energy which are mainly from p-orbitals of ad-atoms, produces high charge(electron/hole) density near the Fermi level results to a very high C_Q in the system. Our calculation also predicts that the Cl functionalization is more viable when a defect present in the graphene, which causes further enhancement of C_Q in the system. The temperature variation calculation shows that C_Q remains large in Cl and N functionalized graphene in a wide range of temperature. Our study proposes that the chemically modified graphene could be a promising electrode material for supercapacitors, in which a very large quantum capacitance ((>600 $\mu F/cm^2$)) can be achieved near room temperature.

Dislocation or defect on pristine graphene also causes charge localization, which in turn may improve the C_Q due to the formation of localized states near Fermi energy, induced by defects. The value of C_Q increases with defect concentration up to 4% and then it decreases. It was also observed that the localized states are spin-polarized induces $0.3\mu B$ magnetic moment for each vacancy created. We were unable to study the vacancy defected graphene with more than 8% defect as the structure itself is unstable.

Interestingly the position of the created vacancy site also has an impact on C$_Q$, very similar to the ad-atom's positions in doped graphene. We observed a significant reduction of C$_Q$ in 4% defect configuration when the distance between two defect sites is less than 5 Å.

The dispersibility of graphene in common organic solvents is an essential condition for making a supercapacitor. Functionalizing graphene with organic functional groups with large aromatic donor and acceptor molecules, which may tune the electronic properties of the system. The results we discussed in this chapter show that the adsorption of particular atoms on graphene has a greater impact on the C$_Q$. Therefore for further study of C$_Q$ here we have selected molecular fragments as dopants that contain these adatoms.

Chapter 4

Enhancement of Quantum Capacitance in graphene electrodes using molecular fragments and radicals functionalization.

In this part of my thesis, I have investigated the quantum capacitance of the graphene-based electrodes by functionalizing them with small organic molecular fragments and their radicals. The main purpose of functionalization of pristine graphene sheets with organic functional groups is the dispersibility of graphene in common organic solvents which is one of the essential requirements for making a supercapacitor (De Oliveira and Miwa 2015, Hwang et al. 2015, Jia et al. 2013). In this work, I have modeled the system considering non-covalent functionalization of graphene with different fragments of aliphatic and aromatic donor/acceptor molecules which are already proven to be suitable for chemical modification of graphene (Lonkar et al. 2015, Milowska et al. 2013, Georgakilas et al. 2012). In the aliphatic group, I have considered fragments such as alkene, alkyne, ketones, amines, amides, nitriles, carboxylic acids, sulphoxides (Umadevi and Sastry 2011). The piperidine ($(CH_2)_5NH$) and dimethyl sulfoxide (DMSO,$(CH_3)_2SO$) are selected as amine and sulfoxide groups for functionalization. Aromatic molecules such as benzene, aniline, phenol, anthracene, toluene, and naphthalene were used for aromatic functionalization of graphene (Wu et al. 2015, de Moraes et al. 2019).

4.1 Methodology

Similar to the ad-atom functionalization of graphene, here also I have investigated quantum capacitance in three different steps.

In the first step, I have investigated the adsorption properties of these molecules and their radicals (Tachikawa 2019). In this case, the orientation of the fragment with respect to the graphene plane plays an important role. We therefore carefully study the absorption of the molecule considering different orientations of the attached fragments/radicals. In each case, the stability of the functionalized structure was examined by estimating average adsorption energies E_{ad} of fragments by using the following equation

$$E_{ad} = \frac{1}{n}[E_{tot} - E_{gr} - nE_{frag}] \tag{4.1}$$

where E_{tot} is the total energy of the functionalized graphene unit cell, E_{gr} is the total energy of pristine graphene in the same unit cell, E_{frag} is the per molecule energy of the fragment and n represents the number of adsorbed molecules present in the unit cell.

A sufficiently large vacuum (height>15Å) was considered in the perpendicular direction of the graphene sheet to avoid the interaction with its periodic images. Depending on the fragment's dimension and to avoid fragment-fragment interactions, different size supercells from 4×4×1 (32C atoms) to 8×8×1 (128C atoms) were used so that the distance between two fragments remain more than 5Å.

The vacancy defected configurations were realized by removing C atoms from the graphene sheet on the same supercell. To model radical adsorbed graphene surface, I have removed one hydrogen atom from each fragment to make radicals, ie. I have removed H from the ring in benzene, from NH_2 group in aniline, from CH_3 group in toluene, from OH group in phenol, from alpha/beta position in naphthalene, from the alpha position in anthracene, etc and placed in the unit cell.

The correction due to the vdW interactions is also incorporated in this calculation using a semiempirical approach (DFT-D2) (Grimme 2006) as implemented in VASP. A 6×6×1 Γ centered k-point mesh was used for reciprocal space sampling in geometry optimization. I have considered 10^{-6}H tolerance in total energy in electronic self-consistency. Finally, a denser $24\times24\times1$ Γ centered k-point grid was used for the precise extraction of electronic structure information such as electron density of states (DOS) and atom projected density of states(PDOS) from the optimized geometries. Finally, we have estimated the C_Q using the equation (2.27) for all the system form the density of states obtained from DFT calculations.

4.2 Aliphatic Molecule functionalization on pristine graphene

Our calculation shows that all the aliphatic molecules are strongly interacting with the graphene surface. We have observed a significant distortion of the graphene structure upon adsorption of acetamide, piperidine, DMSO, butyronitrile, and hexane-1-thiol, whereas the distortion is negligible for alkene, acetic acid, and ketone adsorption. In case of large deformation of the structure, the total adsorption energy for these molecules E_{ad} includes a large energy cost to deform the graphene lattice, which can be calculated from E($\bar{g}$)-E(g), where E($\bar{g}$) is the energy of the deformed graphene. Calculated adsorption energies for different aliphatic molecules on graphene shown in Table.[4.1] indicate that most of the aliphatic molecule considered in this study are well absorb on the graphene surface. The energy-optimized acetone(ketone), piperidine(amine groups), DMSO, and Hexane-1-thiol functionalized graphene are shown in Fig.[4.1].

Although significant geometric distortions were observed in most aliphatic functionalized graphene, the electronic structure of the graphene is not much perturbed. Atom projected density of states for ketone(acetone), amine(piperidine), sulfoxide(DMSO), and Hexane-1-thiol functionalized graphene is shown in Fig.[4.2(a-d)]. Clearly, the Dirac cone structure is preserved in each case. The density of states contributed from aliphatic molecules in the system are highly localized and located in the valence band far from the Fermi level. Since the conduction in pristine graphene is mainly due to the de-localized π cloud from p_z orbitals of carbon, only C p-states are present around the Fermi-energy in the functionalized system. Surprisingly strong adsorption of these molecules on graphene does not produce a significant change in the electronic structure near the Fermi energy. An only noticeable change is observed in the case of thiol

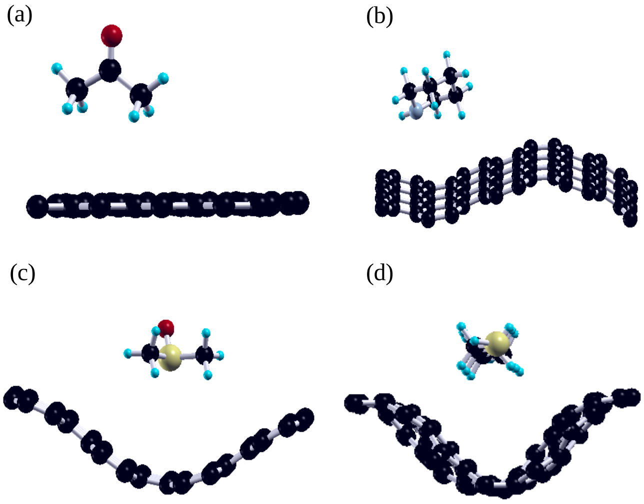

Figure 4.1: Energy-optimized geometry of functionalized graphene with (a)Acetone(ketone), (b)piperidine(amine), (c)DMSO and (d)Hexane-1-thiol. Black, grey, blue, red and yellow ball represents C, N, H, O and S atoms respectively.

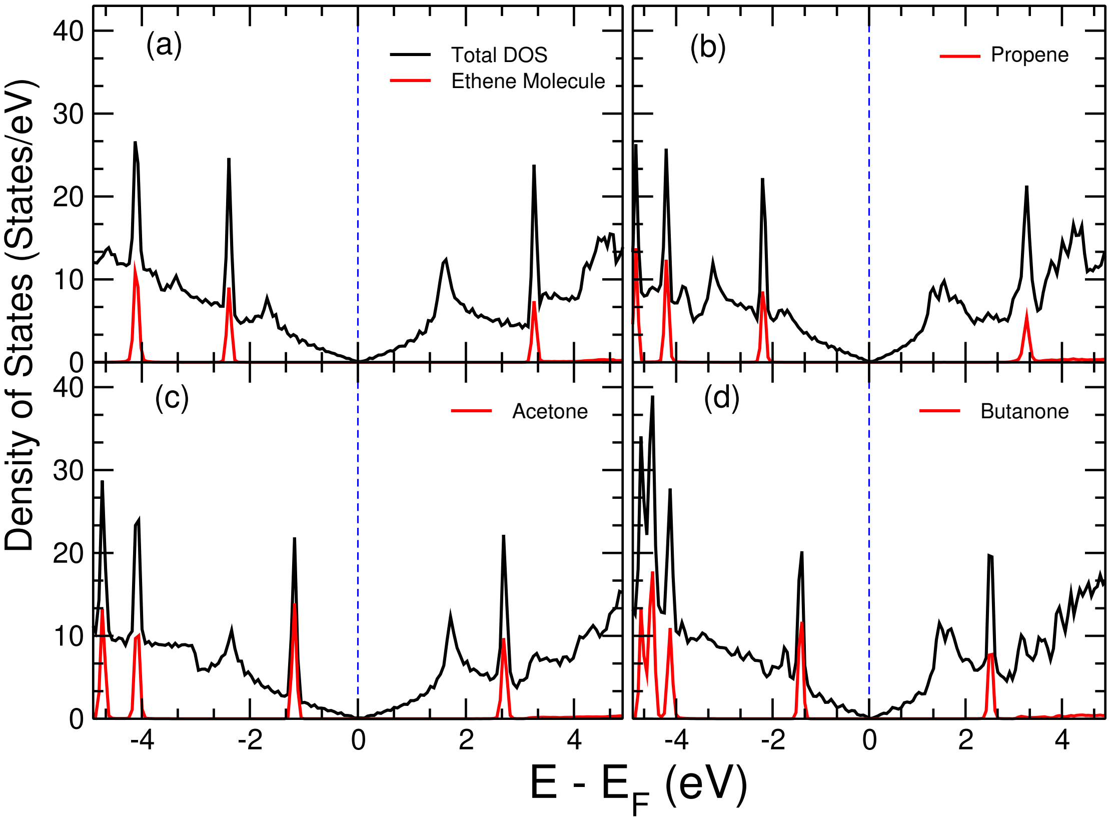

Figure 4.2: Projected density of states for functionalized graphene with (a)Acetone(ketone), (b)piperidine(amine), (c)DMSO (sulfoxide) and (d)Hexane-1-thiol. The colored curve represents dos from the aliphatic molecules. The vertical blue dashed line is the Fermi energy set at E=0.

adsorption, but DOS localization near Fermi energy is negligible. Bader charge analysis shows that a small charge transfer occurs between graphene and the fragments as shown in the Table.[4.1]. Fragment groups such as butyronitrile and hexane-1-thiol behave as electron acceptors on graphene, whereas ethane, acetylene, acetamide, piperidine, acetic-acid, acetone, DMSO are behaving as an electron donor in a functionalized graphene system. This clearly indicates that the interaction between aliphatic molecule and graphene is mainly Van der-Waals type. The overall change in density of states near the Fermi energy is very small for each aliphatic molecule functionalized graphene results in a small change in quantum capacitance compared to pristine graphene tabulated in Table.[4.1]. An atomic defect on pristine graphene causes charge localization, which in turn may improve the quantum capacitance in functionalized graphene. However, I have not observed any significant change in quantum capacitance after introducing vacancy defects in aliphatic functionalized graphene.

Table 4.1: Calculated E_{ad} value, charge transferred and quantum capacitance value at 300 K for various Aliphatic molecules functionalized graphene with single molecule doping.

Configuration	**Adsorption energy(eV)**	**charge transferred(e)**	**Quantum capacitance** ($\mu F/cm^2$)
Pristine Graphene	-	-	1.300
FG-Ethene	-0.241	0.120	1.932
FG-Acetylene	-1.175	0.216	4.493
FG-Acetamide	-1.057	0.909	3.658
FG-Piperidine	-1.147	0.046	3.718
FG-Acetic-Acid	-0.573	0.144	2.532
FG-Acetone	-1.681	0.124	1.711
FG-Butyronitrile	-1.175	-0.077	3.460
FG-DMSO	-0.595	0.142	3.513
FG-Hexane-1-Thiol	-2.268	-0.055	8.171

4.3 Aliphatic Radical functionalization on pristine graphene

There are possibilities of radical formation and radical functionalization during the synthesis process. Also, the radical functionalization may help to create a localized state near the Fermi energy of the system. Therefore, as a next step, I have investigated the electronic structure and quantum capacitance in aliphatic radical functionalized graphene. Radicals are created out of ethene, propene, acetone, and butanone molecules by removing one of the hydrogen atoms from the fragments. The adsorption energies and charge transferred for different aliphatic radical functionalized graphene are listed in the Table.[4.2]. Negative values of the adsorption energy confirm that all aliphatic radicals are stable on top of the graphene sheet. A notable distortion in graphene sheet was observed, in which graphene carbon atoms (near radicals) are attracted towards radicals. Optimized geometry of ethene, propene, acetone, and butanone radical functionalized graphenes are shown in Fig.[4.3]

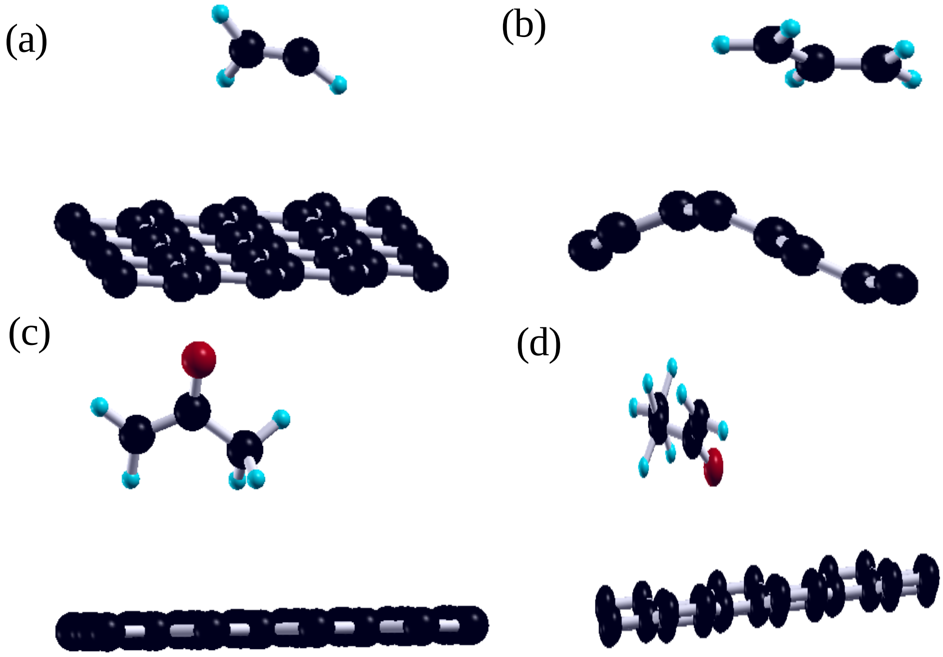

Figure 4.3: Energy-optimized geometry of (a)Ethene, (b)Propene, (c)Acetone and (d)Butanone radical functionalized graphene. Black, blue, and red ball represents C, H and O atoms respectively.

Interestingly, aliphatic radical functionalization shows significant changes in the electronic behavior of graphene. The Dirac cone structure got distorted. From the density of states calculation, I have noticed that the valence band maximum is contributed mainly from the atoms of aliphatic radicals in each case and a sufficient amount of states are accumulated near the Fermi level. For acetone radical, functionalized graphene accumulation of density of state near the Fermi energy is maximum as shown in Fig.[4.4c], as a result, a high quantum capacitance value of 234 $\mu F/cm^2$ is observed in this system.

In the case of other aliphatic radical-functionalized graphene, the density of states calculation also shows similar behavior. A strong peak near E_F appears for each of ethene, propene, and butanone functionalized graphene which is mainly contributed from atoms of the radicals as shown in Fig.[4.4 (a),(b) & (d)] respectively. The calculated values of quantum capacitance for these systems are very high (in the range of 200 $\mu F/cm^2$) listed in Table.[4.2].

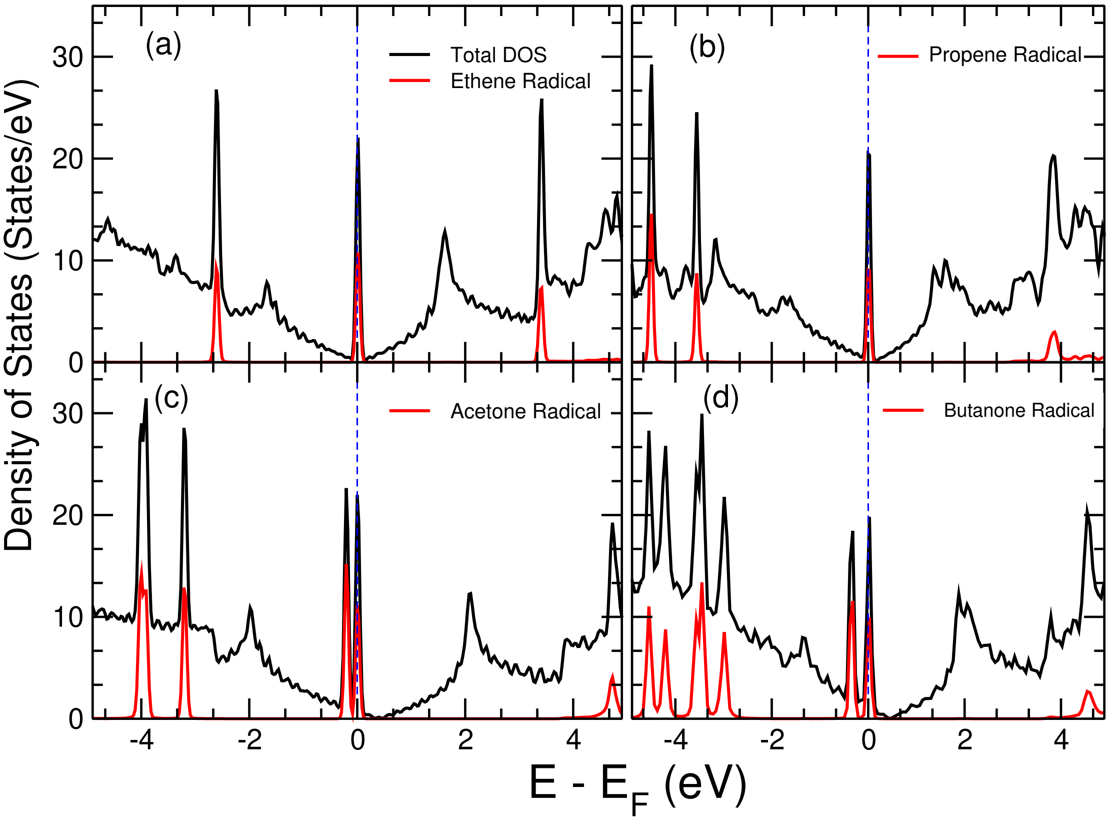

Figure 4.4: Projected density of states for functionalized graphene with (a)Ethene, (b)Propene, (c)Acetone and (d)Butanone radicals. The colored curve represents dos from the aliphatic radical. The vertical blue dashed line is the Fermi energy set at E=0.

4.4 Aromatic molecule functionalization on pristine graphene

Next, I have used a set of aromatic molecules such as benzene, aniline, phenol, anthracene, toluene, and naphthalene and their radicals for the functionalization of graphene. The stable adsorption position of aromatics on graphene was calculated by placing molecules in different possible configurations and comparing the total energies. The perpendicular configuration (ie. molecular plane is perpendicular to the graphene sur-

Table 4.2: Calculated Adsorption value, charge transferred and C_Q value at 300 K for various aliphatic radical functionalized graphene with single radical doping.

Configuration	**Adsorption energy(eV)m**	**charge transferred(e)**	**Quantum capacitance ($\mu F/cm^2$)**
Pristine Graphene	-	-	1.300
G-Ethene	-0.270	-0.011	220.612
G-Propene	-0.310	-0.016	221.294
G-Acetone	-1.818	-0.083	234.676
G-Butanone	-0.932	-0.108	211.494

face)was found to be most favorable for benzene and aniline molecule; whereas a parallel configuration, ie. molecular plane is parallel to the graphene surface was found to be the most stable configuration for phenol, anthracene, toluene, and naphthalene. Interestingly, the atom of molecules that is closest to the graphene surface in perpendicular configurations is sitting at the center of the graphene hexagonal ring. One reason is that this configuration minimizes the repulsion between electrons in π-orbitals and maximizing the attractive interaction between the molecule and the graphene.

Optimized geometric structures of six aromatic functionalized graphene structures are shown in Fig.[4.5]. Out of six aromatic molecules only benzene, aniline, and anthracene functionalization show a noticeable change in the electronic structure of graphene near the Fermi energy. The calculated electronic density of states for six aromatic molecules functionalized graphene are shown in Fig.[4.6]. Although the bandgap in these three systems is zero, the linear dispersion is missing in the band structure. The density of states is localized near the Fermi energy which is mainly contributed from the graphene itself. Bader charge analysis shows that in the case of toluene and anthracene the charge transfer is significant. This calculation shows that the toluene and aniline act as electron donors whereas anthracene behaves as an electron acceptor molecule on the graphene surface. The adsorption energies and charge transferred for different aromatic molecules on the graphene sheet are listed in the Table.[4.3]. There is no significant improvement in the value of quantum capacitance was found in this case. The maximum value observed is 29.09 $\mu F/cm^2$ for benzene functionalized graphene. C_Q values for other aromatic functionalized graphenes are shown in Table.[4.3].

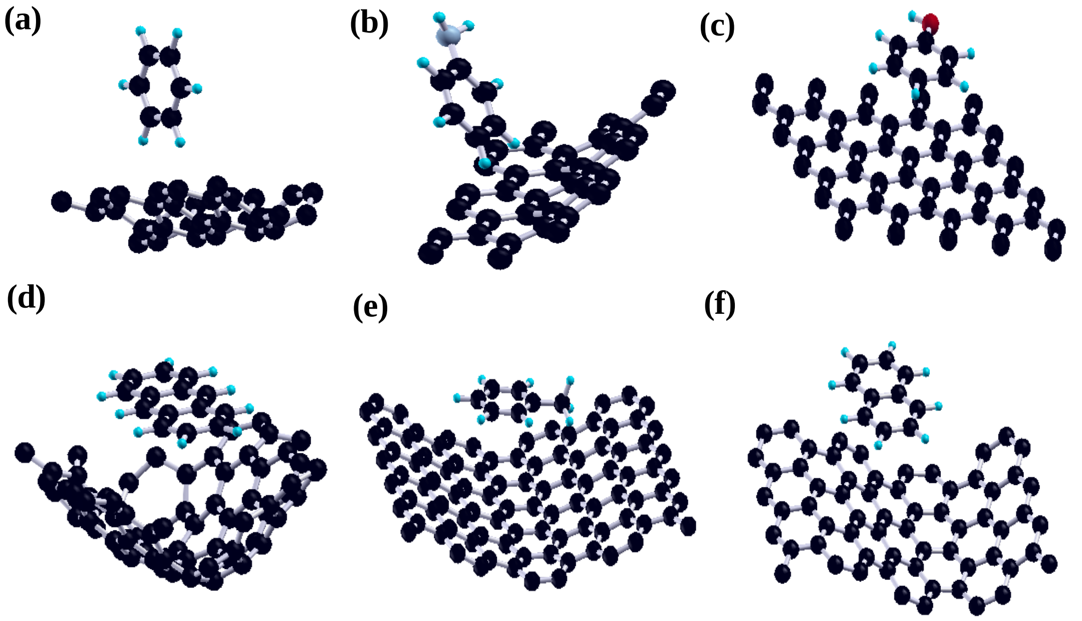

Figure 4.5: Energy-optimized geometry of (a)Benzene, (b)Aniline, (c)Phenol, (d)Anthracene, (e)Toluene and (d)Naphthalene molecule functionalized graphene. Black, blue, red, and grey ball represents C, H, O and N atoms respectively.

In order to enhance the C$_Q$ value, I have introduced vacancy defects in pristine graphene. The distortion in the graphene sheet is more in defective graphene compared to the pristine graphene. In this case, the adsorbed molecule comes close to the defect site and is bonded to the carbon atom of graphene. This gives rise to strong hybridization between π orbitals of graphene and molecule, as a result, the density of states present near the Fermi level get reduced leads to a smaller value of quantum capacitance. There is no significant increment in quantum capacitance for aromatic

Table 4.3: Calculated E_{ad} value, charge transferred and quantum capacitance value at 300 K for various aromatics functionalized graphene with single molecule doping.

Configuration	**Adsorption energy(eV)m**	**charge transferred(e)**	**Quantum capacitance** ($\mu F/cm^2$)
Pristine Graphene	-	-	1.300
G-Benzene	-2.285	-0.062	29.090
G-Aniline	-1.310	0.062	6.248
G-Phenol	-1.182	-0.039	2.490
G-Anthracene	-1.326	-0.373	4.405
G-Toluene	-1.210	0.326	6.342
G-Naphthalene	-0.700	-0.013	3.406

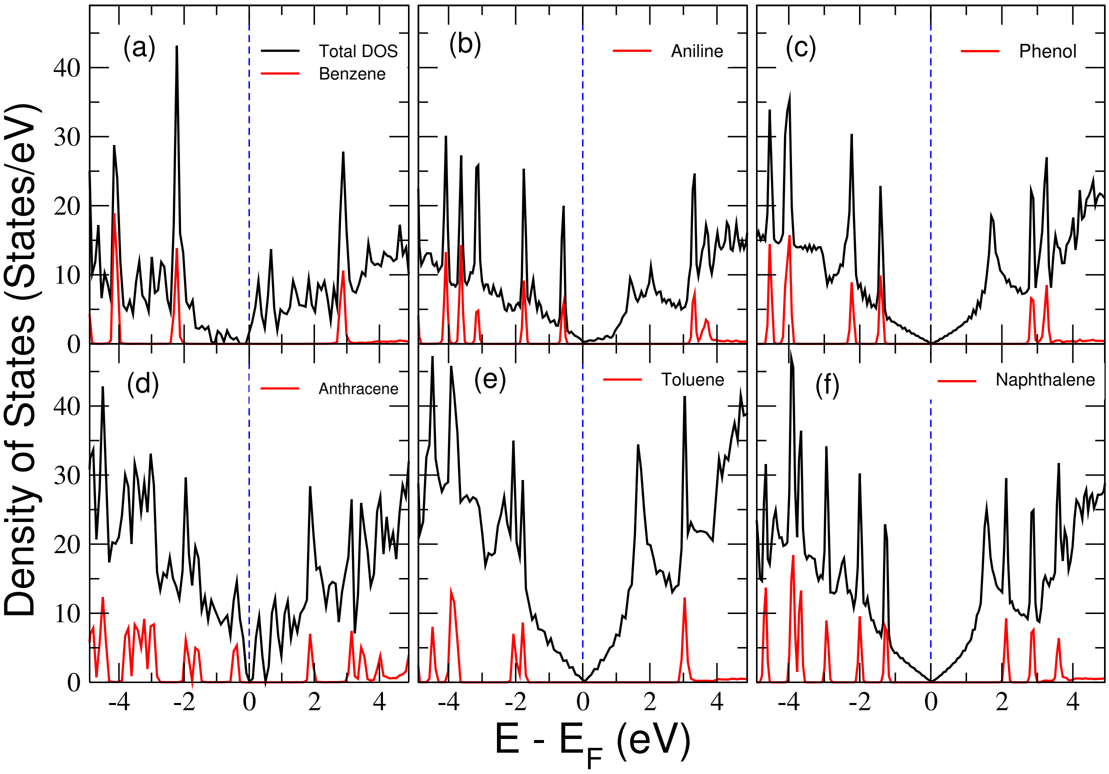

Figure 4.6: Projected density of states for functionalized graphene with (a)Benzene, (b)Aniline, (c)Phenol, (d)Anthracene, (e)Toluene and (d)Naphthalene molecule. The colored curve represents dos from the aromatic molecules. The vertical blue dashed line is the Fermi energy set at E=0.

molecules functionalized on top of vacancy defected graphene surface.

4.5 Aromatic Radical functionalization on pristine graphene

Next, I have investigated the possibility of C_Q enhancement in aromatic radical functionalized graphene. In this case, radicals were formed by removing one H atom from a different position of the molecule and placed in the same supercell which was used in molecule functionalization calculation. Geometry optimization shows different adsorption configurations for different radical functionalization. In the case of benzene and anthracene radicals, radical sites are coming closer to the graphene and bonded with the graphene surface, whereas phenol toluene and naphthalene radicals are sitting parallel to the surface. On the other hand, the aniline radicals are stabilizing in such a way that the unsaturated atom of the molecule keeps maximum distance from the graphene surface. The optimized geometry of aromatic radical adsorbed graphene is given in

Fig.[4.7]. Note that the adsorption energies of aromatic radicals on graphene surface

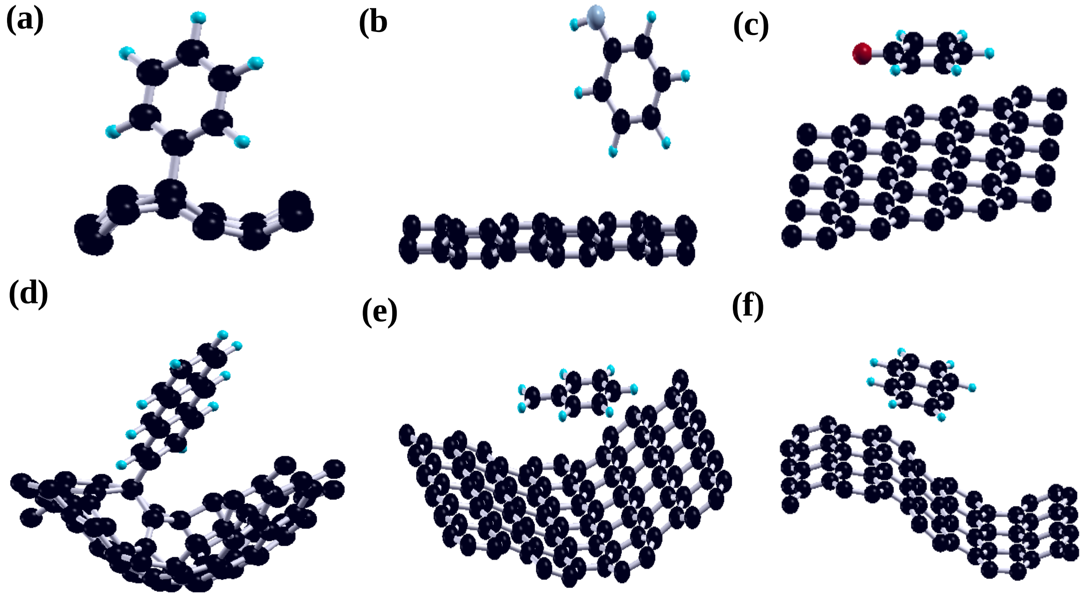

Figure 4.7: Energy-optimized geometry of (a)Benzene, (b)Aniline, (c)Phenol, (d)Anthracene, (e)Toluene and (d)Naphthalene radical functionalized graphene. Black, blue, red, and grey ball represents C, H, O and N atoms respectively.

are more compared to the respective molecule absorptions.

A noticeable change has been observed in the electronic structure of each aromatic radical functionalized graphene compare to the electronic structure of the pristine graphene. The Dirac cone structures are distorted in all cases, and the valence bands become denser compared to the conduction bands. The maximum change in the planar structure of graphene was observed for benzene and anthracene radical functionalized graphene. We observed a bending distortion in the planar geometry of graphene and the radicals get bonded to graphene sublattice. Peaks for benzene and anthracene radical functionalized graphene are lesser compared to the other four. This peak near E_F which are $3p_z$ states from the graphene carbon atom as shown in Fig.[4.8]. In the case of phenol radical doped graphene, states near the Fermi energy are mainly contributed from the oxygen atoms of the radical. Two types of naphthalene radicals can be made from the naphthalene molecule by removing H from alpha- and beta-positions. I have considered both the radicals, which shows a very similar change in electronic behavior shown in Fig.[4.8(f)].

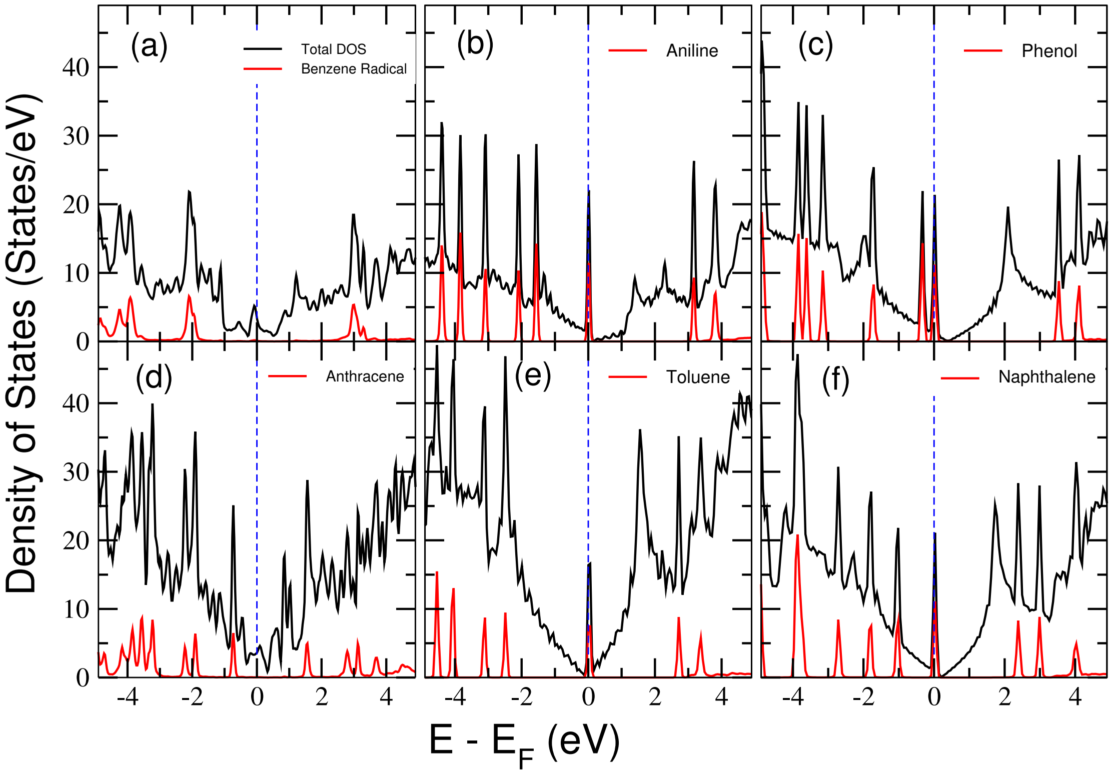

Figure 4.8: Projected density of states for functionalized graphene with (a)Benzene, (b)Aniline, (c)Phenol, (d)Anthracene, (e)Toluene and (d)Naphthalene radical. The colored curve represents dos from the aromatic radicals. The vertical blue dashed line is the Fermi energy set at E=0.

It was observed that the accumulation of large density of state near the Fermi energy for all aromatic radical functionalized graphene and relatively large C_Q was obtained for each system as listed in the Table.[4.4]. The maximum value of $C_Q = 236.62\mu F/cm^2$ obtained for phenol radical doped graphene.

To understand the result I have performed a Bader charge analysis on radical functionalized graphene, which shows that there is significant charge transfer between graphene and the aromatic radicals compared to aromatic molecules. In the case of anthracene and phenol radical doping, the charge transfer is remarkably high. I found that there are 0.46e and 0.27e charge transfer to anthracene and phenol radicals respectively from the graphene sheet. Whereas toluene radical acts as an electron donor to donate +0.3e charge per radical to the graphene sheet. The introduction of the electron-accepting/donating radicals disrupts the homogeneity of the charge distribution. Note that, in the case of benzene and anthracene the quantum capacitance are relatively low.

Table 4.4: Calculated E_{ad} value, charge transferred and quantum capacitance value at 300K for various aromatic radical functionalized graphene with single radical doping.

Configuration	Adsorption energy(eV)m	charge transferred(e)	Quantum capacitance ($\mu F/cm^2$)
Pristine Graphene	-	-	1.300
G-Benzene	-4.191	-0.158	56.522
G-Aniline	-2.321	-0.067	226.040
G-Phenol(para)	-1.261	-0.271	236.624
G-Anthracene	-4.258	-0.461	59.579
G-Toluene	-2.543	0.302	201.542
G-Naphthalene	-0.738	-0.202	213.517

To have a clear insight into the system I have calculated the transferred charge densities for each system. Interestingly, the transfer charges are localized near the unsaturated atoms in the case of aniline, phenol, toluene, and naphthalene radical doped system. Whereas in the case of anthracene and benzene radical doping, the transferred charge is distributed evenly on a comparatively large area. The charge density difference for benzene, anthracene, and phenol radical functionalized graphene is shown in Fig.[4.9]. From the transferred charge density plot one can conclude that the hybridization between graphene and benzene(or anthracene) radical orbitals are much stronger compare to the other radicals adsorptions that push localized states lower in energy deep into the valence band as shown in Fig.[4.8(a & d)] respectively. Hence the electronic density of states near the Fermi level decreases for these two systems and consequently, the quantum capacitance value is reduced to 56.52 $\mu F/cm^2$ & 59.57 $\mu F/cm^2$ for benzene

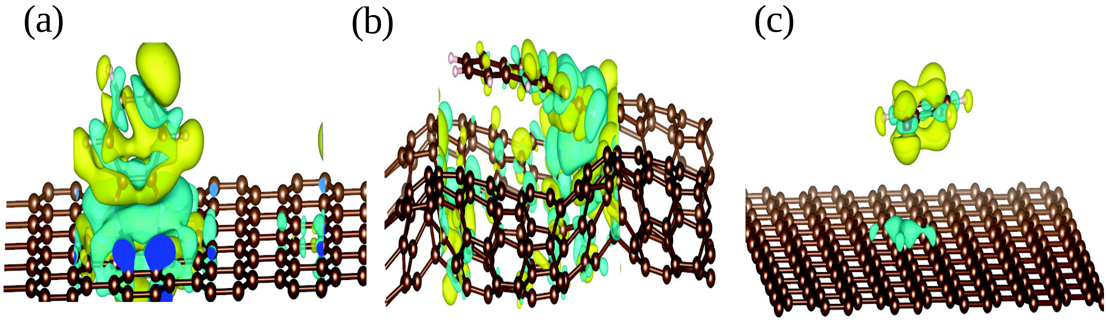

Figure 4.9: Distribution of transferred charge due to (a) benzene (b)anthracene and (c) phenol radical functionalization on graphene. The transferred charges are highly localized in the case of phenol but delocalized in benzene and anthracene radical adsorptions

and anthracene radical functionalization respectively.

4.6 Conclusion

This study investigates quantum capacitance in functionalized graphene doped with various aliphatic and aromatic molecular fragments and their radicals. DFT calculations were performed to analyze the electronic band structure of the functionalized graphene. Our study shows that the C_Q of graphene-based electrodes can be enhanced by functionalizing with aliphatic and aromatic radicals on top of graphene sheets rather than their respective molecules in the pristine graphene surface. These radicals are behaving as magnetic impurities in the system, generates localized density of states near the Fermi energy, consequently, the QC value got increased. The maximum value of quantum capacitance ($\sim$ 237 μF/cm^2) is found for phenol-radical(aromatic) functionalized graphene. Similar value ($\sim$ 235 μF/cm^2) was acquired for acetone-radical (aliphatic) functionalized graphene. These results confirm that the molecules with large aromatic structures are noncovalently attached on the graphene sheets via strong $\pi - \pi$ interactions. The significant p-interactions between donor/acceptor molecules and the graphene were supposed to produce significant charge-transfer effects. The additional charge carriers brought by aromatic molecules and radicals change the carrier concentration in the plane of graphene and lead to the shift of the Fermi level and enhances the quantum capacitance.

Chapter 5

The enhancement of quantum capacitance in chemically modified MoS_2 and h-BN electrodes

5.1 Introduction

Similar to graphene, there are other materials such as MoS_2, h-BN in which layer structures can also be extracted easily from the bulk. MoS_2 belongs to the class of transition metal dichalcogenides. Bulk MoS_2 consists of S-Mo-S layer units, that are kept together by the feeble van der Waals interactions as shown in Fig.(5.1)(Murray and Yoffe 1972). So using physical or chemical methods one or few layers can be easily exfoliated from bulk MoS_2 (Ramakrishna Matte et al. 2010, Chodankar et al. 2020). MoS_2 finds applications in many fields including catalysis, lithium-ion batteries, phototransistors on the basis of their unique morphology, exceptional electrical and mechanical properties (Merki and Hu 2011, Chang and Chen 2011, Li et al. 2011, Phototransistors et al. 2012). However, due to the semiconducting nature of MoS_2 monolayer, it has a very low quantum capacitance that hinders it from supercapacitor applications (Soon and Loh 2007). The lesser electron density of states near Fermi energy of MoS_2 monolayer can be modified using proper functionalization (Li and Zhu 2015, Jiang 2015). A very similar situation may also arise for h-BN layers.

Therefore, in this part of my thesis, I have used different add atoms to functionalized the layer MoS_2 and h-BN. Careful DFT calculations are performed to study the change in electronic band-structure due to functionalization (Mahatha et al. 2012) and subsequently investigated the impact of functionalization on the quantum capacitance. All the calculations are done considering $3\times3\times1$ supercells of MoS_2 layer unit cell, having nine Mo atoms and eighteen sulfur atoms. A single Mo and S atomic sites were selected for substitutional doping. The vacancy defected configurations were studied on the same supercell of MoS_2 with considering different vacancy concentration (Feng et al. 2014). A large vacuum has been considered along the out of the plane direction of MoS_2 (height$>$10Å) layer to avoid the interaction with periodic images.

The study of quantum capacitance in hexagonal boron nitride was done by using a $3\times3\times1$ supercell of h-BN, having nine boron atoms and nine nitrogen atoms. The h-BN top site was the most stable adsorption position for alkali earth metals. Therefore in this study, I have investigated the adsorption of adatoms such as K, Li, and Na on top of h-BN.

The stability of the functionalized structure was investigated by estimating average adsorption energy E_{ad} for ad-atoms using the equation (2.26)

5.2 Quantum capacitance of functionalized MoS_2 monolayer

The electronic bandstructure shows the direct bandgap semiconducting nature of monolayer MoS_2 as shown in Fig.(5.2). The band-edge states are mainly contributed from the d-orbitals of the Mo atoms. As we have already discussed that the electronic bandstructure can be significantly altered by the substitutional doping in MoS_2 monolayer and incorporating vacancy defects. (Wu et al. 2017, Peng et al. 2014, Chang et al. 2014, Zhou et al. 2013, Feng et al. 2014, Xu et al. 2020).

The substitutional doping can be done by selecting the atoms from groups which are nearer to Mo and S atom. Hence I have tried to enhance the quantum capacitance by substituting Mo and S atoms in MoS_2 monolayer with adatoms from various groups in the periodic table. Group-V ad-atoms and halogen family atoms are selected for

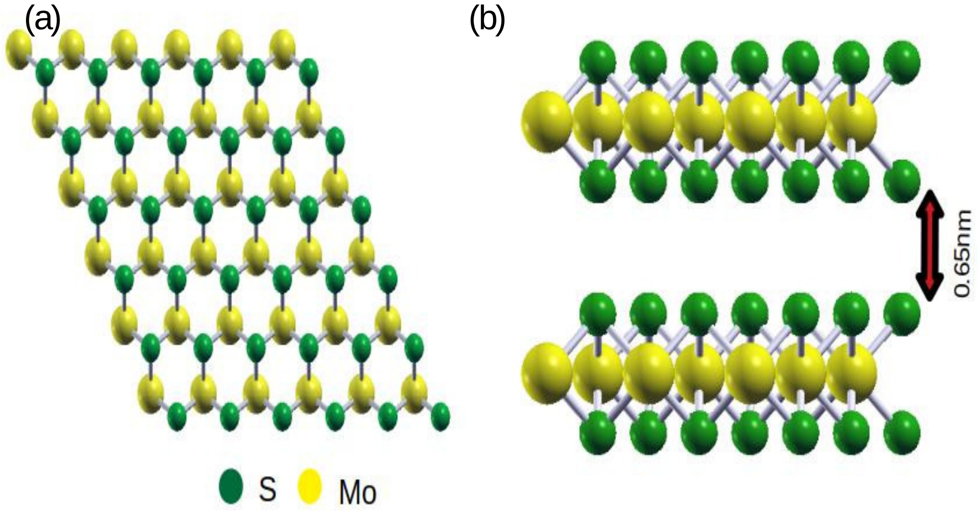

Figure 5.1: The optimized geometric structure of monolayer MoS_2 showing a layer of molybdenum atoms (blue) sandwiched between two layers of sulfur atoms (yellow).

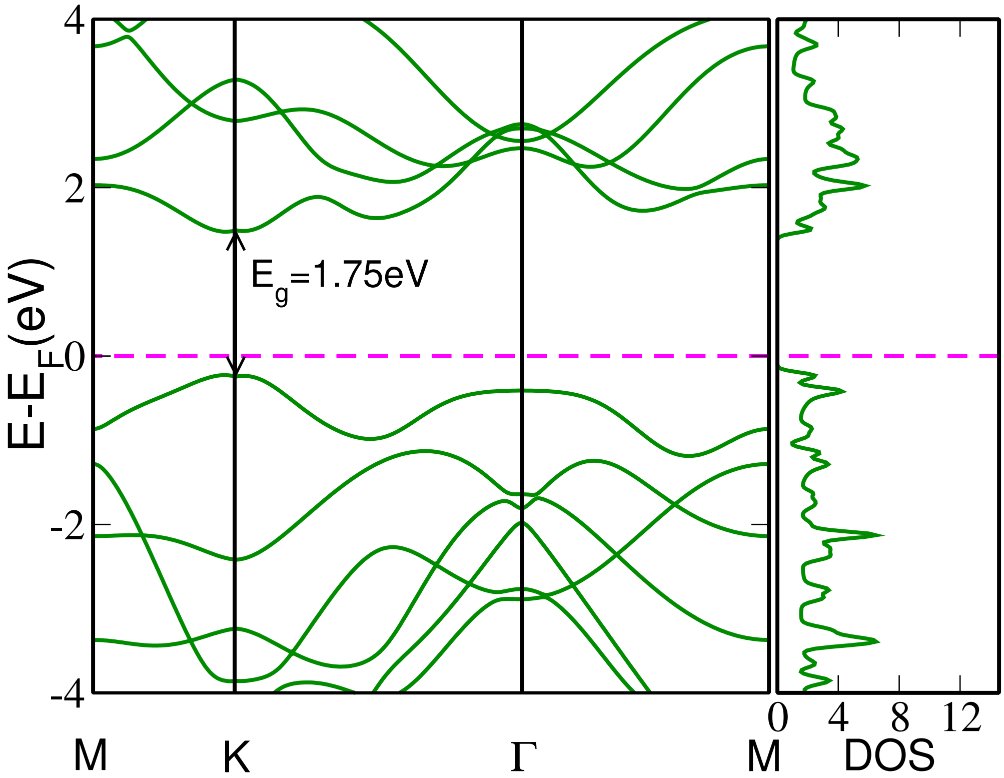

Figure 5.2: Electronic DOS and Bandstructure for MoS_2 Monolayer. Horizontal pink dashed line is the Fermi energy set at E=0.

replacing the S atom whereas transition metal atoms are selected as a replacement for the Mo atom.

The stability of the substituted MoS_2 monolayer structure was examined by estimating average adsorption energy E_{ad} using the equation (2.26). The adsorption energies for various functionalized MoS_2 are listed in the Table.[5.1]. A relatively large negative value of the adsorption energy in each case not only confirms the stability of adatom substituted pristine MoS_2 monolayer but also indicates that these can be easily substituted on the pristine MoS_2 surface.

Table 5.1: Adsorption energy per ad-atoms adsorbs on MoS_2 Monolayer.

ad-atom	**adsorption energy(in eV)**	**ad-atom**	**adsorption energy(in eV)**
N	-2.139	F	-2.039
As	-2.001	Cl	-0.272
Sb	-1.208	Cu	-1.953
Se	-2.091	Ni	-2.142

5.2.1 Substitution of Sulfur with group-V ad-atoms

In the case of pristine MoS_2 monolayer, the value of C_Q is zero due to the semiconducting nature. However, C_Q changes dramatically with substitutional doping. DFT is used with the GGA-PBE method to analyze the substitutional doping effect of the S atom with group-V adatoms. Adatoms such as N, As, Sb, Se was used as group-V substitutional dopants on pristine MoS_2 monolayer as shown in Fig.[5.3].

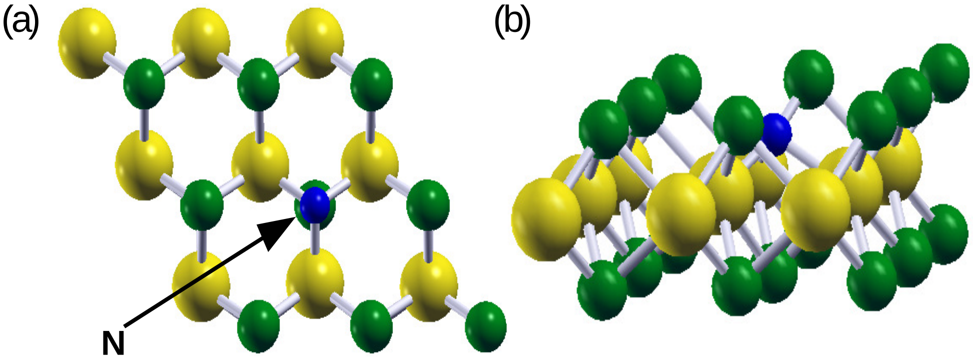

Figure 5.3: The optimized geometric structure of monolayer MoS_2 where Nitrogen replaces Sulfur(a)top view and (b)side view.

In each case, we have observed the accumulation of energy states near the Fermi level. The additional states are mainly contributed from the substituted dopant atoms.

The atom projected density of states for S atom substituted with group V adatoms are shown in Fig.[5.4]. Significant enhancement in quantum capacitance is observed in each modified system except Se doped systems, which shows only 0.595 μF/cm^2 quantum capacitance. The maximum quantum capacitance value of 203 μF/cm^2 was calculated for the nitrogen substituted MoS_2 monolayer as shown in Fig.[5.9]. Relatively large C_Q values of 189 μF/cm^2 and 188 μF/cm^2 have been found for As and Sb doped system respectively.

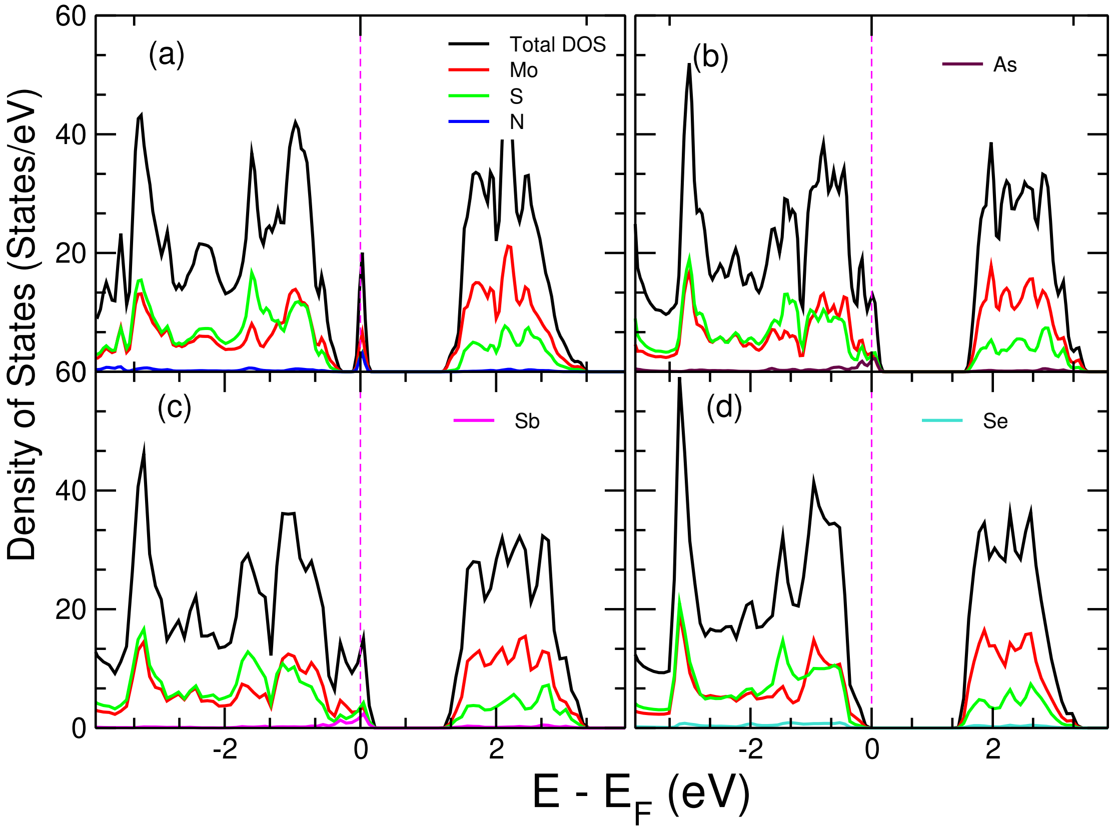

Figure 5.4: Atom projected density of states for functionalized MoS_2 with (a)N, (b)As, (c)Sb and (d)Se atoms. Colored curve represents dos from the doped atom. Vertical majenta dashed line is the Fermi energy set at E=0.

Next, We have investigated the microscopic origin of enhanced C_Q in functionalized MoS_2. One of the main reasons could be the charge redistribution in the presence of substituted ad-atom. To analyze the charge redistribution, the change in electron density associated with functionalized MoS_2 has been calculated. Fig.[5.5] shows the excess charge density (red) and the charge deficiency(green) due to the charge redistribution upon substitutional doping of MoS_2 with N, As, Sb, and Se ad-atoms. The homogeneity in the charge distribution gets significantly disrupted because of the substituted adatoms. Large charge localization near the ad-atom indicated that the accumulation of state near the Fermi energy which in turn enhances the C_Q of the functionalized materials.

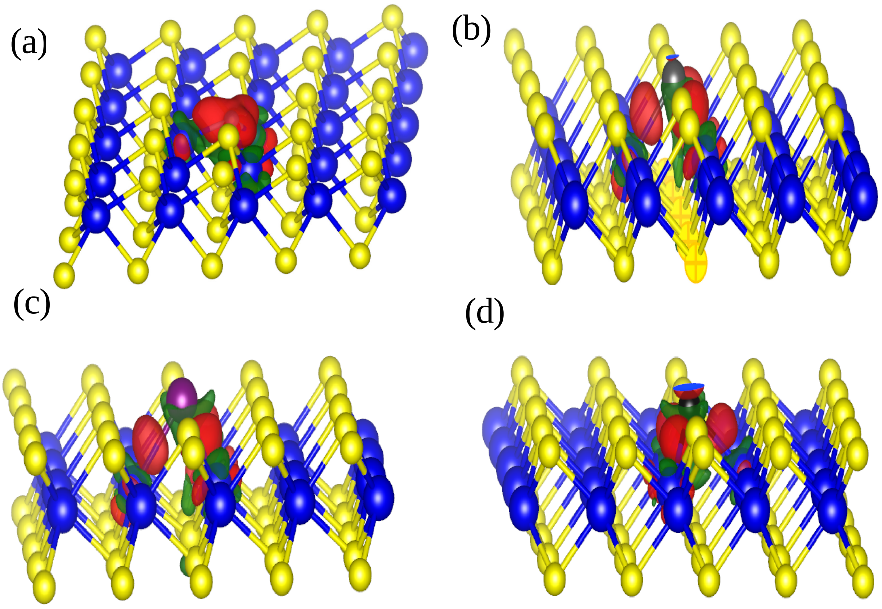

Figure 5.5: Change in electron density associated with Functionalized MoS_2 Monolayer with (a)N, (b)As, (c)Sb and (d)Se doping. Red and green isosurface represents the charge accumulation and electron deficiency in the system. The blue and yellow balls represents Mo and S atoms in MoS_2 Monolayer.

5.2.2 Substitution of Sulfur with group VII ad-atoms

Group-VII adatoms such F and Cl are also used as substitutional dopants for S atom on pristine MoS_2 monolayer is shown in Fig.[5.6]. The atom projected density of states is shown in Fig.[5.7].

It is clear from the DOS plot that these two ad-atom help to accumulate the state near the Fermi energy which in turn improves the quantum capacitance of the system. Our calculation shows that the fluorine substitutes MoS_2 gives a C_Q value of 139 μF/cm^2 at room temperature, whereas the value is significantly increased to 252 μF/cm^2 for Cl-functionalized system as shown in Fig.[5.9].

The electron density difference associated with functionalized MoS_2 with group seven adatoms are shown in Fig.[5.8]. Clearly, the charge localization near the ad-atom

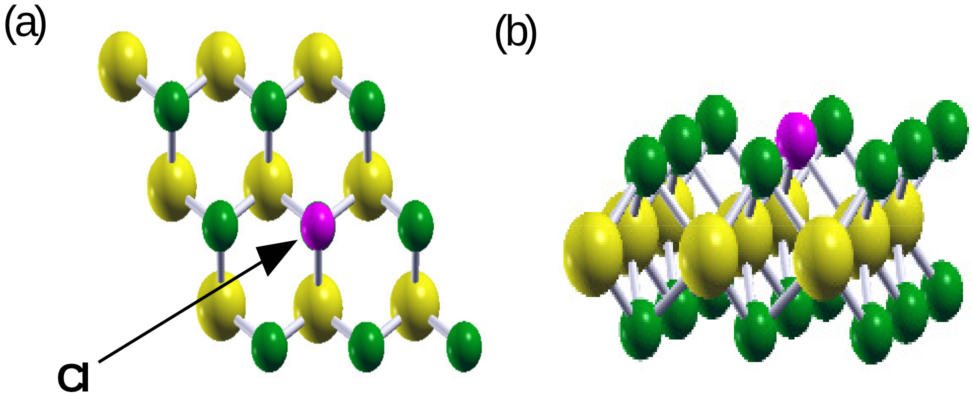

Figure 5.6: The optimized geometric structure of monolayer MoS_2 where Clorine replaces Sulfur(a)top view and (b)side view.

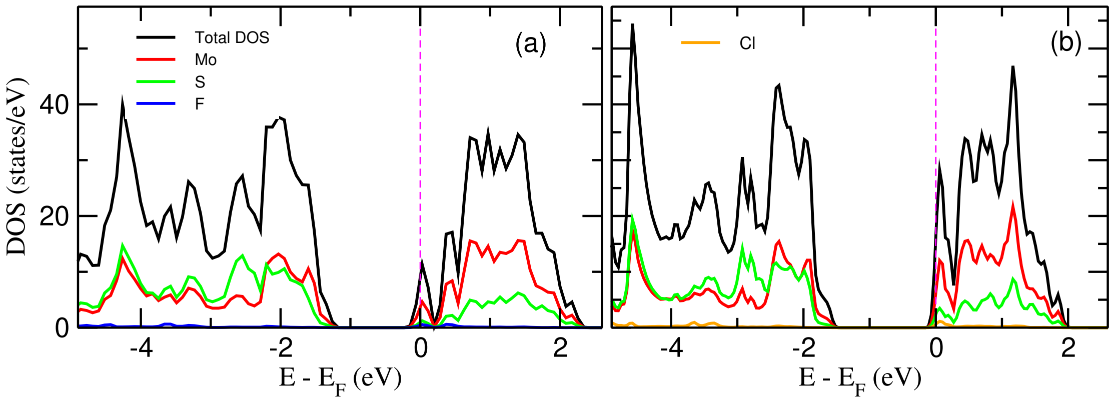

Figure 5.7: Atom projected density of states for functionalized MoS_2 with (a)F and (b)Cl atoms. Colored curve represents dos from the doped atom. Vertical majenta dashed line is the Fermi energy set at E=0.

assists to improve the quantum capacitance in the system.

5.2.3 Substitution of Mo with Transition Metal(TM) ad-atoms

In the next part of our investigation, we have used transition metal adatoms such as Co, Cu, Ni, and V to substitute one Mo atom in pristine MoS_2 monolayer as shown in Fig.[5.10]. A noticeable change in electronic structure has been observed in each functionalized system compare to the pristine MoS_2 monolayer. The atom projected density of states for Mo atom substituted with TM ad-atoms is shown in Fig.[5.11]. All the ad-atoms introduce a new peak of DOS near Fermi energy.

As a consequence, a large enhancement in the quantum capacitance was observed

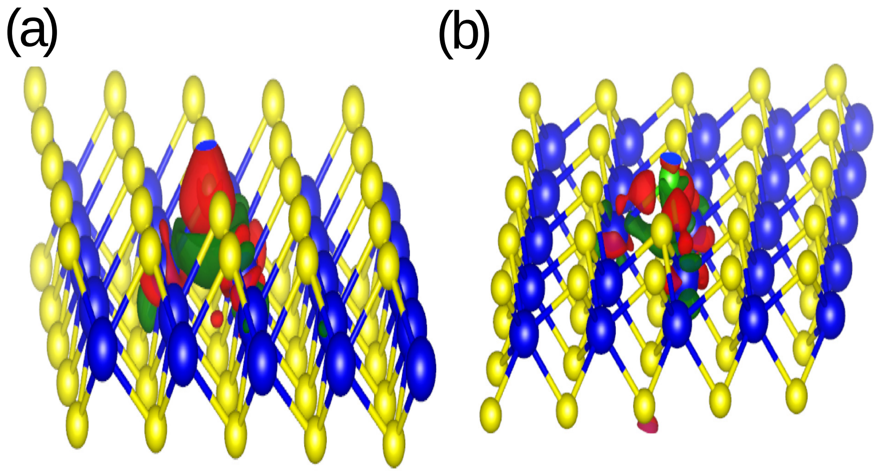

Figure 5.8: Isosurface plots for electron density associated with Functionalized MoS_2 Monolayer with (a)F and (b)Cl. Red and green isosurface represnts the charge accumulation and electron deficiency in the system. The blue and yellow balls represents Mo and S atoms in MoS_2 Monolayer.

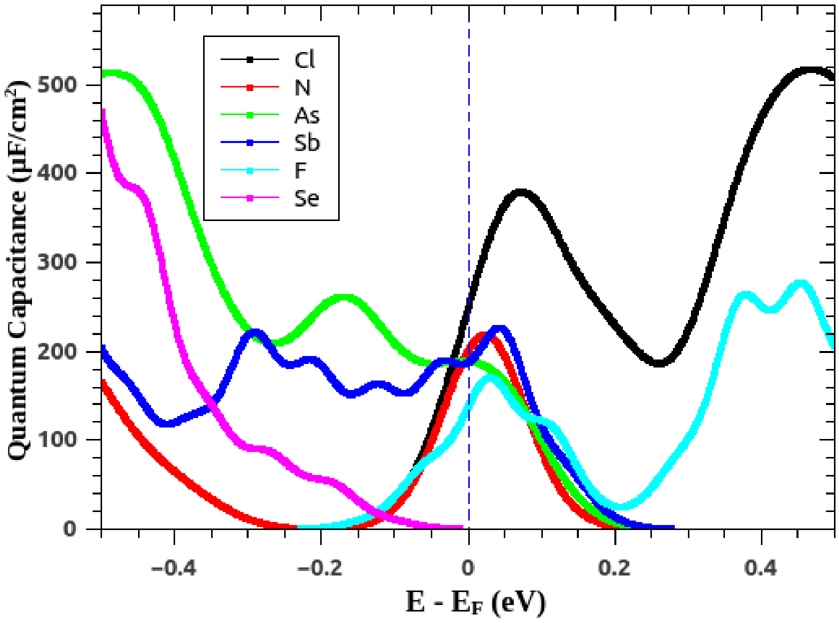

Figure 5.9: The different color curve represents the energy variations of quantum capacitance for MoS_2 Monolayer functionalized with various ad-atoms(Group 5 & 7).

in TM-functionalized MoS_2. Computed values of C_Q for TM doped MoS_2 are listed in Table.[5.2] and the energy variation of C_Q is shown in Fig.[5.12]. To understand the charge redistribution for these systems we have also calculated the difference of

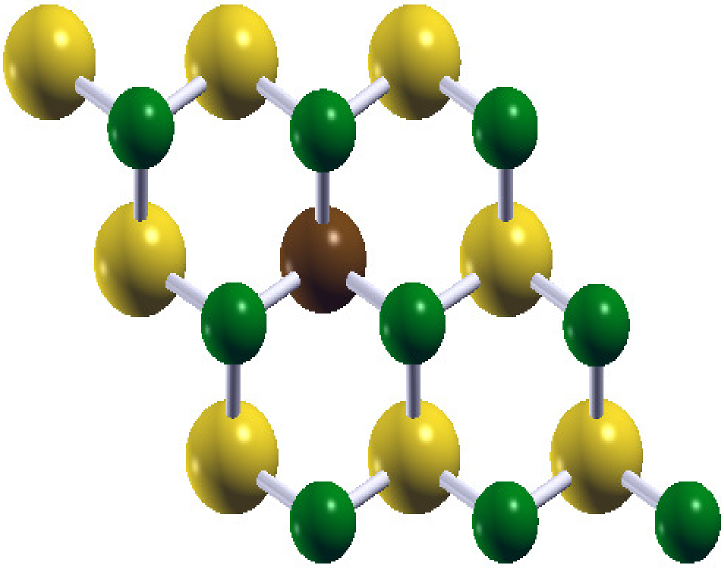

Figure 5.10: The optimized geometric structure of monolayer MoS_2 where Vanadium replaces Molybdenum.

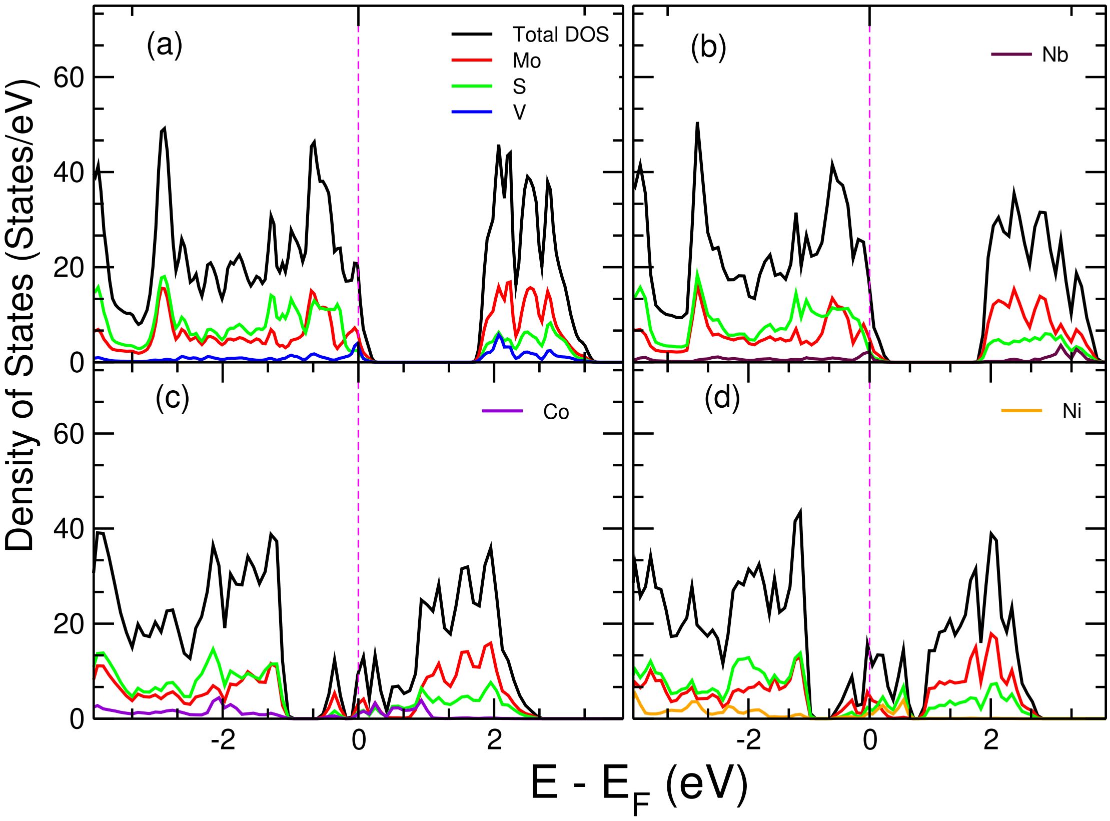

Figure 5.11: Atom projected density of states for functionalized MoS_2 with (a)V, (b)Nb, (c)Co and (d)Ni atoms. Colored curve represents dos from the doped atom. Vertical majenta dashed line is the Fermi energy set at E=0.

electron density and plotted in Fig.[5.13]

Table 5.2: Details of C_Q value calculated at Fermi energy for various ad-atom functionalized MoS_2.

Configuration	**C_Q (μF/cm^2)**	**Configuration**	**C_Q (μF/cm^2)**
FG - Co	152.794	FG - Ni	202.439
FG - Cu	191.658	FG - V	263.721

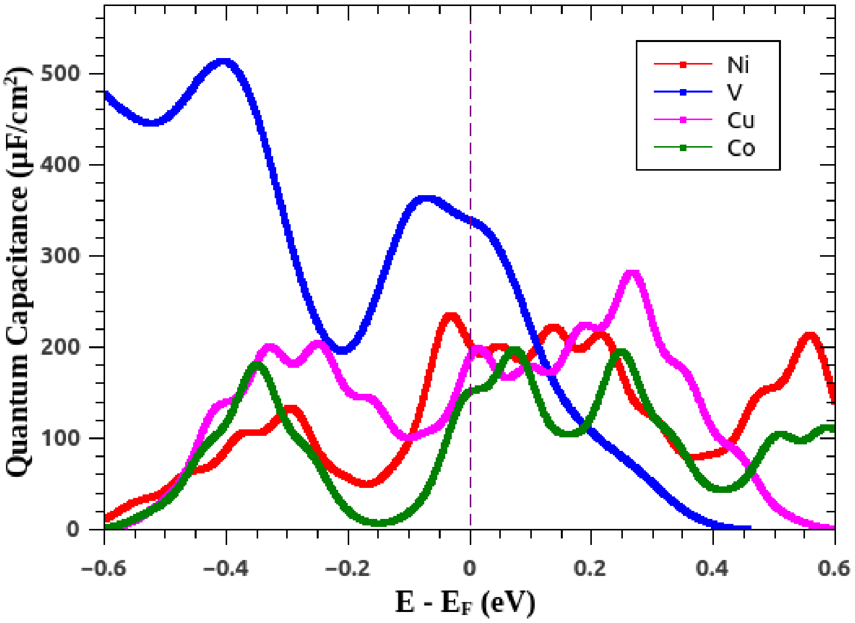

Figure 5.12: The different color curve represents the energy variations of quantum capacitance for MoS_2 Monolayer functionalized with various ad-atoms.

The calculation shows that the charge inhomogeneity increases as we move from group five to group seven to transition metal adatoms doped systems. The maximum charge re-distribution on MoS_2 monolayer caused by cobalt doping as shown in Fig.[5.13]. This may be due to the strong on-site c interaction dominant in the case of transition metals.

5.2.4 Impact of vacancy defects

Similar to graphene functionalization, vacancy defects have also been incorporated to study the variation in quantum capacitance as shown in Fig.[5.14]. The change in the electronic density of states is due to a vacancy defect is shown in Fig.[5.15]

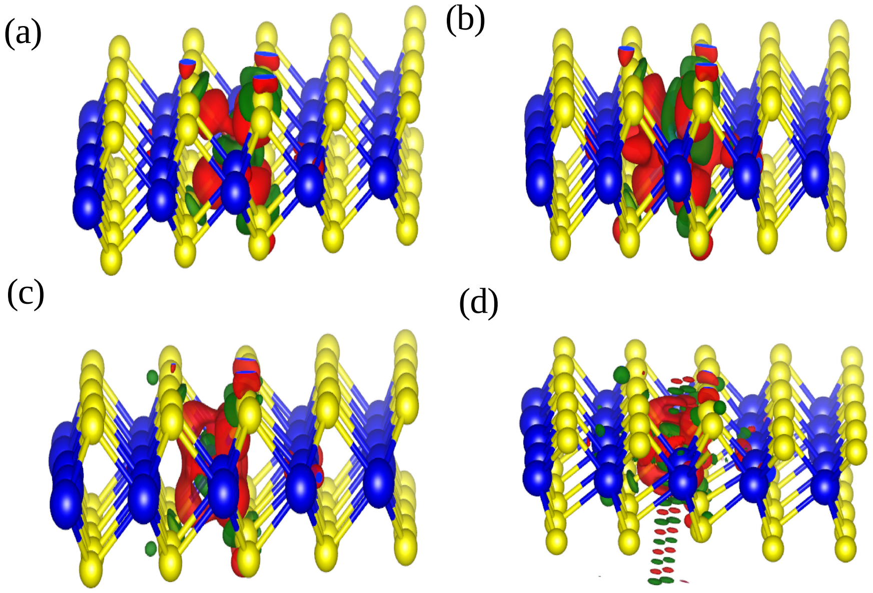

Figure 5.13: Change in electron density associated with Functionalized MoS_2 monolayer with (a)V, (b)Nb, (c)Co and (d)Ni doping. The blue and yellow balls represents Mo and S atoms in MoS_2 Monolayer. The electron accumulation and charge deficiency is represented by the red and green isosurface respectively

.

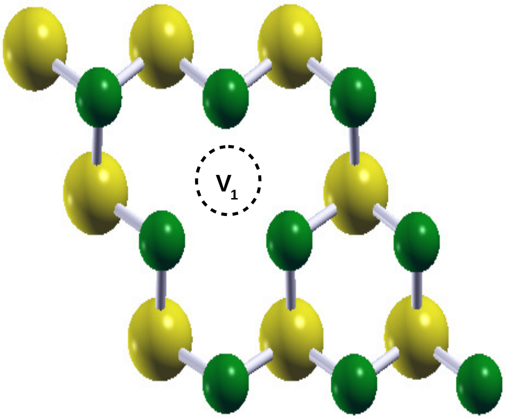

Figure 5.14: The optimized geometric structure of monolayer MoS_2 with monovacancy at Molybdenum site.

We have observed that the sulfur vacancy in the system is comparatively less effective on C_Q value. The calculated value of C_Q f are 0.190 μF/cm^2, 2.5 μF/cm^2 and 33 μF/cm^2 for 5.5 %, 11%, and 16.5% vacancy respectively. On the other hand 11.5% of Mo vacancy greatly improved the quantum capacitance value up to 209 μF/cm^2. The energy variation of C_Q is shown in Fig.[5.16].

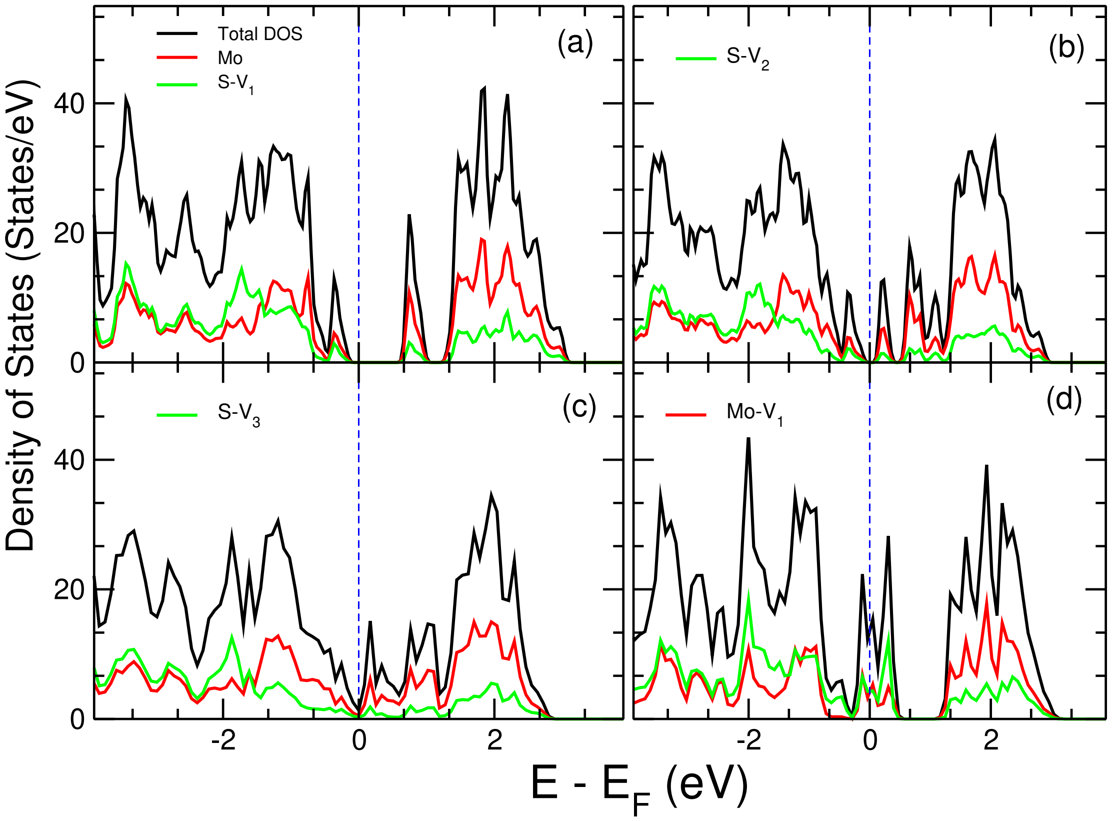

Figure 5.15: Atom projected density of states for MoS_2 Monolayer with (a)One sulfur vacancy, (b)two sulfur vacancy, (c)three sulfur vacancy, (d)one Mo vacancy. Vertical blue dashed line is the Fermi energy set at E=0.

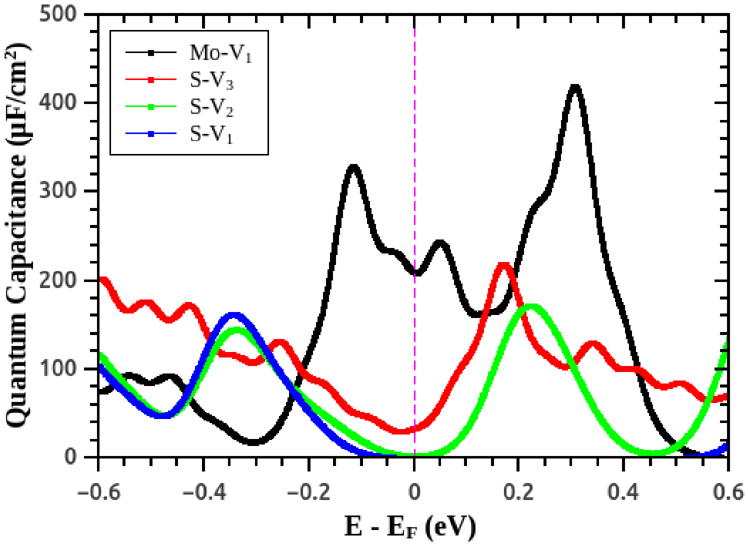

Figure 5.16: The different color curve represents the energy variations of quantum capacitance for MoS_2 functionalized with various ad-atoms

Results show the enhancement in quantum capacitance by changing the semiconducting nature of MoS_2.

Interestingly in most of the cases, the MoS_2 monolayer shows metallic behavior upon the incorporation of vacancy defect that enhances the possibilities of using modified MoS_2 as a suitable material for supercapacitor electrode applications.

5.3 Effect of functionalization on quantum capacitance for hexagonal boron nitride (h-BN)

In the final stage of my work, I have selected another 2D material namely the hexagonal boron nitride(h-BN), which has not been considered as a suitable material for supercapacitor electrode due to its inadequately large bandgap (5.95 eV) (Cassabois et al. 2016). Attempts have been made to overcome this limitation by constructing a van der Waals heterostructure of h-BN with another 2D material. Bhauriyal et.al proposed an electrode of graphene/h-BN heterostructure as an electrode material for Al batteries. They showed graphene/h-BN heterostructure can deliver both a high voltage (2.14 V) as well as a high storage capacity (183 mA h/g), whereas monolayers of graphene and h-BN are either good at delivering higher storage capacity or better net voltage (Bhauriyal et al. 2019).

Functionalization converts h-BN from wide bandgap semiconductor to a metallic system with DOS at the Fermi level (Weng et al. 2016, Cassabois et al. 2016). Thus my attempt was to functionalized these materials with suitable adatoms so that it would be useful for supercapacitor applications. I therefore choose alkali earth metals like K, Li, and Na as shown in Fig.[5.17(a)]. These adatoms improved the electronic density of states at the Fermi level. As a result, the quantum

Table 5.3: Calculated C_Q value at 300 K for various adatom functionalized h-BN.

Configuration	**Quantum Capacitance**($\mu F/cm^2$)
h-BN - K	29.6006
h-BN - Li	38.4761
h-BN - Na	61.5025

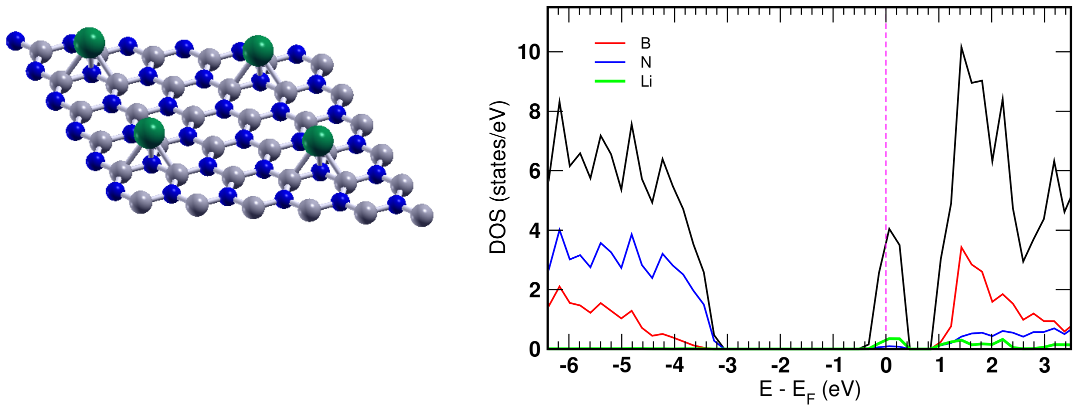

Figure 5.17: (a)Geometric structure for Li doped h-BN and (b)Atom PDOS for Li doped h-BN.

capacitance value got enhanced as listed in Table.[5.3]. The obtained values of quantum capacitance are 29 $\mu F/cm^2$, 38 $\mu F/cm^2$, 61 $\mu F/cm^2$ for K, Li, and Na functionalized h-BN respectively which are not as significant as we obtain for the other systems.

5.4 Conclusion

In conclusion, I have investigated the quantum capacitance of functionalized MoS_2 and h-BN layer materials. The functionalization has been done by replacing Mo and S atoms in MoS_2 monolayer with ad-atoms. Groups five and halogen family atoms were selected for replacing the S atom whereas transition metal atoms were selected as a replacement for the Mo atom. The maximum quantum capacitance value calculated for a single layer of nitrogen substituted MoS_2 is 203 μF/cm^2. And the chlorine substituted system has a value of C_Q 252 μF/cm^2. The computational results show a significant enhancement in quantum capacitance while functionalizing MoS_2 monolayer with transition metals. The substitution with vanadium gives a maximum C_Q of 263 μF/cm^2. The major reason for enhancement is the generation of new electronic states near the Fermi-energy caused by the charge re-distribution on MoS_2 monolayer. Functionalized hexagonal boron nitride with alkali earth metals like K, Li, and Na enhance the C_Q values, however not much improvement in the C_Q value has been observed in these systems. The vacancy defected systems have also been investigated. In the case of MoS_2, the sulfur vacancy is having less effect on C_Q. But a single Mo vacancy greatly improved the quantum capacitance value up to 209 μF/cm^2.

Chapter 6

Summary and Future Work

6.1 Summary

To summarize my work in this thesis, I have performed a detailed investigation of the electronic band structure and quantum capacitance of a group of two-dimensional materials after functionalization towards their use in supercapacitor electrodes. I have used density functional theory as a tool to carry out my investigation. Graphene, the wonder two-dimensional materials have been considered first and functionalized variously. Obtained DFT results show that quantum capacitance in graphene-based electrodes can be significantly increased using chemical modification. Enhancement is possible by incorporating ad-atoms and vacancy defects in the graphene sheet. The functionalization of graphene with ad-atoms of different groups in the periodic table has been looked at effectively.

Our investigation on ad-atom functionalized graphene demonstrates that the quantum capacitance mainly relies upon the sub-lattice positions for adsorption and the concentration of ad-atoms. Doping with ad-atoms gives rise to the creation of new electronic states near the Dirac point and a shift of Fermi level, which in turn assists with accumulating more amounts of charge carriers in functionalized graphene in comparison with pristine graphene. Newly generated DOS that are present in the vicinity of the Fermi-energy, provides a high charge (electron/hole) density near the Fermi level result in an unusually high quantum capacitance in the system.

We found that the improvement was enormous when graphene was functionalized with Sn, N, Cl, and P ad-atoms with specific concentrations. The quantum capacitance of Sn functionalized graphene was found to be 249.477 μF/cm^2. Nitrogenated graphene typically yields a high C_Q of 279.385 μF/cm^2 which was later extended to 423.73 μF/cm^2 in the presence of oxygen atoms in the system. Maximum improvement was observed for Cl functionalization which shows as large as 1141.655 μF/cm^2 quantum capacitance. Our investigation also predicts that Cl functionalization is more feasible when deformation present in the graphene that also provides additional enhancement of C_Q in the framework. Eventually, the temperature variation study of quantum capacitance shows that C_Q remains very large in Cl and N functionalized graphene in a wide range of temperatures.

Next, we have functionalized graphene with the different organic molecules and their radicals. Our investigation shows that the quantum capacitance in graphene-based electrodes can also be improved by the functionalization of graphene with the aliphatic and aromatic molecules and their radicals. Results show that aromatic/aliphatic molecules and their radicals are well-adsorbed on the graphene sheets through strong π-interactions. A significant charge transfer and charge re-distribution happen in donor/acceptor molecule doped graphene. The extra charge carriers brought by aromatic/aliphatic molecules and their radicals change the carrier concentration in graphene that gives rise to the shift of the Fermi level. The improvement is more prominent when graphene is functionalized with radicals instead of their respective molecules. These radicals are acting as impurities in the system, produce localized density of states close to the Fermi energy. A very high C_Q (above 200μF/cm2) compared to pristine graphene has been observed.

At the final stage of our investigation, I have considered two other well-known two-dimensional materials such as MoS_2 and h-BN. They are semiconducting in nature. Therefore functionalization has been done to improve their functionality and make them suitable for supercapacitor electrode applications. Our study shows that the quantum capacitance (C_Q) of MoS_2 electrodes can be enhanced significantly by introducing ad-atoms and vacancy defects in the monolayer MoS_2 sheet. A marked quantum capacitance above 200 μ F/cm^2 has been observed in the functionalized monolayer MoS_2. Calculations show that the quantum capacitance of MoS_2 monolayer enhances with substitutional doping of Mo with transition metal adatoms. The substitution with vanadium gives a maximum C$_Q$ of 263 μF/cm^2. The major reason for enhancement is the generation of new electronic states near the Fermi-energy caused by the charge re-distribution on MoS$_2$ monolayer. The vacancy defected MoS$_2$ has also been investigated. Our calculation shows that the sulfur vacancy is having less effect on C$_Q$, whereas a single Mo vacancy greatly improved the quantum capacitance value up to 209 μF/cm^2.

Functionalized hexagonal boron nitride with alkali earth metals like K, Li, and Na enhance the C$_Q$ values, however not much improvement in the C$_Q$ value has been observed in these systems.

6.2 Future Scope of work

Design and investigation of functionalized materials for supercapacitor application is a new and highly demanding field of research. In this thesis, I have developed and reported a systematic route to improve and investigate the quantum capacitance in various two-dimensional materials. However, there are many open challenges that need to be addressed to improve the supercapacitor performances. Some of them are listed below

- There are possibilities of improving the quantum capacitance of supercapacitor electrodes considering hybrid structures of graphene, MoS$_2$ and h-BN, detail electronic behavior of such system is yet to be explored.
- Impact of chemical modifications on the capacitor performance of graphene-ionic liquid systems remains largely unexplored, which needs further investigation.
- A good theoretical model for the calculation of total ion density at the surface and the interface of supercapacitor electrodes is not available, which is very essential for the proper estimation of the performance of a supercapacitor. In the future, I would like to continue my research in this area and develop a feasible model for the calculation of total ion density at the surface of different supercapacitor electrodes.

References

Ahmad, S. and Mukherjee, S. (2014). A Comparative Study of Electronic Properties of Bulk MoS 2 and Its Monolayer Using DFT Technique : Application of Mechanical Strain on MoS 2 Monolayer. (October):52–59.

Aikebaier, F., Pertsova, A., and Canali, C. M. (2015). Effects of short-range electron-electron interactions in doped graphene. *Physical Review B - Condensed Matter and Materials Physics*, 92(15).

Allen, M. (2009). Honeycomb carbon – A study of graphene. *American Chemical Society*, page 184.

Amiri, A., Shanbedi, M., Ahmadi, G., Eshghi, H., Kazi, S. N., Chew, B. T., Savari, M., and Zubir, M. N. M. (2016). Mass production of highly-porous graphene for high-performance supercapacitors. *Scientific Reports*.

Bhauriyal, P., Bhattacharyya, G., Rawat, K. S., and Pathak, B. (2019). Graphene/hbn heterostructures as high-capacity cathodes with high voltage for next-generation aluminum batteries. *Journal of Physical Chemistry C*, 123(7):3959–3967.

Bhushan, B. S. and Srivastava, A. (2018). Integrated and differential quantum capacitance of graphene: A DFT study. *AIP Conference Proceedings*, 1953.

Bissett, M. A., Kinloch, I. A., and Dryfe, R. A. W. (2015). Characterization of MoS 2 –Graphene Composites for High-Performance Coin Cell Supercapacitors. *ACS Applied Materials & Interfaces*, 7(31):17388–17398.

Blöchl, P. E. (1994a). Projector augmented-wave method. *Phys. Rev. B*, 50(24):17953–17979.

Blöchl, P. E. (1994b). Projector augmented-wave method. *Physical Review B*, 50(24):17953–17979.

Bottari, G., Ángeles Herranz, M., Wibmer, L., Volland, M., Rodríguez-Pérez, L., Guldi, D. M., Hirsch, A., Martín, N., D'Souza, F., and Torres, T. (2017). Chemical functionalization and characterization of graphene-based materials. *Chemical Society Reviews*, 46(15):4464–4500.

Bouša, D., Luxa, J., Mazánek, V., Jankovský, O., Sedmidubský, D., Klímová, K., Pumera, M., and Sofer, Z. (2016). Toward graphene chloride: Chlorination of graphene and graphene oxide. *RSC Advances*, 6(71):66884–66892.

Brousse, T., Bélanger, D., Chiba, K., Egashira, M., Favier, F., Long, J., Miller, J. R., Morita, M., Naoi, K., Simon, P., and Sugimoto, W. (2017). Materials for electrochemical capacitors. *Springer Handbooks*, pages 495–561.

Burt, R., Breitsprecher, K., Daffos, B., Taberna, P. L., Simon, P., Birkett, G., Zhao, X. S., Holm, C., and Salanne, M. (2016). Capacitance of Nanoporous Carbon-Based Supercapacitors Is a Trade-Off between the Concentration and the Separability of the Ions. *Journal of Physical Chemistry Letters*, 7(19):4015–4021.

Cassabois, G., Valvin, P., and Gil, B. (2016). Hexagonal boron nitride is an indirect bandgap semiconductor. *Nature Photonics*, 10(4):262–266.

Centre, S. and Kumar, C. (2014). High performance supercapacitor electrode material based on in situ reduced Graphene oxide wrapped Manganese Carbonate. *International Journal of Latest Research in Science and Technology*, 3(3):65–69.

Chang, J., Larentis, S., Tutuc, E., Register, L. F., and Banerjee, S. K. (2014). Atomistic simulation of the electronic states of adatoms in monolayer MoS2. *Applied Physics Letters*, 104(14):1–15.

Chang, K. and Chen, W. (2011). In situ synthesis of MoS2/graphene nanosheet composites with extraordinarily high electrochemical performance for lithium ion batteries. *Chemical Communications*, 47(14):4252–4254.

Chen, L., Li, X., Ma, C., Wang, M., and Zhou, J. (2017). Interaction and Quantum Capacitance of Nitrogen/Sulfur Co-Doped Graphene: A Theoretical Calculation. *Journal of Physical Chemistry C*, 121(34):18344–18350.

Chodankar, N. R., Nanjundan, A. K., Losic, D., Dubal, D. P., and Baek, J. B. (2020). Graphene and molybdenum disulphide hybrids for energy applications: an update. *Materials Today Advances*, 6.

Cities, M. T. (2016). Graphene Quantum Capacitance Varactors. (April 2015).

Cooper, D. R., D'Anjou, B., Ghattamaneni, N., Harack, B., Hilke, M., Horth, A., Majlis, N., Massicotte, M., Vandsburger, L., Whiteway, E., and Yu, V. (2012). Experimental Review of Graphene. *ISRN Condensed Matter Physics*, 2012:1–56.

de Moraes, E. E., Tonel, M. Z., Fagan, S. B., and Barbosa, M. C. (2019). Density functional theory study of π-aromatic interaction of benzene, phenol, catechol, dopamine isolated dimers and adsorbed on graphene surface. *Journal of Molecular Modeling*, 25(10).

De Oliveira, I. S. and Miwa, R. H. (2015). Organic molecules deposited on graphene: A computational investigation of self-assembly and electronic structure. *Journal of Chemical Physics*, 142(4).

Dimakis, N., Valdez, D., Flor, F. A., Salgado, A., Adjibi, K., Vargas, S., and Saenz, J. (2017). Density functional theory calculations on alkali and the alkaline Ca atoms adsorbed on graphene monolayers. *Applied Surface Science*, 413:197–208.

Dobrota, A. S., Paš, I. A., Mentus, S. V., and Skorodumova, N. V. (2016). A general view on the reactivity of the oxygen-functionalized graphene basal plane. *Phys. Chem. Chem. Phys. Phys. Chem. Chem. Phys*, 18(18):6580–6586.

Dreyer, D. R., Park, S., Bielawski, W., and Ruoff, R. S. (2010). The chemistry of graphene oxide.

Dröscher, S., Roulleau, P., Molitor, F., Studerus, P., Stampfer, C., Ensslin, K., and Ihn, T. (2010). Quantum capacitance and density of states of graphene. *Applied Physics Letters*, 96(15).

Dž, K., Korać, F., and Gutić, S. (2015). Bulletin of the Chemists and Technologists of Bosnia and Herzegovina Graphite , Graphite Oxide , Graphene Oxide , and Reduced Graphene Oxide as Active Materials for Electrochemical Double Layer Capacitors : A comparative Study.

Editor, G., Hobza, P., Cozzi, F., Annunziata, R., Benaglia, M., Kim, K., Aguirre, G., Estrada, J., Siegel, J. S., Chem, P. C., Amicangelo, J. C., Gung, B. W., Irwin, D. G., Romano, N. C., Chem, P., Phys, C., Morgado, C. A., Hillier, I. H., Burton, N. A., Mcdouall, J. J. W., Chem, P., Phys, C., Riley, K. E., and Hobza, P. (2008). acid bases.

El-Kady, M. F., Shao, Y., and Kaner, R. B. (2016). Graphene for batteries, supercapacitors and beyond. *Nature Reviews Materials*, 1(7):16033.

Elias, D. C., Gorbachev, R. V., Mayorov, A. S., Morozov, S. V., Zhukov, A. A., Blake, P., Ponomarenko, L. A., Grigorieva, I. V., Novoselov, K. S., Guinea, F., and Geim, A. K. (2011). Dirac cones reshaped by interaction effects in suspended graphene. *Nat Phys*, 7(9):701–704.

Erickson, B. K., Erni, R., Lee, Z., Alem, N., Gannett, W., and Zettl, A. (2010). Determination of the Local Chemical Structure of Graphene Oxide and Reduced Graphene Oxide. pages 4467–4472.

Fang, T., Konar, A., Xing, H., and Jena, D. (2007). Carrier statistics and quantum capacitance of graphene sheets and ribbons. *Appl. Phys. Lett. Additional information on Appl. Phys. Lett. Journal Homepage*, 91.

Fedorov, M. V. (2014). Screening of Ion−Graphene Electrode Interactions by Ionic Liquids.pdf. (ii).

Feng, L. P., Su, J., Chen, S., and Liu, Z. T. (2014). First-principles investigations on vacancy formation and electronic structures of monolayer MoS2. *Materials Chemistry and Physics*, 148(1-2):5–9.

Fujimoto, Y. (2015). Formation, energetics, and electronic properties of graphene monolayer and bilayer doped with heteroatoms. *Advances in Condensed Matter Physics*, 2015.

Georgakilas, V., Otyepka, M., Bourlinos, A. B., Chandra, V., Kim, N., Kemp, K. C., Hobza, P., Zboril, R., and Kim, K. S. (2012). Functionalization of graphene: Covalent and non-covalent approach. *Chemical Reviews*, 112(11):6156–6214.

Gómez-Navarro, C., Meyer, J. C., Sundaram, R. S., Chuvilin, A., Kurasch, S., Burghard, M., Kern, K., and Kaiser, U. (2010). Atomic structure of reduced graphene oxide. *Nano Letters*, 10(4):1144–1148.

Grimme, S. (2006). Semiempirical GGA-Type Density Functional Constructedwith a Long-Range Dispersion Correction. *Journal of computational chemistry*, 27:1787–1799.

Gu, D. and Fein, J. B. (2015). Adsorption of metals onto graphene oxide: Surface complexation modeling and linear free energy relationships. *Colloids and Surfaces A: Physicochemical and Engineering Aspects*.

Hanlumyuang, Y. and Sharma, P. (2014). Quantum capacitance: A perspective from physics to nanoelectronics. *Jom*, 66(4):660–663.

Hirunsit, P., Liangruksa, M., and Khanchaitit, P. (2016). Electronic structures and quantum capacitance of monolayer and multilayer graphenes influenced by Al, B, N and P doping, and monovacancy: Theoretical study. *Carbon*, 108:7–20.

Huang, X., Qi, X., Boey, F., and Zhang, H. (2012). Graphene-based composites. *Chemical Society Reviews*, 41(2):666–686.

Hussain, A., Ullah, S., and Farhan, M. A. (2016). Fine tuning of band-gap of graphene by atomic and molecular doping: A density functional theory study. *RSC Advances*, 6:55990–56003.

Hwang, H., Kim, H., and Cho, J. (2011). MoS2 nanoplates consisting of disordered graphene-like layers for high rate lithium battery anode materials. *Nano Letters*, 11(11):4826–4830.

Hwang, Y. H., Chun, H. S., Ok, K. M., Lee, K. K., and Kwak, K. (2015). Density Functional Investigation of Graphene Doped with Amine-Based Organic Molecules. *Journal of Nanomaterials*, 2015.

Ito, J., Nakamura, J., and Natori, A. (2008). Semiconducting nature of the oxygen-adsorbed graphene sheet. *Journal of Applied Physics*, 103(11).

Iyakutti, K., Kumar, E. M., Lakshmi, I., Thapa, R., Rajeswarapalanichamy, R., Surya, V. J., and Kawazoe, Y. (2015). Effect of surface doping on the band structure of graphene: a DFT study. *Journal of Materials Science: Materials in Electronics*, pages 1–13.

Iyakutti, K., Mathan Kumar, E., Thapa, R., Rajeswarapalanichamy, R., Surya, V. J., and Kawazoe, Y. (2016). Effect of multiple defects and substituted impurities on the band structure of graphene: a DFT study. *Journal of Materials Science: Materials in Electronics*, 27(12):12669–12679.

Jeong, H. M., Lee, J. W., Shin, W. H., Choi, Y. J., Shin, H. J., Kang, J. K., and Choi, J. W. (2011). Nitrogen-doped graphene for high-performance ultracapacitors and the importance of nitrogen-doped sites at basal planes. *Nano Letters*, 11(6):2472–2477.

Jha, P. K., Singh, S. K., Kumar, V., Rana, S., Kurungot, S., and Ballav, N. (2017). High-Level Supercapacitive Performance of Chemically Reduced Graphene Oxide. *Chem*, 3(5):846–860.

Jia, T. T., Sun, B. Z., Lin, H. X., Li, Y., and Chen, W. K. (2013). Bonding of hydroxyl and epoxy groups on graphene: Insights from density functional calculations. *Jiegou Huaxue*, 32(10):1475–1484.

Jiang, J., Cao, D., Jiang, D. E., and Wu, J. (2014). Kinetic charging inversion in ionic liquid electric double layers. *Journal of Physical Chemistry Letters*, 5(13):2195–2200.

Jiang, J.-W. (2015). Graphene versus MoS2: A short review. *Frontiers of Physics*, 10(3):287–302.

Kang, B., Liu, H., and Lee, J. Y. (2014). Oxygen adsorption on single layer graphyne: a DFT study. *Phys. Chem. Chem. Phys.*, 16(3):974–980.

Karthika, P. (2012). Functionalized Exfoliated Graphene Oxide as Supercapacitor Electrodes. *Soft Nanoscience Letters*, 02(October):59–66.

Kaverzin, A. A., Strawbridge, S. M., Price, A. S., Withers, F., Savchenko, A. K., and Horsell, D. W. (2011). Electrochemical doping of graphene with toluene. *Carbon*, 49(12):3829–3834.

Ke, Q. and Wang, J. (2016). Graphene-based Materials for Supercapacitor Electrodes - A Review. *Journal of Materiomics*, 2(1):37–54.

Kim, T. Y., Lee, H. W., Stoller, M., Dreyer, D. R., Bielawski, C. W., Ruoff, R. S., and Suh, K. S. (2010). High-Performance Supercapacitors. XXX(Xx).

Kim, T. Y., Lee, H. W., Stoller, M., Dreyer, D. R., Bielawski, C. W., Ruoff, R. S., and Suh, K. S. (2011). High-performance supercapacitors based on poly(ionic liquid)-modified graphene electrodes. *ACS Nano*.

Kliros, G. S. (2010). A phenomenological model for the quantum capacitance of monolayer and bilayer graphene devices. *Romanian Journal of Information Science and Technology*, 13(4):332–341.

Kliros, G. S. (2015). Chapter 13 Quantum Capacitance of Graphene Sheets and Nanoribbons. 183:171–183.

Kliros, G. S. (2016). Quantum Capacitance of Graphene.

Kotov, V. N., Uchoa, B., Pereira, V. M., Guinea, F., and Castro Neto, A. H. (2012). Electron-electron interactions in graphene: Current status and perspectives. *Reviews of Modern Physics*, 84(3):1067–1125.

Kresse, G. and Furthmüller, J. (1996a). Efficiency of ab-initio total energy calculations for metals and semiconductors using a plane-wave basis set. *Computational Materials Science*, 6(1):15–50.

Kresse, G. and Furthmüller, J. (1996b). Efficient iterative schemes for ab initio total-energy calculations using a plane-wave basis set. *Physical Review B*, 54(16):11169–11186.

Kumar, N. A., Dar, M. A., Gul, R., and Baek, J. B. (2015). Graphene and molybdenum disulfide hybrids: Synthesis and applications. *Materials Today*, 18(5):286–298.

Lazar, P., Karlický, F., Jurecka, P., Kocman, M., Otyepková, E., Šafářová, K., and Otyepka, M. (2013). Adsorption of small organic molecules on graphene. *Journal of the American Chemical Society*, 135(16):6372–6377.

Li, B., Saito, T., and Okamoto, N. (2018). First principles calculation of the structure and quantum capacity of acidic functional groups on graphene-based capacitor. *2018 International Conference on Electronics Packaging and iMAPS All Asia Conference, ICEP-IAAC 2018*, pages 539–542.

Li, X. and Zhu, H. (2015). Two-dimensional MoS2: Properties, preparation, and applications. *Journal of Materiomics*, 1(1):33–44.

Li, Y., Wang, H., Xie, L., Liang, Y., Hong, G., and Dai, H. (2011). MoS2 nanoparticles grown on graphene: An advanced catalyst for the hydrogen evolution reaction. *Journal of the American Chemical Society*, 133(19):7296–7299.

Lin, H., Fratesi, G., and Brivio, G. P. (2015). Graphene magnetism induced by covalent adsorption of aromatic radicals. *Physical Chemistry Chemical Physics*, 17(3):2210–2215.

Lin, Y. C., Dumcenco, D. O., Huang, Y. S., and Suenaga, K. (2014). Atomic mechanism of the semiconducting-to-metallic phase transition in single-layered MoS 2. *Nature Nanotechnology*, 9(5):391–396.

Lonkar, S. P., Deshmukh, Y. S., and Abdala, A. A. (2015). Recent advances in chemical modifications of graphene. *Nano Research*, 8(4):1039–1074.

Ma, G., Peng, H., Mu, J., Huang, H., Zhou, X., and Lei, Z. (2013). In situ intercalative polymerization of pyrrole in graphene analogue of MoS2 as advanced electrode material in supercapacitor. *Journal of Power Sources*, 229:72–78.

Mahatha, S. K., Patel, K. D., and Menon, K. S. (2012). Electronic structure investigation of MoS 2 and MoSe 2 using angle-resolved photoemission spectroscopy and abinitio band structure studies. *Journal of Physics Condensed Matter*, 24(47).

Majumdar, D. (2016). Functionalized-Graphene/Polyaniline Nanocomposites as Proficient Energy Storage Material: An Overview. *Innov Ener Res*, 5.

Marsden, A. J., Brommer, P., Mudd, J. J., Dyson, M. A., Cook, R., Asensio, M., Avila, J., Levy, A., Sloan, J., Quigley, D., Bell, G. R., and Wilson, N. R. (2015). Effect of oxygen and nitrogen functionalization on the physical and electronic structure of graphene. *Nano Research*.

Merki, D. and Hu, X. (2011). Recent developments of molybdenum and tungsten sulfides as hydrogen evolution catalysts. *Energy and Environmental Science*, 4(10):3878–3888.

Milowska, K. Z., Birowska, M., and Majewski, J. A. (2013). Mechanical, electronic, and transport properties of functionalized graphene monolayers from ab initio studies. *AIP Conference Proceedings*, 1566(December 2015):123–124.

min Ding, Y., jie Shi, J., Zhang, M., he Jiang, X., xia Zhong, H., Huang, P., Wu, M., and Cao, X. (2016). Improvement of n-type conductivity in hexagonal boron nitride monolayers by doping, strain and adsorption. *RSC Advances*, 6(35):29190–29196.

Mirlin, A. D. (2005). Electron transport in graphene. 666(2004):2005–2006.

Mkhoyan, K. A., Contryman, A. W., Silcox, J., Stewart, D. A., Eda, G., Mattevi, C., Miller, S., and Chhowalla, M. (2009). Atomic and electronic structure of graphene-oxide. *Nano Letters*, 9(3):1058–1063.

Mo Jeong, H., Woo Lee, J., Ho Shin, W., Jeong Choi, Y., Joon Shin, H., Ku Kang, J., and Wook Choi, J. (2011). Nitrogen-Doped Graphene for High-Performance Ultracapacitors and the Importance of Nitrogen-Doped Sites at Basal Planes. *Nano Letters*, 11(6):2472–2477.

Mousavi-Khoshdel, M., Targholi, E., and Momeni, M. J. (2015). First-Principles Calculation of Quantum Capacitance of Codoped Graphenes as Supercapacitor Electrodes. *Journal of Physical Chemistry C*, 119(47):26290–26295.

Mousavi-Khoshdel, S. M. and Targholi, E. (2015). Exploring the effect of functionalization of graphene on the quantum capacitance by first principle study. *Carbon*, 89:148–160.

Mukherjee, S. and Kaloni, T. P. (2012). Electronic properties of boron- and nitrogen-doped graphene: A first principles study. *Journal of Nanoparticle Research*, 14(8).

Murray, R. B. and Yoffe, A. D. (1972). The band structures of some transition metal dichalcogenides: Band structures of the titanium dichalcogenides. *Journal of Physics C: Solid State Physics*, 5(21):3038–3046.

Nakada, K. and Ishii, A. (2011). DFT Calculation for Adatom Adsorption on Graphene. *Graphene Simulation*.

Neilson, D., Perali, A., and Zarenia, M. (2016). Many-body electron correlations in graphene. *Journal of Physics: Conference Series*, 702(1).

Novoselov, K. S., Geim, A. K., Morozov, S. V., Jiang, D., Katsnelson, M. I., Grigorieva, I. V., Dubonos, S. V., and Firsov, A. A. (2005). Two-dimensional gas of massless Dirac fermions in graphene. *Nature*, 438(7065):197–200.

Olaniyan, O., Mapasha, R. E., Momodu, D. Y., Madito, M. J., Kahleed, A. A., Ugbo, F. U., Bello, A., Barzegar, F., Oyedotun, K., and Manyala, N. (2016). Exploring the stability and electronic structure of beryllium and sulphur co-doped graphene: a first principles study. *RSC Adv.*, 6(91):88392–88402.

Ooi, N., Rajan, V., Gottlieb, J., Catherine, Y., and Adams, J. B. (2006). Structural properties of hexagonal boron nitride. *Modelling and Simulation in Materials Science and Engineering*, 14(3):515–535.

Paek, E., Pak, A. J., and Hwang, G. S. (2012). A Computational Study of the Interfacial Structure and Capacitance of Graphene in [BMIM][PF6] Ionic Liquid. *Journal of the Electrochemical Society*.

Paek, E., Pak, A. J., Kweon, K. E., and Hwang, G. S. (2013). On the origin of the enhanced supercapacitor performance of nitrogen-doped graphene. *Journal of Physical Chemistry C*, 117(11):5610–5616.

Pak, A. J., Paek, E., and Hwang, G. S. (2013). Tailoring the performance of graphene-based supercapacitors using topological defects : A theoretical assessment. *Carbon*, 68(512):734–741.

Pak, A. J., Paek, E., and Hwang, G. S. (2014). Tailoring the performance of graphene-based supercapacitors using topological defects: A theoretical assessment. *Carbon*.

Parq, J. H., Yu, J., Kwon, Y. K., and Kim, G. (2010). Tunable charge donation and spin polarization of metal adsorbates on graphene using an applied electric field. *Physical Review B - Condensed Matter and Materials Physics*.

Peng, X., Peng, L., Wu, C., and Xie, Y. (2014). Two dimensional nanomaterials for flexible supercapacitors. *Chemical Society Reviews*, 43(10):3303–3323.

Perdew, J. P., Burke, K., and Ernzerhof, M. (1996). Generalized gradient approximation made simple. *Physical Review Letters*, 77(18):3865–3868.

Perdew, J. P., Burke, K., and Ernzerhof, M. (1997). Generalized Gradient Approximation Made Simple [Phys. Rev. Lett. 77, 3865 (1996)]. *Phys. Rev. Lett.*, 78(7):1396.

Phototransistors, S.-l. M., Yin, Z., Li, H., Li, H., Jiang, L., Shi, Y., Sun, Y., Lu, G., Zhang, Q., Chen, X., and Zhang, H. (2012). Single-Layer MoS 2 Phototransistors**.

Plachinda, P., Evans, D., and Solanki, R. (2017). Electrical properties of covalently functionalized graphene. *AIMS Materials Science*, 4(2):340–362.

Pumera, M. (2014). Heteroatom modified graphenes: electronic and electrochemical applications. *J. Mater. Chem. C*.

Ramakrishna Matte, H. S., Gomathi, A., Manna, A. K., Late, D. J., Datta, R., Pati, S. K., and Rao, C. N. (2010). MoS2 and WS2 analogues of graphene. *Angewandte Chemie - International Edition*, 49(24):4059–4062.

Rani, P., Bhandari, R., and Jindal, V. K. (2015). Band gap modulation of graphene with increasing concentration of Li/B doping. *Advanced Science Letters*, 21(9):2826–2829.

Rani, P. and Jindal, V. K. (2013). Designing band gap of graphene by B and N dopant atoms. *RSC Adv.*

Res, I. E. and Majumdar, D. (2016). Innovative Energy & Research Functionalized-Graphene / Polyaniline Nanocomposites as Proficient Energy Storage Material : An Overview. *Innovative Energy & Research*, 5(2):1000145.

Roychoudhury, S., Motta, C., and Sanvito, S. (2016). Charge transfer energies of benzene physisorbed on a graphene sheet from constrained density functional theory. *Physical Review B*, 93(4):1–8.

Rubio-Pereda, P. and Takeuchi, N. (2013). Density functional theory study of the organic functionalization of hydrogenated graphene. *Journal of Physical Chemistry C*, 117(36):18738–18745.

Sherrill, C. D. (2000). An Introduction to Hartree-Fock Molecular Orbital Theory What Problem Are We Solving ? Motivation and the Hartree Product. pages 1–8.

Shim, Y., Jung, Y., and Kim, H. J. (2011). Graphene-based supercapacitors: A computer simulation study. *Journal of Physical Chemistry C*, 115(47):23574–23583.

Shim, Y., Kim, H. J., and Jung, Y. (2012). Graphene-based supercapacitors in the parallel-plate electrode configuration: Ionic liquids versus organic electrolytes. *Faraday Discussions*, 154:249–263.

Song, C., Wang, J., Meng, Z., Hu, F., and Jian, X. (2018). Density Functional Theory Calculations of the Quantum Capacitance of Graphene Oxide as a Supercapacitor Electrode. *ChemPhysChem*, 19(13):1579–1583.

Soon, J. M. and Loh, K. P. (2007). Electrochemical double-layer capacitance of MoS2 nanowall films. *Electrochemical and Solid-State Letters*, 10(11):250–254.

Sruthi, T. and Kartick, T. (2019). Route to achieving enhanced quantum capacitance in functionalized graphene based supercapacitor electrodes. *Journal of Physics Condensed Matter*, 31(47).

Stauber, T., Parida, P., Trushin, M., Ulybyshev, M. V., Boyda, D. L., and Schliemann, J. (2017). Interacting Electrons in Graphene: Fermi Velocity Renormalization and Optical Response. *Physical Review Letters*.

Stoller, M. D., Park, S., Yanwu, Z., An, J., and Ruoff, R. S. (2008). Graphene-Based ultracapacitors. *Nano Letters*, 8(10):3498–3502.

Su, Q., Pang, S., Alijani, V., Li, C., Feng, X., and Müllen, K. (2009). Composites of craphene with large aromatic molecules. *Advanced Materials*, 21(31):3191–3195.

Sun, M. and Peng, Y. (2014). Study on structural, electronic and magnetic properties of Sn atom adsorbed on defective graphene by first-principle calculations. *Applied Surface Science*, 307:158–164.

Sun, S., Qi, Y., and Zhang, T. Y. (2015). Dissecting graphene capacitance in electrochemical cell. *Electrochimica Acta*, 163:296–302.

Superzeure, E. X. and Superieure, E. X. (1964). I i ˜ ˜. 155(1962).

Tachikawa, H. (2019). Surface Science Methyl radical addition to the surface of graphene nano fl akes : A density functional theory study. *Surface Science*, 679(September 2018):196–201.

Takahashi, T., Sugawara, K., Noguchi, E., Sato, T., and Takahashi, T. (2014). Band-gap tuning of monolayer graphene by oxygen adsorption. *Carbon*.

Taluja, Y., SanthiBhushan, B., Yadav, S., and Srivastava, A. (2016). Defect and functionalized graphene for supercapacitor electrodes. *Superlattices and Microstructures*, 98:306–315.

Tan, Z., Chen, G., and Zhu, Y. (2015). Carbon-Based Supercapacitors Produced by Activation of Graphene-surporting materials. *Science*, 1(June):211–225.

Terrones, M., Botello-Méndez, A. R., Campos-Delgado, J., López-Urías, F., Vega-Cantú, Y. I., Rodríguez-Macías, F. J., Elías, A. L., Muñoz-Sandoval, E., Cano-Márquez, A. G., Charlier, J. C., and Terrones, H. (2010). Graphene and graphite nanoribbons: Morphology, properties, synthesis, defects and applications. *Nano Today*, 5(4):351–372.

Umadevi, D. and Sastry, G. N. (2011). Molecular and ionic interaction with graphene nanoflakes: A computational investigation of CO2, H2O, Li, Mg, Li+, and Mg2+ interaction with polycyclic aromatic hydrocarbons. *Journal of Physical Chemistry C*, 115(19):9656–9667.

Vanderbilt, D. (2006). Theory of Pseudopotentials. *Bangalore Summer School*.

Vatamanu, J., Ni, X., Liu, F., and Bedrov, D. (2015). Tailoring graphene-based electrodes from semiconducting to metallic to increase the energy density in supercapacitors. *Nanotechnology*, 26(46):464001.

Wang, G., Zhang, L., and Zhang, J. (2012). A review of electrode materials for electrochemical supercapacitors. *Chemical Society Reviews*, 41(2):797–828.

Wang, L., Chen, X., Zhu, W., Wang, Y., Zhu, C., Wu, Z., Han, Y., Zhang, M., Li, W., He, Y., and Wang, N. (2014). Detection of resonant impurities in graphene by quantum capacitance measurement. *Physical Review B - Condensed Matter and Materials Physics*, 89(7):1–6.

Weng, Q., Wang, X., Wang, X., Bando, Y., and Golberg, D. (2016). Functionalized hexagonal boron nitride nanomaterials: Emerging properties and applications. *Chemical Society Reviews*, 45(14):3989–4012.

Wood, B. C. (2015). First principles-inspired design strategies for graphene-based supercapacitor electrodes. *PhD Proposal*, 1.

Wu, G., Tang, X., Meyyappan, M., and Lai, K. W. (2015). Chemical functionalization of graphene with aromatic molecule. *IEEE-NANO 2015 - 15th International Conference on Nanotechnology*, (December 2016):1324–1327.

Wu, P., Yin, N., Li, P., Cheng, W., and Huang, M. (2017). The adsorption and diffusion behavior of noble metal adatoms (Pd, Pt, Cu, Ag and Au) on a MoS2 monolayer: A first-principles study. *Physical Chemistry Chemical Physics*, 19(31):20713–20722.

Xia, J. (2010). Charge Transport and Quantum Capacitance of Graphene. (December).

Xia, J., Chen, F., Li, J., and Tao, N. (2009). Measurement of the quantum capacitance of graphene.

Xu, Q., Yang, G., Fan, X., and Zheng, W. (2019). Improving the Quantum Capacitance of Graphene-Based Supercapacitors by the Doping and Co-Doping : First-Principles Calculations.

Xu, Q., Yang, G. M., and Zheng, W. T. (2020). DFT calculation for stability and quantum capacitance of MoS2 monolayer-based electrode materials. *Materials Today Communications*, 22.

Yang, G. M., Zhang, H. Z., Fan, X. F., and Zheng, W. T. (2015). Density functional theory calculations for the quantum capacitance performance of graphene-based electrode material. *Journal of Physical Chemistry C*, 119(12):6464–6470.

Yang, Q. and Achenie, L. E. (2018). Exploration of bulk and interface behavior of gas molecules and 1-butyl-3-methylimidazolium tetrafluoroborate ionic liquid using equilibrium and nonequilibrium molecular dynamics simulation and quantum chemical calculation. *Physical Chemistry Chemical Physics*, 20(15):10121–10131.

Yankowitz, M., Xue, J., and Leroy, B. J. (2014). Graphene on hexagonal boron nitride. *Journal of Physics Condensed Matter*, 26(30).

Yeh, N.-c. (2008). A Perspective of Frontiers in Modern Condensed Matter Physics. 18(2):13–15.

Yu, G. L., Jalil, R., Belle, B., Mayorov, A. S., Blake, P., Schedin, F., Morozov, S. V., Ponomarenko, L. a., Chiappini, F., Wiedmann, S., Zeitler, U., Katsnelson, M. I., Geim, a. K., Novoselov, K. S., and Elias, D. C. (2013). Interaction phenomena in graphene seen through quantum capacitance. *Proceedings of the National Academy of Sciences of the United States of America*, 110(9):3282–6.

Zeng, J., Zhang, R. Q., and Treutlein, H. R. (2012). Quantum simulations of materials and biological systems. *Quantum Simulations of Materials and Biological Systems*, pages 1–197.

Zhan, C., Lian, C., Zhang, Y., Thompson, M. W., Xie, Y., Wu, J., Kent, P. R. C., Cummings, P. T., Jiang, D.-e., and Wesolowski, D. J. (2017). Computational Insights into Materials and Interfaces for Capacitive Energy Storage. (April).

Zhan, C., Neal, J., Wu, J., and Jiang, D. E. (2015). Quantum Effects on the Capacitance of Graphene-Based Electrodes. *Journal of Physical Chemistry C*, 119(39):22297–22303.

Zhan, C., Zhang, Y., Cummings, P. T., and Jiang, D.-e. (2016). Enhancing graphene capacitance by nitrogen: effects of doping configuration and concentration. *Phys. Chem. Chem. Phys.*, 18(6):4668–4674.

Zhang, L. L., Zhou, R., and Zhao, X. S. (2009). Carbon-based materials as supercapacitor electrodes. *Journal of Materials Chemistry*, 38(29):2520–2531.

Zhou, W., Zou, X., Najmaei, S., Liu, Z., Shi, Y., Kong, J., Lou, J., Ajayan, P. M., Yakobson, B. I., and Idrobo, J. C. (2013). Intrinsic structural defects in monolayer molybdenum disulfide. *Nano Letters*, 13(6):2615–2622.

Zhu, J., Childress, A. S., Karakaya, M., Srivastava, A., Lin, Y., Rao, A. M., and Podila, R. (2016). Defect-engineered graphene for bulk supercapacitors with high energy and power densities.

6.3 LIST OF PUBLICATIONS BASED ON THESIS WORK

- **Sruthi T.** and Kartick Tarafder.(2019) ”Enhancement of quantum capacitance by chemical modification of graphene supercapacitor electrodes: a study by first principles.”
  Bulletin of Material Science **42**, 257
  DOI: http://dx.doi.org/10.1007/s12034-019-1952-8

- **Sruthi T.** and Kartick Tarafder. (2019). ”Route to achieving enhanced quantum capacitance in functionalized graphene based supercapacitor electrodes.”
  Journal of Physics: Condensed Matter, **31**(47), 475502.
  DOI: http://dx.doi.org/10.1088/1361-648X/ab2ac0

- **Sruthi T** and Kartick Tarafder(2020). ”Enhancement of quantum capacitance in graphene electrodes by chemical modifications using aliphatic/aromatic molecules and their radicals”.
  Physica B: Physics of Condensed Matter
  DOI: https://doi.org/10.1016/j.physb.2020.412676

- **Sruthi T**, Nayana Devaraj, and Kartick Tarafder(2020). ”Theoretical investigation of quantum capacitance in the functionalized MoS_2-monolayer”.
  (*Electron.Struct3(2021)025003*)
  DOI: https://doi.org/10.1088/2516-1075/abc4c5

Conference Presentations

1. **Sruthi T** and Dr. Kartick Tarafder. "THE EFFECT OF STRONG CORRELETION IN FUNCTIONALIZED GRAPHENE : A DFT STUDY". International Meeting on Highly Correlated Systems (IMHCS) 2017 at SCHOOL OF PURE AND APPLIED PHYSICS MAHATMA GANDHI UNIVERSITY ,KOTTAYAM,2017.
   Poster Presentation
2. **Sruthi T** and Dr. Kartick Tarafder. "Enhancement of Quantum Capacitance by Chemical Modification of Zigzag Graphene Nano-ribbon Supercapacitor Electrodes: A First Principle Calculation". Indo-US Bilateral Workshop on Nanotechnology for Clean Energy Generation and Storage Organised by Nanotech Research, Innovation and Incubation Centre PSG Institute of Advanced Studies Coimbatore-641 004, India & SUNY Polytechnic Institute Colleges of Nanoscale Science and Engineering Albany, New York, USA Funded by Indo-US Science and Technology Forum, 2018.
   Oral Presentation
3. **Sruthi T** and Dr. Kartick Tarafder. "Density functional theory calculations for the enhanced quantum capacitance of chemically modified graphene nanoribbon supercapacitor electrodes. ". 29th Annual General Meeting Of Materials Research Society Of India & National Symposium On Advances In Functional And Exotic Materials, 2018.
   Poster Presentation
4. **Sruthi T** and Dr. Kartick Tarafder. "Enhancement of Quantum Capacitance by Chemical Modification of Graphene Supercapacitor Electrodes: A Study From

First Principles". Materials & Technologies for Energy Conversion and Storage (M-TECS 2018)Organized by Bhabha Atomic Research Centre in association with Materials Research Society of India-Mumbai Chapter at DAE Convention Centre, Anushaktinagar, Mumbai, 2018.
Poster Presentation

5. **Sruthi T** and Dr. Kartick Tarafder. "The effect of functionalization in MoS2 monolayer : A DFT STUDY". International Conference on Current Trends in Functional Materials(CTFM-2020), Organized National Institute of Technology, Karnataka.
   Poster presentation

CURRICULUM VITAE

SRUTHI T

Father's name : T Thulaseedasan Bhattathiri

Date of birth : 03/06/1991

Permanent Address :

W/O Dr Sukesh A K
Pranavam House Mobile : +91-9495579305
PO: Padannakad E-mail : sruty111@gmail.com
Kerala, India - 671314

Academic Qualifications :

Master of Science Score : 84%

Kannur University,
Kerala, India

Bachelor of Science Score : 91%

Kannur University,
Kerala, India

Research Publications : 4

Conferences and Workshops attended : 5